OPTIMIZING GENETICALLY ENCODED CALCIUM INDICATORS TO MEASURE PRESYNAPTIC CALCIUM TRANSIENTS

by

Andrew Alexander Edward Gilyan

Submitted in partial fulfilment of the requirements
for the degree of Master of Science

at

Dalhousie University
Halifax, Nova Scotia
September 2012

DALHOUSIE UNIVERSITY

DEPARTMENT OF PHYSIOLOGY AND BIOPHYSICS

The undersigned hereby certify that they have read and recommend to the Faculty of Graduate Studies for acceptance a thesis entitled "OPTIMIZING GENETICALLY ENCODED CALCIUM INDICATORS TO MEASURE PRESYNAPTIC CALCIUM TRANSIENTS" by Andrew Alexander Edward Gilyan in partial fulfilment of the requirements for the degree of Master of Science.

Dated: September 27th, 2012

Supervisor: _____

Readers: _____

_____

_____

DALHOUSIE UNIVERSITY

DATE: September 27th, 2012

AUTHOR: Andrew Alexander Edward Gilyan

TITLE: OPTIMIZING GENETICALLY ENCODED CALCIUM INDICATORS TO MEASURE PRESYNAPTIC CALCIUM TRANSIENTS

DEPARTMENT OR SCHOOL: Department of Physiology and Biophysics

DEGREE: MSc CONVOCATION: May YEAR: 2013

_____

Signature of Author

DEDICATION

I dedicate this Master of Science thesis to my late grandfather, Edward “Eddy” Kelly.

TABLE OF CONTENTS

LIST OF TABLES....viii

LIST OF FIGURES....ix

ABSTRACT....xi

LIST OF ABBREVIATIONS USED....xii

ACKNOWLEDGEMENTS....xiv

CHAPTER 1: INTRODUCTION....1

1.1 CALCIUM SIGNALLING IN NEURONS....1
1.2 MEASURING INTRACELLULAR CALCIUM TRANSIENTS....3
1.2.1 Electrophysiology....3
1.2.2 Synthetic Fluorescent Calcium Indicator Dyes....5
1.2.3 Genetically Encoded Calcium Indicators....7
1.3 GCaMP-BASED CALCIUM SENSORS....10
1.3.1 Development of GECIs Based on Circular Permuted GFP....10
1.3.2 Optimization of GCaMP Sensors....12
1.3.3 The Structure and Functional Properties of Calmodulin....13
1.4 OBJECTIVES OF THIS STUDY....18

CHAPTER 2: MATERIALS AND METHODS....21

2.1 GENERATION OF GCaMP3 MUTANT CONSTRUCTS....21
2.1.1 Primer Phosphorylation and Site Directed Mutagenesis PCR....21
2.1.2 Generating GCaMP3 Constructs with Multiple Mutations....23
2.1.3 Transformation of Plasmid DNA Obtained from SDM PCR and Subcloning....24
2.1.4 Isolation of Small Amounts of Plasmid DNA from *E. coli* for Sequence Verification....25
2.2 GCaMP3 VARIANT CONSTRUCT VERIFICATION....26

2.3 *IN VITRO* ASSESSMENT OF GCaMP3 VARIANTS....26
2.3.1 Protein Expression....26
2.3.2 Calcium Titration Assay....28
2.3.3 Determination of K_d, Hill Coefficients, Dynamic Ranges, and Basal Fluorescence of GCaMP3 Variants....29
2.3.4 Statistical Analysis of Calcium Titration Data....30
2.4 ASSESSMENT OF GCaMP3 VARIANTS IN NEURONS....31
2.4.1 Primary Cell Culture of Hippocampal Neurons....31
2.4.2 Subcloning GCaMP3 Calcium Affinity Variants into a Vector for Neuronal Protein Expression....32
2.4.3 Transfection of pE(GCaMP3) Constructs....33
2.4.4 Stimulation and Cellular Imaging....34
2.4.5 Image Analysis....35
2.4.6 Statistical Analysis of Neuronal Data....37

CHAPTER 3: RESULTS....39

3.1 *IN VITRO* CHARACTERIZATION OF GCaMP MUTATIONS....39
3.1.1 Single Point Mutations in EF Motifs....39
3.1.1.1 Position 12 Mutations of GCaMP3....39
3.1.1.2 Position 3 Mutations of GCaMP3....41
3.1.1.3 Position 5 Mutations of GCaMP3....42
3.1.1.4 Position 9 Mutations of GCaMP3....43
3.1.1.5 Position 2 Mutations of GCaMP3....44
3.1.1.6 Position 11 Mutations of GCaMP3....45
3.1.2 Linker Mutations of GCaMP3....46
3.1.3 Generation of GCaMP Variants with High Calcium Affinity Using a Combinatorial Approach....47
3.1.4 Generation of GCaMP Variants with Low Calcium Affinity Using a Combinatorial Approach....49
3.2 CHARACTERIZATION OF GCaMP MUTATIONS IN CULTURED HIPPOCAMPAL NEURONS....51
3.2.1 Detection of Presynaptic Calcium Transients in Neurons….....52
3.2.2 GCaMP Mutants with Higher Calcium Affinity....53

3.2.3 GCaMP Mutants with Lower Calcium Affinity.....56

CHAPTER 4: DISCUSSION.....59

4.1 GENERATION OF GCaMP VARIANTS WITH A LARGER RANGE OF CALCIUM AFFINITY.....59

4.1.1 High Calcium Affinity Sensor.....59

4.1.2 Low Calcium Affinity Sensors.....61

4.2 FURTHER IMPROVEMENTS TO THE HIGH AND LOW AFFINITY GCaMP3 VARIANTS.....62

4.2.1 Further Increases in Calcium Affinity.....62

4.2.2 Improvements of the Signal-to-Noise Ratio with which GCaMPs Detect Small Calcium Transients.....64

4.2.3 Further Improvements of Low Calcium Affinity Sensors.....65

4.3 APPLICATIONS FOR GCaMP3 AFFINITY VARIANTS.....67

4.3.1 Measurement of Action-Potential Evoked Presynaptic Calcium Transients.....67

4.3.2 "Mapping" of Calcium Micro- and Nanodomains.....68

4.3.3 Compartmentalization of Calcium Homeostasis in Neurons at Rest and under Conditions of Sustained Calcium Influx.....69

REFERENCES.....71

APPENDIX A: PRIMER SEQUENCES.....83

APPENDIX B: TABLES.....86

APPENDIX C: FIGURES.....96

LIST OF TABLES

Table 1 K_d, Hill coefficients, dynamic ranges, and basal fluorescence of *in vitro* characterization for single point mutant GCaMP3 variants.....86

Table 2 K_d, Hill coefficients, dynamic ranges, and basal fluorescence of *in vitro* characterization for linker mutation GCaMP3 variants.....88

Table 3 K_d, Hill coefficients, dynamic ranges, and basal fluorescence of *in vitro* characterization for mutant combination GCaMP3 variants.....89

Table 4 Neuronal data for high calcium affinity GCaMP3 variant.....91

Table 5 Neuronal data for individual mutant constructs comprising the high calcium affinity GCaMP3 variant.....93

Table 6 Neuronal data for low calcium affinity GCaMP3 variants.....94

LIST OF FIGURES

Figure 1 Schematic representation of compartmentalized calcium signaling in neurons.....96

Figure 2 Schematic representation illustrating FRET-based calcium indicators, circular permutation of GFP, and GCaMP-based calcium indicators.....98

Figure 3 Overview of the optimization of the GECI, GCaMP, to generate GCaMP3.....100

Figure 4 Schematic representation of the calcium chelating protein, calmodulin.....101

Figure 5 Schematic diagram illustrating the loop of an EF motif.....102

Figure 6 Overlay of the four calcium binding EF motifs.....103

Figure 7 *In vitro* characterization of GCaMP3 constructs containing mutations at position 12 of the calcium binding EF motifs.....104

Figure 8 *In vitro* characterization of GCaMP3 constructs containing mutations at position 3 of the calcium binding EF motifs.....105

Figure 9 *In vitro* characterization of GCaMP3 constructs containing mutations at position 5 of the calcium binding EF motifs.....106

Figure 10 *In vitro* characterization of GCaMP3 constructs containing mutations at position 9 of the calcium binding EF motifs.....107

Figure 11 *In vitro* characterization of GCaMP3 constructs containing mutations at position 2 of the calcium binding EF motifs.....108

Figure 12 *In vitro* characterization of GCaMP3 constructs containing mutations at position 11 of the calcium binding EF motifs.....109

Figure 13 Overview of the 25 amino acid residue flexible linker region connects the N- and C- terminal domains of CaM.....110

Figure 14 *In vitro* characterization of GCaMP3 constructs containing mutations within the linker region of CaM.....112

Figure 15 *In vitro* characterization of GCaMP3 constructs containing multiple increasing calcium affinity mutations within the EF motifs and linker region of CaM.....113

Figure 16 *In vitro* characterization of GCaMP3 constructs containing multiple decreasing calcium affinity mutations within the EF motifs and linker region of CaM.....114

Figure 17 Images showing dissociated hippocampal neurons transfected with tdTomato-Bassoon and the high calcium affinity GC3 variant.....115

Figure 18 Fluorescence changes of GCaMP3 and GC3_K21A_K77G_N97D in response to electrical stimulation.....117

Figure 19 Normalized fluorescence changes in response to 2 second stimulus trains for GCaMP3 and GC3_K21A_K77G_N97D.....119

Figure 20 SNR for GC3 and GC3_K21A_K77G_N97D in response to a single stimulus and bursts of 2 and 4 stimuli at 40 Hz.....120

Figure 21 Average fluorescence change for mutations comprising the high calcium affinity GCaMP3 variant in response to a single stimulus and bursts of 2 and 4 stimuli at 40 Hz.....121

Figure 22 SNR for GC3 and select mutations comprising the high calcium affinity variant in response to a single stimulus and bursts of 2 and 4 stimuli at 40 Hz.....123

Figure 23 Normalized fluorescence changes in response to 2 second stimulus trains for GCaMP3 and the low calcium affinity GCaMP3 variants.....124

Figure 24 Fluorescence changes for GCaMP3 and the low calcium affinity sensors.....125

Figure 25 Average change in fluorescence in response to a single stimulus and bursts of 2 and 4 stimuli at 40 Hz for the low calcium affinity GCaMP3 sensors.....127

Figure 26 Average SNR for GC3 and the low calcium affinity sensors in response to a single stimulus and bursts of 2 and 4 stimuli at 40 Hz.....128

ABSTRACT

Neurotransmitter release is modulated by multiple regulatory mechanisms that control several stages of synaptic vesicle (SV) exocytosis. At the final stage, SV fusion with the presynaptic membrane requires calcium influx through voltage-gated calcium channels, and regulatory mechanisms that alter the surface expression or conductance of calcium channels have large effects on neurotransmitter release. To determine how these mechanisms contribute to synapse-specific modulations of neurotransmitter release and synaptic strength, we require a means to monitor presynaptic calcium transients at individual synapses. Genetically encoded calcium indicators (GECIs), engineered proteins that change their fluorescence emission properties upon calcium binding, generally lack the sensitivity to measure such transients in response to isolated stimuli. Therefore, we modified the GECI, GCaMP3, by altering its sensitivity for calcium. Our results suggest the modified GCaMP-based presynaptically targeted GECIs are excellent tools to quantify presynaptic calcium transients at individual synapses in response to isolated action potentials.

LIST OF ABBREVIATIONS USED

°C	Degrees Celsius
A	Alanine
AMPA	2-amino-3-(5-methyl-3-oxo-1,2- oxazol-4-yl)propanoic acid
ANOVA	Analysis of Variance
APs	Action Potentials
APV	2-amino-5-phosphonovaleric acid
ATP	Adenosine Triphosphate
BAPTA	bis-(*o*-aminophenoxy)-ethane-*N,N,N',N'*-tetraacetic acid
Ca^{2+}	Calcium
$CaCl_2$	Calcium Chloride
CaM	Calmodulin
CCD	Charged Coupled Device
cDNA	complementary Deoxyribonucleic Acid
CIP	Calf Intestinal Phosphatase
CMV promoter	CytoMegalovirus promoter
cpEGFP	circularly permuted Enhanced Green Fluorescent Protein
D	Aspartic Acid
DNQX	6,7-dinitroquinoxaline-2,3-dione
E	Glutamic Acid
E. coli	*Escherichia coli*
EDTA	Ethylenediaminetetraacetic acid
EGFP	Enhanced Green Fluorescent Protein
EGTA	Ethylene Glycol Tetraacetic Acid
F	Fluorescence
F_{max}	Maximum Fluorescence
F_{min} or F_0	Minimum Fluorescence
FRET	Forster/fluorescence Resonance Energy Transfer
G	Glycine
GC3	GCaMP3
GECIs	Genetically Encoded Calcium Indictors
GFP	Green Fluorescent Protein
HBS	Hepes Buffered Saline
Hepes	-(2-hydroxyethyl)-1-piperazineethanesulfonic acid
IPTG	Isopropyl-beta-D-thiogalactopyranoside
K	Lysine
KCl	Potassium Chloride
K_d	Dissociation Constant
LB medium	Luria-bertani medium
M	Methionine
MEM	Minimal Essential Medium
MgCl	Magnesium Chloride
MLCK	Methionine-Leucine-Cysteine-Lysine leader sequence
MOPS	3-(N-morpholino)propanesulfonic acid

N	Asparagine
Na^+	Sodium
Na_2HP0_4	Disodium Hydrogen Phosphate
NaCl	Sodium Chloride
$NaH_2P0_4 \cdot 2H_2O$	Dihydrogen Sodium Phosphate
NaOH	Sodium Hydroxide
ND	Not Determined
Ni-NTA	Nickel Nitriloacetate
NMDARs	*N*-methyl-*D*-aspartate-type glutamate receptors
NS	Not Significant
OD_{600}	Optical Density of sample measured at wavelength of 600 nm
PMCA	Plasma Membrane Calcium ATPase
PNK	Polynucleotide Kinase
Q	Glutamine
R	Arginine
RNA	Ribonucleic Acid
RNase A	Ribonuclease A
rpm	Revolutions per Minute
S	Serine
SDM PCR	Site Directed Mutagenesis Polymerase Chain Reaction
SERCA pumps	Smooth Endoplasmic Reticulum Calcium pumps
SNR	Signal-to-Noise Ratio
SV	Synaptic Vesicle
T	Threonine
TBE	tris(hydroxymethyl)amino methane, boric acid, EDTA buffer
Tris-HCl	tris(hydroxymethyl)amino methane and hydrochloric acid
Tukey HSD	Tukey Honestly Significant Difference Test
V	Valine
V/cm	Volts per centimetre
v/v	Volume to Volume
VGCC	Voltage-Gated Calcium Channels
vs	Versus
w/v	Weight to Volume
Y	Tyrosine
ΔF	Change in Fluorescence

ACKNOWLEDGEMENTS

First and foremost, I would like to express my most sincere gratitude to my supervisor, Dr. Stefan Krueger, for his excellent guidance, expertise, and continued support and help throughout the course of this project.

Thank you to my supervisory committee members Drs. Alan Fine, Barbara Karten, and Doug Rasmusson for their helpful suggestions, feedback, and discussions.

A major thank you goes to the current and former members of our lab, especially Annette Kolar, Dylan Quinn, Kristen Chafe, Christina Selenz, and Jacob Matz for their technical expertise and unconditional assistance and support. Without you all, this work could not have been accomplished. I would also like to thank the labs of Dr. Alan Fine, Dr. Barbara Karten, Dr. Jim Fawcett, Dr. Brent Johnston, and Dr. Chris Sinal for providing technical support and equipment.

To my family who has provided their continuous support and encouragement throughout my Master's Thesis, I thank you.

Finally, I would like to thank NSERC for funding through the GCS award as well as from the NSHRF funding agency.

CHAPTER 1 INTRODUCTION

1.1 CALCIUM SIGNALLING IN NEURONS

Calcium plays a vital role in the regulation of many essential cellular processes and signalling events across a variety of tissues and organisms (Brownlee, 2000; Clapham, 1995; Takahashi et al, 1999). Calcium is a universal second messenger regulating many enzymes. However, persistent calcium elevation can lead to apoptotic and necrotic cell death (Clapham, 1995). Therefore, the ion's concentration is maintained at very low cytosolic levels, ranging from 30 to 100 nM (Maravall et al, 2000; Nakajima et al, 1993). In neurons, which contain high densities of voltage-gated calcium channels, low basal calcium concentrations are achieved through a plethora of efficient calcium buffering proteins, including parvalbumin, calretinin, and calbindin-D28K, and rapid extrusion mechanisms (Celio, 1990; Baimbridge et al, 1993; Clapham, 1995; and Edmonds et al, 2000). Such mechanisms include transporting Ca^{2+} to the extracellular space via high-affinity, low capacity plasma membrane Ca^{2+} ATPase (PMCA) pumps as well as low-affinity, high capacity Na^{+}/Ca^{2+} exchangers; intraorganellar storage of the ions by means of smooth endoplasmic reticulum calcium (SERCA) pumps, and mitochondrial Ca^{2+} uniporters (Bianchi et al, 2004; Clapham, 1995; Reuter and Porzig, 1995). The autonomous regulation of calcium influx in the cytosol by the ubiquitously distributed calcium buffers and extrusion mechanisms causes calcium signalling to be highly localized to subcellular compartments within neurons (Berridge, 1998). Moreover, these spatially defined elevations of cytosolic calcium maintain their highest amplitude at the point of entry, but quickly taper off to create diffusion gradients as the distance from each source increases (Chad and Eckert, 1984). Furthermore, cytosolic calcium transients

arise from various extracellular and intracellular sources of influx and differ in their contribution to the regulation of internal signaling processes and events depending on their identity, location, and characteristics (Berridge, 1993; Clapham, 1995; Tsien and Tsien, 1990).

Much is known about the various axonal, dendritic, and somatic sources of calcium influx that lead to compartmentalized signaling in neurons. Along the plasma membrane of axons, extracellular calcium enters the cytosol through N- and P/Q-type voltage-gated calcium channels (VGCCs) in response to membrane depolarizing action potentials (APs) (Catteral, 2000; Spafford and Zamponi, 2003; Jaffe et al, 1992). The rapid influx of calcium through VGCCs forms spatially defined regions of calcium that quickly diffuse from the mouth of the channels that are denoted as 'calcium domains' (Chad and Eckert, 1984). Each domain can be further characterized as being either a 'microdomain' or a 'nanodomain' depending on the degree of signal summation that arises from clusters of open VGCCs or from single, isolated VGCCs, respectively (Kasai, 1993; Llinás et al, 1992). The concentrations of calcium within these domains reportedly range from tens of nanomolar to hundreds of micromolar in value (Heidelberger et al, 1994; Roberts and Hudspeth, 1990; Llinas et al, 1992; Neher, 1998). As an example for calcium signalling in micro- and nanodomains, presynaptic VGCCs are predominantly located at the active zone to facilitate neurotransmitter release. The local Ca^{2+} increase through VGCCs at presynaptic specializations is detected by the synaptic vesicle membrane glycoprotein, synaptotagmins. Since synaptotagmins have a low affinity for calcium, synaptic vesicles have to be located within the calcium micro- or nanodomain to undergo calcium-triggered exocytosis (Südhof, 1995).

The cascade of events resulting in neurotransmitter release at presynaptic sites facilitates synaptic communication with neighboring neurons and may activate another source of calcium influx. The neurotransmitter glutamate, for instance, can bind to *N*-methyl-*D*-aspartate-type glutamate receptors (NMDARs) in the postsynaptic membrane to induce dendritic influxes of calcium (Berridge, 1998; Müller and Connor, 1991). In addition to the axonal and dendritic sources of calcium, intracellular calcium stores within the extensive endoplasmic reticulum network represent another important source of calcium that can have profound effects on shaping neuronal Ca^{2+} signals (Kostyuk and Verkhratsky, 1994; Simpson et al, 1995; Garaschuk et al, 1997) (Figure 1). To understand regulatory mechanisms in neurons that require calcium signalling, accurate measurements of calcium transients in subcellular domains, micro- and nanodomains are necessary.

1.2 MEASURING INTRACELLULAR CALCIUM TRANSIENTS

1.2.1 Electrophysiology

Several calcium measurement techniques have been implemented in various neuronal preparations to ascertain information regarding synaptic transmission and the functioning of neural networks. Electrophysiological methods provide measurements of calcium conductances across the plasma membrane with excellent temporal resolution. However, this technique is accompanied by several significant limitations. Electrophysiological techniques generally have a poor spatial resolution, as this approach integrates calcium conductances across the plasma membrane of electrotonically

accessible parts of the cell. In some instances, measurements of calcium conductances in electrotonically well-isolated compartments of neurons can be made by patch-clamping these structures directly (e.g. Stanley and Atrakchi, 1990; Schneggenburger et al, 1999). However, this approach is limited to large, experimentally accessible subcellular structures, often in specialized preparations, such as Calyx-type synapses. A second limitation of electrophysiological calcium measurements is that not all sources of cytosolic calcium transients can be measured. As electrodes for electrophysiology are placed at the plasma membrane, calcium mobilized from other sources that do not contact this membrane, such as intracellular stores, cannot be sampled. Experimental protocols for conducting electrophysiological recordings are also very invasive in nature as they impale the membrane of recording site of the cell of interest. Recordings with whole-cell access often result in a 'wash out' effect, which is the dilution of the constituents of a cell, such as proteins involved in calcium signalling and buffering, amongst others. Another limitation with this technique is that in order to isolate a specific ion's currents, all other ionic currents must be inhibited. This requirement results in an unphysiological environment that can skew the data recovered of the isolated current of interest. Finally, electrophysiological recordings have been proven to be very difficult to perform in an *in vivo* preparation due to the accessibility to cells of interest. Due to the drawbacks of these methods, more effective techniques to measure isolated calcium transients were in need of development so researchers could further expand their understanding of neuronal calcium dynamics.

1.2.2 Synthetic Fluorescent Calcium Indicator Dyes

The use of fluorescent small molecule synthetic calcium indicator dyes has addressed several limitations of electrophysiological approaches. These dyes report information with high spatial resolution, can monitor different sources of calcium influx concomitantly, do not require extensive pharmacology to isolate calcium conductances, and are more easily applied *in vivo*. Therefore, indicator dyes have become widely used over the last three decades to study questions of calcium signalling as well as to monitor action potentials in neurons and cardiomyocytes (Higley and Sabatini, 2008; Rochefort et al, 2008). These bright indicator dyes, which are mostly based on the calcium chelating molecule bis-(*o*-aminophenoxy)-ethane-*N,N,N',N'*-tetraacetic acid (BAPTA), an ethylene glycol tetraacetic acid (EGTA) homologue, are photostable, and demonstrate large Ca^{2+} dependent fluorescence changes (Paredes et al, 2008). Furthermore, a multitude of dyes have been generated ranging in their affinity for calcium, as their application as sensors are only effective when utilized with calcium concentrations similar to their own dissociation constant (K_d). For instance, high affinity dyes can be applied to detect small calcium transients with high sensitivity while low affinity dyes are not saturated by, and are accurate reporters of, large calcium transients. Dyes that range in their affinity for calcium include Fura 2, Fluo 3, Rhod 2, BTC, and Mag-fura 2, and have respective K_d of 224 nM, 400 nM, 1 μM, 7 μM, and 25 μM (Takahashi et al, 1999). Dyes such as these allow researchers to select an appropriate calcium sensor depending on the type of calcium environment under investigation.

Although the implementations of calcium dyes have further advanced our understanding of neuronal processes underlying calcium signalling, several limitations

must be considered with this approach as well. First and foremost, the use of indicator dyes to measure cytosolic calcium transients is often problematic in experiments probing calcium transients in (1) discrete populations of cells in organized tissue or (2) at specific subcellular locations in a single cell. Indicator dyes can be loaded into cells either through a patch pipette or by bulk application of a membrane-permeable acetomethoxy ester of the dye. When attempting to record calcium transients from discrete populations of cells in a tissue slice or in vivo, the dye often has to be applied through a patch pipette to permit the identification of cell type and prevent signal contamination. However, this method has many of the drawbacks of conventional electrophysiology (difficulty to use in vivo, invasive and prone to "wash out" artefacts, and limitation of recordings to a single or few cells). Regardless of the loading method, synthetic indicators also lack the ability to be easily targeted to specific subcellular locations, such as synaptic specializations, as they become distributed throughout the cytosol or intraorganellar space upon loading (Takahashi et al, 1999). This feature often prevents the efficient use of calcium dyes in experiments probing calcium transients in micro- or nanodomains. Moreover, fluorescent ion indicators that can readily traverse the membrane can compartmentalize in an undesirable fashion (Takahashi et al, 1999). Many positively charged dyes, for example, become trapped in mitochondria, preventing their effective use to measure cytosolic transients (Steinberg et al, 1987; Malgaroli et al, 1987).

Synthetic indicators are also generally restricted to acute experiments due to issue of cytotoxicity, photodamage and photobleaching, and leakage of the dye to extracellular space from loaded cells (Takahashi et al, 1999; Becker and Fay, 1987; McDonough and Button, 1989). Dye leakage is regulated in part by anion transport systems and is partially

dependent on the cell type. It is especially problematic in long-term experiments, during which dye leakage can lead to progressive deterioration of the signal. Dye leakage may also make it difficult to accurately compare signals measured at different times during a long-term experiment, even when concentration changes are carefully monitored. Some techniques can be employed to avoid dye leakage. They include conjugating the indicator with membrane impermeable dextrans, inhibiting the ion transport systems, or continuously loading the dye; however, these workarounds are invasive, may limit data interpretation, and be potentially difficult or laborious depending on the preparation, respectively (Di Virgilio et al, 1988; Di Virgilio et al, 1990; Schlatterer et al, 1992; Munsch and Deitmer, 1995).

In summary, the use of synthetic indicator dyes has dramatically improved our understanding of cellular calcium signalling in neurons as well as non-neuronal cells. However, several limitations such as the inability to target dyes to specific cell populations and subcellular compartments as well as dye compartmentalization and leakage issues has restricted their use in some paradigms and led to the development of genetically encoded calcium indicators (GECIs), which are discussed in the next section.

1.2.3 Genetically Encoded Calcium Indicators

Another approach that has garnered significant attention over the last decade is the use of GECIs. These sensors have the potential to overcome the limitations of small-molecule calcium indicators as they are expressible within genetically defined neuronal populations through use of tissue-specific promoters (Hasan et al, 2004; Kuhn et al, 2012). The generation of transgenic mice or use of viral delivery methods allows fairly

convenient use of GECIs in vivo. Used in this way, the expression of GECIs remains relatively constant over time, allowing long-term experiments. This strategy allows the ability to monitor the neuronal activity across multiple brain regions and cell types, with examples including, neurons in the adult mouse retina (Borghuis et al, 2011), the hippocampus (Dombeck et al, 2010), and the mouse somatosensory cortex (Mittmann et al, 2011). Moreover, unlike small molecule-dyes, GECIs can easily be targeted to specific subcellular domains by constructing chimeric proteins in which the GECI is tagged with a cellular targeting sequence or fused to a protein that is targeted to a subcellular domain. This approach has been utilized to image synaptic activity by tethering indicators to synaptic vesicles (Dreosti et al, 2009), assessing mitochondrial calcium handling (Filippin et al, 2005), and investigate localized calcium signals at the nucleus (Miyawaki et al, 1997), endoplasmic reticulum (Palmer et al, 2004), Golgi (Griesbeck et al, 2001), and the plasma membrane (Nagai et al, 2004; Shigetomi et al, 2010). Moreover, the generation of various transgenic organisms incorporated with GECIs has facilitated cell specific expression of calcium sensors within tissues that are difficult to load with dyes (Heim et al, 2007; Kerr et al, 2000; Reiff et al, 2005; Higashijima et al, 2003; Hasan et al, 2004. Ji et al, 2004).

GECIs are polypeptide calcium sensors comprised of one or two optical reporter elements, such as green fluorescent protein (GFP) or its derivatives, conjugated with a calcium binding protein, such as calmodulin (CaM) or troponin C (Romoser et al, 1997; Miyawaki et al, 1997; Baird et al, 1999; Heim and Griesbeck, 2004; Mank et al, 2006). They transduce calcium binding evoked structural changes of the sensor protein into an observable fluorescence change of the attached fluorophore. The initial GECI detection

strategy pioneered by Roger Tsien, Atsushi Miyawaki, and colleagues, utilized Forster/fluorescence resonance energy transfer (FRET) between two fluorophores. This technique exploits the conformational change of the sensor domain upon Ca^{2+} binding to alter the relative distance and orientation between the donor and acceptor fluorophores resulting in the modulation of their emission spectra (Miyawaki et al, 1997; Knopfel et al, 2010; Palmer et al, 2006; Kotlikoff, 2007) (Figure 2A).

The first series of FRET based sensors designed by Miyawaki et al (1997), termed 'cameleons', were successfully expressed in the cytosol and endoplasmic reticulum of HeLa cells, maintained K_d values of 11 μM and 70 nM and reported calcium concentrations in the range from $<10^{-7}$ to $>10^{-4}$ M. They demonstrated two combinations of donor and acceptor fluorophores which were blue or cyan fluorescent proteins fused with enhanced green or yellow fluorescent proteins. These fluorophore combinations exhibited excitation wavelength and emission ratios of 380-510/445 and 440-535/480 nm, respectively. Since their advent, the cameleons have been progressively modified to decrease their pH sensitivity (Miyawaki et al, 1999; Griesbeck et al, 2001), improve their dynamic range by exchanging the calcium binding component of the sensor (Heim and Griesbeck, 2004), and optimize the interactions between the donor and acceptor, as well as between calmodulin and its target binding peptide (Truong et al, 2001; Nagai et al, 2004; Palmer et al, 2006). Although not as bright as synthetic dyes, current derivatives of the original cameleons are able to detect calcium transients in response to spike bursts or even single action potentials in hippocampal slices (Wallace et al, 2008) as well as in vivo in vertebrate and invertebrate preparations (Mank et al, 2008, Wallace et al, 2008).

1.3 GCaMP-Based Calcium Sensors

1.3.1 Development of GECIs Based on Circular Permuted GFP

In contrast to FRET-based sensors, which require continuous monitoring of fluorescence at two different wavelengths, GECIs with a single optical element require fluorescence measurements at only a single wavelength and are thus much easier to employ (Figure 2C). Therefore, single fluorophore GECIs are more frequently used. In particular, GECIs of the GCaMP family are increasingly popular (Chalasani et al, 2007; Dreosti et al, 2009; Dombeck et al, 2010; Mao et al, 2008) as they are currently the most sensitive GECIs (Tian et al, 2009; Muto et al, 2011, Zhao et al, 2011a), Unlike FRET-based calcium indicators, the most current generation of these sensors approach signal-to-noise characteristics of small molecule indicator dyes. Since GCaMP-based GECIs have been extensively utilized in this Masters project, their development and continuing evolution will be summarized below.

The generation the GCaMP family of GECIs is based on the concept of circular permutations to the GFP fluorophore, initially developed by Baird and Tsien (1999). This permutation interchanges the amino and carboxyl regions of the enhanced GFP moiety and reconnects the original termini with a short peptide spacer sequence, thus generating new N and C termini (Figure 2B). The exchange still allows the GFP to fold correctly, generate internal chromophores, and maintain the stability of their excited states (Baird et al, 1999). Furthermore, the circular permuted GFP can tolerate the insertion of proteins that profoundly affect the indicator's fluorescence.

Two research groups independently utilized the circular permutation approach to generate the first generation of single wavelength fluorescent calcium indicators (Nagai et al, 2001; Nakai et al, 2001). Their approaches were similar as each group incorporated either a circularly permutated yellow fluorescent protein (termed pericams; Nagai et al, 2001) or a circularly permuted enhanced GFP (cpEGFP) (named GCaMP1; Nakai et al, 2001) with the new C terminus fused to CaM (of *Homo sapiens*) and N terminus with CaM-binding M13 peptide, which was derived from chicken skeletal myosin light chain kinase. The binding of free Ca^{2+} to CaM causes a conformational change magnified by the M13 peptide, which performs as an actuator due to its preferential binding to the calcium-bound form of CaM (Rhoads and Friedberg, 1997). In turn, this change reorganizes the environment of the fluorophore resulting in a fluorescence intensity increase that is a function of Ca^{2+} concentration with reversible spectral properties (Nagai et al, 2001). Although both sensors exploited the 144-145 fluorophore break identified in the initial circular permutation studies, amino acids 145-148 are removed in GCaMP1 (Nakai et al, 2001). Moreover, GCaMP1 exhibited a higher K_d when used in cells, resulting in an improved signal over background ratio (Nakai et al, 2001; Pologruto et al, 2004). However, limitations of the first generation of GCaMP1 included pH sensitivity and required folding temperatures below 37°C (Nakai et al, 2001). Nonetheless, these sensors exemplified the ability of single fluorophore indicators to measure cytosolic Ca^{2+} with relatively high signal strength characteristics at the time of their inception.

1.3.2 Optimization of GCaMP Sensors

Since their advent, engineering an improved GCaMP indicator has been a priority, as their initial properties, such as signal-to-noise ratio (SNR), transition kinetics, fluorescent intensity, and photostability have lagged behind that of synthetic indicators. As a result of dedicated efforts from multiple research groups, the initial GCaMP scaffold introduced by Nakai et al (2001) has since been optimized to produce a sensor closer in performance to that of dyes.

The first efforts to improve GCaMP1 were performed by Ohkura et al, (2005). They utilized a site-directed mutagenesis approach to replace the amino acids Valine and Serine with Alanine and Glycine at positions 163 and 175 within the cpEGFP, respectively. The substitutions in the resulting variant, named GCaMP1.6, reduce steric hindrance and provide more efficient chromophore formation of the GFP. Compared with the original GCaMP, GCaMP1.6 exhibited a 40-fold increase in fluorescence, lower pH sensitivity, slightly higher affinity, and higher selectivity for divalent cations similar in radius to Ca^{2+} (Ohkura et al, 2005). Furthermore, the alanine at position 206 was replaced with Lysine (A206K) (Tallini et al, 2006) to prevent GFP dimerization (Zacharias et al, 2002). Following a PCR-based random substitution protocol performed on GCaMP1.6, two more amino acid substitutions were identified to further increase brightness 6-fold (Aspartic acid-180-Tyrosine and Valine-93-Isoleucine) (Tallini et al, 2006). However, of more importance was the addition of an N-terminal 35-residue polyHis RSET linked to the MLCK leader sequence (Methionine-Leucine-Cysteine-Lysine) to provide environmental stability above 30°C. The resulting sensor was termed GCaMP2.

Although much improved compared to the original GCaMP1, GCaMP2 still produced inferior signals to that of synthetic indicator dyes, not enabling their detection of Ca^{2+} transients during low firing rates within neurons. The X-ray determination of the Ca^{2+}-bound and Ca^{2+}-free states of GCaMP2's crystal structure (Wang et al, 2008; Akerboom et al, 2009) significantly facilitated strategies for researchers striving to modify GCaMPs signals to approach those produced by indicator dyes. Continuing with the site directed mutagenesis approach, Akerboom and colleagues (2009) attempted to further increase the brightness of the sensor, in addition to reducing the dimerization observed in GCaMP2, utilizing these crystal structures. The M13 peptides of GCaMP2 were found dimerize to the CaM domain of another GCaMP leading to a possible decrease in signal. The replacement of Aspartic Acid with the bulkier Tyrosine at position 381 (D381Y), located on the flexible linker region of CaM which packs against the cpEGFP opening, addressed this issue. However, of more importance, all mutations investigated were performed on the GCaMP2-T116V (Threonine-116-Valine) template due to this mutation's noted ability to increase the wild type EGFP excited-state proton transfer. This mutation resulted in a dynamic range increase ($\Delta F/F_0 = 8.4$), and in turn, successfully improved the SNR of the sensor (Akerboom et al, 2009). Although not all pertinent mutations were kept in subsequent versions of GCaMP (i.e. D381Y), the mutation sites identified in this study could not have been predicted without GCaMPs structural data.

Tian et al, (2009) also utilized the data obtained by Akerboom et al, (2009) as well as the previously discussed optimization studies to implement a protein structure-guided mutagenesis combined with a rationalized library screening protocol. The result

was the generation of GCaMP3. In addition to retaining the important T116V point mutant, the generation of GCaMP3 contained amino acid substitutions of Asparagine-363-Aspartic Acid (N363D or CaM N60D), which increased the fluorescence change for small transients without affecting basal fluorescence, and Methionine-153-Lysine (M153K) within the EGFP component of the sensor. Although the sensors kinetics were similar to that of GCaMP2, the implementation of GCaMP3 resulted in a brighter GECI for AP triggered responses within pyramidal neurons in cultured brain slices, exhibited greater protein stability, SNR, and dynamic range properties than its predecessor. Moreover, GCaMP3 had an increased affinity for calcium compared to GCaMP2 (Tian et al, 2009). Upon testing GCaMP3s abilities by imaging neural activity across various *in vivo* preparations such as worms, flies, and mice, the indicator exhibited the ability to detect calcium transients triggered by single APs in the soma and proximal dendrites, with faster kinetics, better SNR and photostability than previously reported FRET based indicators D3cpV and TN-XXL (Tian et al, 2009; Wallace et al, 2008; Mank et al, 2008). Furthermore, its use has reduced physiological defects during long-term overexpression experiments previously experienced with previous generations of GECIs (Garaschuk et al, 2007) (see Figure 3 for overview of GCaMP optimization).

Many other research groups have produced significant data with the use of GCaMP3. For example, specific applications of the sensor allowed calcium dynamics to be observed in the optic lobe of walking Drosophila (Seelig et al, 2010), and in mouse hippocampal neurons during virtual navigation (Dombeck et al, 2010). Thus, the widespread application of GCaMP3 across many experimental paradigms illustrates the importance of its generation for those interested in monitoring calcium dynamics.

While previous studies devoted to improving the sensitivity of GCaMP have mainly focused on the cpEGFP domain of the protein, relatively little work has addressed how mutations in the calcium-binding calmodulin component change the properties of GCaMPs (with the exception of Tian et al's (2009) CaM N60D, and Akerboom et al's (2009) mutation in the linker region, which did not show a significant effect on their own). However, structure-function relationships of calmodulin itself have been extensively studied.

1.3.3 The Structure and Functional Properties of Calmodulin

Calmodulin belongs to the 'EF hand' family of calcium binding proteins that is highly conserved across species. This small acidic protein, which is of 148 amino acid length, consists of two somewhat homologous (46%) globular domains that do not form direct contacts between one another, separated by a flexible linker region (Starovasnik et al, 1992; Sorensen et al, 2002; Kuboniwa et al, 1995; Faga et al, 2003). Each domain contains two Ca^{2+} binding sites called EF hand motifs (labelled numerically I through IV from the N terminus) of α-helix-loop-α-helix conformation that sequester Ca^{2+} in a cooperative fashion amongst site pairs within their respective domains (Tsalkova and Privalov, 1985) (Figure 4). The 12 residue loop region of each EF hand motif is composed of six chelating residues arranged in a multidentate coordination shell that either directly or indirectly bind calcium through glutamate, aspartate, or asparagine side chains at positions 1, 3, 5, and 12, the mainchain carbonyl at position 7, and a bridging water molecule that interacts with the amino acid at position 9 (Ye et al, 2005). These six

residues are denoted as the +X, +Y, +Z, -Y, -X, and -Z (1, 3, 5, 7, 9, and 12) positions on the axes of the near-octahedral shell (Figure 5).

Upon motif comparison, a high conservation of residues is observed across the four binding sites of GCaMP3s CaM, especially in regards to aspartic acid at chelating positions 1, 3, and 5 (with the exception of asparagine in motif III), glycine at position 6, and glutamic acid at chelating position 12 (Wu and Reid, 1997) (see Figure 6 for EF motif overlay).

The extensive investigation of CaM has been facilitated in large part by studies utilizing directed mutagenesis techniques performed primarily on the EF hand residues to further understand their Ca^{2+} affinity properties. For example, protein studies of *Drosophila melanogaster* CaM have revealed that the independent replacement of glutamic acid with glutamine at chelating position 12 (-Z) in each of the four motifs eliminates Ca^{2+} binding affinity at that site (Maune et al, 1992). Moreover, a reduction of calcium affinity was also observed within the EF motif of the same domain to significantly reduce the calcium binding of the mutant protein compared to that of the wild type protein (Maune et al, 1992). Synthetic peptide studies have also investigated the effects of substituting amino acid residues at positions 3 (+Y), 5 (+Z) and 9 (-X) of the EF motifs (Procyshyn and Reid, 1994a; Procyshyn and Reid, 1994b; Reid and Procyshyn, 1995). Their results indicated that the replacement of aspartic acid at positions 3 and 5 with asparagine reduces the calcium affinity of the EF motif containing the point mutation. Furthermore, a separate protein study reported that even a very conservative mutation (aspartic acid to glutamic acid) at conserved position 5 (+Z) of site IV was also able to produce a drastic reduction in site affinity for calcium in addition to

significantly reducing the calcium affinity of site III within the same domain (Wu and Reid. 1997). Similar calcium affinity reductions were observed upon the independent insertion of asparagine at position 9 of EF motifs III and IV for peptides performed by the same research group as well (Procyshyn and Reid, 1994a). Thus, positions 3, 5, and 9 serve a major role in shaping CaMs calcium binding properties. However, position 12 of each EF motif is elementary in maintaining not only each EF motifs calcium binding capabilities, but also of the neighboring sites within the same domain. This last point illustrates that coordination or cooperativity exists between EF motifs of the same domain to affect the overall calcium affinity of CaM.

More recently, residues outside of the four EF hand motifs have been more thoroughly explored. According to studies investigating the flexible interdomain linker region, basic residues of arginine (CaM position 74), and lysine (CaM positions 75 and 77) were deemed critical for both stabilizing the apo-conformation of the N-terminal domain and lowering its affinity for calcium (Faga et al, 2003; VanScyoc et al, 2002; Sorensen et al, 2002) Furthermore, a mild increase in affinity of sites I and II was observed when the position 74 arginine was replaced with the nonpolar alanine (VanScyoc et al, 2002). This study conducted a second similar mutation on the linker region closer to C-terminal EF motifs (CaM position 90) that resulted in a mild increase in calcium affinity for sites III and IV, in addition to sites I and II. These results indicate that not only can the overall affinity of CaM be tuned by targeting residues that are distant to the binding loops, but the alteration of these residues can also affect the binding capabilities of both domains concomitantly. Collectively, these studies show that calmodulin cooperatively binds calcium with its four EF hand motifs and that its K_d is

exquisitely sensitive to mutations in these motifs, as well as to amino acid residue exchanges in the linker between N- and C-terminal lobes of the protein.

1.4 OBJECTIVES OF THIS STUDY

GCaMP3 has been shown to be sensitive enough to detect calcium transients in response to isolated APs in the somata and proximal dendrites of neurons (Tian et al, 2009). However, we have found that they are insufficient for the detection of action potential-induced transients in smaller compartments, such as in axons, and presynaptic varicosities. The inability to measure transients in these compartments of relatively smaller volume arises because the number of GECI molecules per imaged area is much lower than when somata or thick proximal dendrites are imaged. Therefore, the overall signal and SNR are very much reduced. Moreover, the SNR of current GCaMP sensors may also be insufficient to detect postsynaptic calcium transients in response to NMDA receptor activation, which may also be smaller in amplitude than transients elicited by somatic VGCC opening induced by action potentials. Therefore, the first objective of this study is to **increase the sensitivity of current GCaMP sensors to enable the quantifiable detection of calcium transients that occur in smaller neuronal compartments.**

A number of strategies increase the sensitivity or SNR of a GECI such as GCaMP3 for small calcium transients, some of which of have been utilized by previous GECI optimization studies discussed above. The approach of increasing the dynamic range $[(F_{max}-F_{min})/F_{min}]$ of a sensor has already proven to be successful towards

improving SNR (Akerboom et al, 2009; Tian et al, 2009). Also, an increase of the basal fluorescence (F_{min}) of the sensor while keeping the dynamic range constant has led to increases in the sensitivity of the sensor (Ohkura et al, 2005; Tallini et al, 2006; Tian et al, 2009). Finally, for the sensitive detection of small transients, the calcium affinity, i.e. dissociation constant (K_d) for calcium and the Hill coefficient, likely has large effects on the sensitivity of the sensor. Previous mutations in the cpGFP, and to a small part in the CaM regions, have led to small changes in the apparent K_d of the sensor (Ohkura et al, 2005; Tallini et al, 2006; Tian et al, 2009, Muto et al, 2011, Zhao et al, 2011b). However, it has not been systematically explored whether K_d and Hill coefficient of the currently used sensor mutants are optimal for the detection of small calcium transients. This affinity issue will be addressed by performing a mutagenesis screen of the CaM domain, as outlined below.

Calcium concentrations are known to vary by more than 2 orders of magnitude in many cells, including neurons (Clapham, 1995; Berridge, 1998). In comparison, current GCaMP-based calcium sensors have a much narrower effective measurement range, encompassing approximately one order of magnitude around their K_d for the ion. It is for this reason that vast assortments of small-molecule indicator dyes exhibiting different K_d values, ranging from tens of nM (Quin2, Fura-2) to hundreds of μM (X-rhod 5N), have been developed. Similarly, FRET-based GECIs with a variety of K_d values have also been generated (Miyawaki et al, 1997; Palmer et al, 2006, Mank et al, 2008). In contrast, current GCaMPs have fairly high calcium affinities and easily saturate with large calcium transients (Tian et al, 2009; Zhao et al, 2011b). Therefore, the second objective of this study was to **create GCaMP variants with lower calcium affinities, between 2 – 20**

μM, to complement the existing GCaMPs and allow their use in applications where high calcium transients are expected, such as in calcium nanodomains.

Similar to present GCaMPs, these lower affinity sensors to be generated should have a larger dynamic range and therefore higher sensitivity than current FRET-based sensors. Unlike some of the developed low-affinity FRET-based sensors (Miyawaki et al, 1997; Palmer et al, 2006), they should also have a high Hill coefficient that is similar to that of high affinity GECIs to allow for the sensitive detection of calcium concentrations in the micromolar range. In addition to optimized K_d values and Hill coefficient, the lower susceptibility of GCaMPs to photobleaching and increased ease of use (single wavelength imaging) should make them more desirable than FRET-based sensors.

To accomplish the two objectives outlined in this study, the calcium affinity of GCaMP3 will be either increased or lowered by enhancing or interfering with calcium binding of the four EF hand motifs of CaM through a series of site directed mutations. These guided mutations will be chosen based on the previously mentioned structure-function studies of calmodulin (Wu and Reid, 1997; Ye et al, 2005; Starovasnik et al, 1992; Maune et al, 1992; Gao et al, 1993) at calcium chelating positions 3, 5, 9, and 12 as well as on select other residues in the EF motifs and the linker region connecting the N- and C-terminal CaM lobe (Procyshyn and Reid, 1994; Sorensen et al, 2002; VanScyoc et al, 2002; Faga et al, 2003). Mutant GCaMP3s will be expressed and purified from bacteria to assess changes in their K_d, Hill coefficient, and dynamic range. Finally, all mutants with desirable changes will be expressed in neurons to assess their value as calcium sensors in excitable cells.

CHAPTER 2 MATERIALS AND METHODS

2.1 GENERATION OF GCAMP3 MUTANT CONSTRUCTS

A site directed mutagenesis approach was utilized to generate GECIs with altered calcium affinities. Amino acid residues that are highly conserved at positions 2, 3, 5, 9, 11, and 12 within the four calcium binding EF Motifs of CaM and the interdomain linker region of CaM were targeted for amino acid substitution in attempts to alter GC3s calcium affinity.

2.1.1 Primer Phosphorylation and Site Directed Mutagenesis PCR

Primer pairs were selected for the Site Directed Mutagenesis Polymerase Chain Reaction (SDM PCR) protocol to exchange nucleotide base pairs that result in the substitution of amino acid residues at desired locations within the calmodulin component of GC3. Primers pairs to perform the mutagenesis were obtained from Integrated DNA Technologies, Coralville, IA, USA. Primers were selected as follows (see Appendix A for primer sequences). Either, primers that were largely complementary and contained the desired mutation roughly in the middle of each primer were designed with the aid of an online SDM PCR Primer selection tool (www.bioinformatics.org/primerx). Alternatively, a primer pair was chosen in which one of the primers, either forward or reverse, had the intended mutation located at the 5' end and the other primer annealed to the GCaMP cDNA region immediately abutting the site of the mutation. We encountered a higher success rate with the second type of primer pair that includes the mutation at the 5' end of one of the primers. Moreover, this type of primer pair providing more flexibility upon designing additional mutations at the same site as only one extra primer was needed

containing the desired mutation, whereas primer pairs containing the mutation roughly in the middle required the design of an entirely new pair of primers to perform a different mutation at the same site. Abutting primers with the mutation at the 5' end of one primer had to be phosphorylated for subsequent ligation of the blunt-ended PCR product into a circular plasmid for successful transformation. For this purpose, an Eppendorf Mastercycler personal PCR machine was utilized to phosphorylate each primer pair. Oligonucleotides were phosphorylated with T4 Polynucleotide Kinase (PNK) (New England Biolabs, Pickering, ON, CA) at 37°C for 1 h according to the manufacturer's instructions. Following primer phosphorylation, SDM PCR reactions were performed to produce amplified plasmid DNA products containing the desired nucleotide substitutions located within the CaM component of GCaMP3. The original template DNA used for initial rounds of SDM PCR was pRSET(GCaMP3), courtesy of Loren Looger (Howard Hughes Medical Institute, Ashburn, VA, USA). The PCR reactions were performed with Phusion Hot Start High-Fidelity DNA Polymerase (New England Biolabs) according to the manufacturer's instructions with final primer, dNTPs, and Phusion DNA Polymerase concentrations of 0.5 μM, 0.2 mM and 0.02 U/μl, respectively. Annealing temperatures for the primers were determined depending on their sequence length and cytosine-guanine composition. Following PCR, each sample was treated with 1 μl of the restriction enzyme DpnI (New England Biolabs) for 3h at 37°C as DpnI digests methylated DNA (the template plasmid DNA) to ensure the PCR product contains only mutated plasmids.

Samples of nucleic acids (PCR products or DNA fragments during subcloning procedures described below for the generation of GC3 constructs containing multiple

mutations) were routinely separated according to their migration behaviour due to their molecular size (kb) by agarose gel electrophoresis. Each sample was mixed with Orange G loading dye (5:1 ratio) and loaded on a 1.5% preparative agarose gel made with 0.5% TBE buffer (22.4 mM Tris Base, 22.4 mM Boric Acid, 0.5 mM EDTA pH 8.0). Electrophoresis was performed using 0.5% TBE as the running buffer in an electrophoresis cell connected to a PowerPac Basic Power Supply (Bio-Rad, Hercules, CA, USA) for 30 min at 100V. Gels were then exposed to ultraviolet light and the desired linearized DNA bands were excised and extracted using a QIAEX II Gel Extraction Kit (Qiagen, Toronto, ON, CA) in accordance to the manufacturer's instructions. Ligations were performed for either 1 h at 24°C or overnight at 16°C with T4 DNA Ligase and 1X DNA Ligation Buffer (New England Biolabs).

2.1.2 Generating GCaMP3 Constructs with Multiple Mutations

Several of the GC3 constructs generated contained more than one amino acid substitution to achieve larger shifts in the calcium affinity than observed for the individual mutations. To obtain constructs with multiple mutations, two different approaches were implemented. The first approach involved performing additional rounds of SDM using DNA templates of GC3 variants that contained amino acid substitutions introduced by previous rounds of SDM PCR. The second approach involved subcloning mutation containing inserts of GC3 into a different GC3 construct having different mutations (outside of the insert region). This approach utilized unique target sites for the restriction enzymes PstI located between EF motifs I and II of CaM (CaM Q49), ClaI at the Isoleucine located in position 2 of EF motif IV (CaM I130), and XhoI located 5' of the cpEGFP component of GC3. Therefore, separate digestions were designed for

mutation combination by selecting two of the three restriction enzymes for each digestion depending on the location of the mutations. Inserts containing mutations were excised with the respective restriction enzymes (New England Biolabs) that encompass the desired mutations of separate GC3 DNA templates. For example, to generate a GC3 construct that contains both the D24N and E104Q CaM mutations, PstI and ClaI restriction enzymes would be selected as D24N is located 5' of PstI and 3' of ClaI while E104Q is located 5' of ClaI and 3' of PstI, resulting in two separate inserts from their respective GC3 templates that each contain a mutation. After digestion, the inserts were combined by ligating the excised fragments together with T4 DNA Ligase (New England Biolabs).

2.1.3 Transformation of Plasmid DNA Obtained from SDM PCR and Subcloning

To verify the success of SDM PCR and subcloning protocols used to obtain mutated GC3 constructs, we first transformed each ligation into electrocompetent bacteria with the use of a Micropulser Electroporator (Bio-Rad). Electrocompetent *E. coli* (Top Ten - Invitrogen, Burlington, CA, USA) were prepared using a high efficiency competence protocol according to Bio-Rad's instructions. Aliquots (100 µl) of the bacteria were inoculated with 1 µl of plasmid DNA solution (0.2 µg/µl), pipetted into an electroporation cuvette (Scientific USA, Ocala, FL, USA) and placed within the capacitor of the electroporator. The bacterial solutions with plasmids were electrically stimulated to transfer the DNA into the bacteria. Following electroporation, the bacteria were incubated in LB (Luria-Bertani) medium (Becton, Dickinson and Company, Sparks, MD, USA) for 30 min at 37°C and gentle agitation. The plasmid containing bacteria were then plated onto antibiotic selective LB agar for overnight incubation at 37°C. The GC3

construct used during SDM and subcloning protocols was propagated in a pRSET vector containing a gene for carbenicillin/ampicillin antibiotic resistance.

2.1.4 Isolation of Small Amounts of Plasmid DNA from *E. coli* for Sequence Verification

Individual colonies from antibiotic selective LB agar plates were used to create starter cultures for the purpose of isolating small amounts of DNA (10-25 µg) employing an alkaline lysis protocol modified from Birnboim and Doly (1979). Briefly, bacterial pellets from small (2 ml) overnight cultures in antibiotic selective LB media were resuspended in 250 µl of P1 buffer (50 mM Tris-HCl, pH 8.5, 10 mM EDTA, 100 µg/ml RNase A) and transferred to a microcentrifuge tube. To lyse the bacteria, 250 µl of P2 buffer (200 mM NaOH, 1% SDS w/v) was added to the tubes, gently mixed and left to stand for 5 min before 350 µl of the neutralization P3 buffer (3.0 M potassium acetate, pH 5.5) was added, mixed, and placed on ice for 10 min to precipitate the genomic DNA and cellular debris. After centrifugation for 15 min at 14 000 rpm (24104 x g) and 4°C in a tabletop centrifuge, the supernatant was transferred to a clean microcentrifuge tube and 0.7 volumes of isopropanol was added to precipitate the plasmid DNA. Another high speed centrifugation was then performed for 30 min and the supernatant decanted. The DNA pellet was then washed with cold 70% ethanol and centrifuged a final time at high speed for 5 min. The resulted pellet was air dried and resuspended in 50 µl of 10 mM Tris-HCl pH 8.

2.2 GCaMP3 Variant Construct Verification

To verify ligations performed in subcloning protocols, diagnostic digests were performed using two unique sites located in the GC3 mutant variants. The restriction digest was subjected to gel electrophoresis and the ligation was deemed successful if the linearized bands resembled that of an original template GCaMP3 construct digested concomitantly. In order to verify the presence and identity of mutations, the reading frame, and nucleotide sequence of altered GCaMP3 constructs from subcloning and SDM PCR procedures, 100 ng of each sample was sent to Macrogen (Seoul National University College of Medicine, Seoul, Korea) for nucleotide sequencing. The reverse complement primer pET-24a (5'- GGGTTATGCTAGTTATTGCTCAG-3') was used to sequence pRSET(GC3) constructs by initiating sequence reading 3' of the calmodulin component of GC3.

2.3 *In vitro* Assessment of GCaMP3 Variants

2.3.1 Protein expression

To examine the altered calcium affinities of our GC3 constructs, we prepared them for protein expression by first transforming each plasmid DNA into electrocompetent BL21 *E. coli* bacteria that contain a T7 RNA polymerase gene under control of the IPTG- (Isopropyl-beta-D-thiogalactopyranoside) inducible *lac* promoter. Starter cultures were created by selecting single bacterial colonies from LB agar plates for the inoculation of 2 ml of LB media containing a 0.1 μg/ml of Carbenicillin (Gold BioTechnology Inc., St. Louis, MO, USA). These starter cultures were incubated on a

shaker overnight at 37°C. The following morning, bacterial cultures were transferred to 200 ml of LB medium containing 0.1 μg/ml of Carbenicillin and incubated on a shaker at 37°C until the bacterial culture reached an OD_{600} of 0.5-0.8. The cultures were then induced for protein expression with 0.5 μM IPTG (Gold BioTechnology Inc.) and incubated on a shaker at 24-28°C for 14-18 h. Bacterial pellets (15 min centrifugation at 5000 rpm (3075 x g) at 4°C) were resuspended in 4 ml of nickel nitriloacetate (Ni-NTA) Binding Buffer (300 mM NaCl, 50 mM Na_2HP0_4, 10 mM imidazole, pH 8.0), and placed on ice for 1 h with 1 mg/ml of lysozyme (Worthington Biochemical Corporation, Lakewood, NJ, USA) for bacterial cell wall degradation. The remainder of the protocol was performed at 4°C. Bacteria then underwent high frequency sonication in four 30 sec bursts with a 30 sec cooling period between each burst to disrupt the cell membrane followed by centrifugation at 14000 rpm (24104 x g) for 30 min to pellet the cellular debris. The supernatant containing our proteins of interest was decanted to new Eppendorf tubes in which 200 μl of Ni-NTA His-Bind resin (Novagen, Madison, WI, USA) per 1 ml of lysate was added and placed on a shaker for 1 h to allow our for chelation of His-tagged proteins. The loaded Ni-NTA resin was then transferred to Poly-Prep Chromatography Columns (Bio-Rad, Hercules, CA, USA) and allowed to settle. Upon lysate flow through, 8 ml of Ni-NTA Wash Buffer (300 mM NaCl, 47.5 mM Na_2HP0_4, 2.5 mM $NaH_2P0_4 \cdot 2H_2O$, 20 mM imidazole, pH 8.0) was applied. To elute the His-Tagged GC3 proteins from the resin, 1 ml of Ni-NTA Elution Buffer (300 mM NaCl, 47.5 mM Na_2HP0_4, 2.5 mM $NaH_2P0_4 \cdot 2H_2O$, 250 mM imidazole, pH 8.0) was added to the columns. The purified proteins were then collected and concentrated with Amicon Ultra-0.5 ml Centrifugal Filter Units (10K MW cutoff) (Millipore, Billerica, MA, USA)

using the protocol provided. In brief, proteins were added to the centrifugal filter units and spun at 14000 rpm (24104 x g) for 3 min. They were then re-buffered by adding 500 ml of KME buffer (0.1 M KCl, 0.03 M MOPS Buffer, 0.005 M EGTA, pH 7.2) and subjected to ultrafiltration until the volume was reduced to 70 µl. This procedure was repeated five times, thus diluting any small-molecule contaminants approximately 10,000-fold. A final collection spin was performed at 1000 rpm (123 x g) for 2 min. Protein concentrations were quantified using the Pierce BCA Protein Assay Kit (Thermo Scientific, IL, USA) according to the manufacturer's instructions.

2.3.2 Calcium Titration Assay

An *in vitro* calcium titration assay was performed to determine calcium affinity, Hill coefficient, *in vitro* dynamic range and basal fluorescence of our mutated constructs. In all assays, we included GCaMP3 for comparison. Titration solutions used for this assay contained 0.01, 0.03, 0.05, 0.10, 0.20, 0.316, 0.50, 1.00, 2.00, 3.16, 5.62, 10.0, 20.0, 31.6, 56.2, 100, 316, and 5000 µM of free Ca^{2+} and were created by mixing the calcium-free and calcium containing buffers of the EGTA-Based Calcium Calibration Buffer Kits purchased from Biotium (Hayward, CA, USA) or Invitrogen. Since EGTA has a pK_a of 6.9 at a pH of 7.0, EGTA-based calcium buffers are ideally suited to maintain concentrations of free Ca^{2+} in the 10 nM – 10 µM range. Total calcium concentrations needed to achieve the desired free calcium concentrations were calculated according to Bers et al., 2010 using the MaxChelator calculation tool available online (http://maxchelator.stanford.edu). All titration solutions were utilized when measuring the low calcium affinity GC3 mutants while only solutions ranging between 0.01 and 10.0 µM of free calcium were utilized to assess the high calcium affinity GC3 mutants.

Purified proteins of each GCaMP3 mutant variant were added to the calcium titration solutions in a small volume (2.5 µl per 50 µl) to a final protein concentration of 25 µg/ml in triplicates on a black 96-well plate to minimize background fluorescence during readings. Fluorescence recordings for each assay were measured using excitation and emission wavelengths of 488 nm and 518 nm, respectively, on a Fluoroskan Ascent FL plate fluorescent plate reader (Thermo Electron Corporation, Gormley, ON, Canada) or a BMG LABTECH FLUOstar Omega fluorescent plate reader (Fisher Scientific, Ottawa, ON, CA) courtesy of Dr. Brent Johnston (Department of Microbiology and Immunology, Dalhousie University) and Dr. Chris Sinal (Department of Pharmacology, Dalhousie University), respectively.

2.3.3 Determination of K_d, Hill Coefficients, Dynamic Ranges, and Basal Fluorescence of GCaMP3 Variants

Data obtained from the *in vitro* calcium titration analysis were utilized to determine the average calcium dissociation constants (K_d), Hill coefficients, dynamic ranges, and basal fluorescence for GCaMP3 and GCaMP3 mutant variants. For each assay performed with a GCaMP variant, the normalized fluorescence was calculated as $(F - F_{min})/(F_{max} - F_{min})$, plotted against the calcium titration solutions ($pKCa^{2+}$) and fitted with a sigmoidal curve. The graphs depicted in Figures 7-12 and 14-16 represent averages of these curves for all assays performed on a certain GCaMP variant. For the determination of K_d the log $(F - F_{min})/(F_{max} - F)$ was plotted against the log $c(Ca^{2+})$. A linear regression analysis was then performed to calculate the x-axis intercept, corresponding to the K_d of the construct analysed (Tables 1-3), and the slope,

corresponding to the Hill coefficient. Averages and standard errors of affinity constants and Hill coefficients calculated for each assay are given in tables 1-3.

The dynamic range for each construct was individually calculated for each assay performed for the constructs as the maximum fluorescence observed divided by the minimum fluorescence observed [$(F_{max}-F_{min})/F_{min}$]. An average of the dynamic range value reported for each assay performed per construct indicated the average dynamic range observed for each construct (Tables 1-3). The basal fluorescence of each GC3 mutation variant was simply calculated as the minimum fluorescence of each mutant subtracted by the minimum fluorescence of the wild type GCaMP3 run concomitantly within the same assay. The average basal fluorescence was then calculated for each GC3 mutant construct and reported in tables 1-3.

2.3.4 Statistical Analysis of Calcium Titration Data

A statistical analysis was performed to determine if the K_d, Hill coefficient, dynamic range, and basal fluorescence significantly differed for each mutational construct from that of GCaMP3. The GC3 mutations that resided in the same EF motif position were included alongside the GCaMP3 control construct in separate ANOVA/Tukey HSD tests to determine significance (p-values) (Table 1). For mutations in the interdomain linker, we individually compared a set of mutations of basic residues at the N-terminus of the linker (R74A, K75G, K77G), acidic residues in the middle part of the linker (D80R, E84R) and a mutation at the C-terminus of the linker, close to EF motif III (R90G, Table 2). To determine the significance of reported values for the combination mutants, these constructs were again tested with three different

ANOVA/Tukey HSD tests that included the high calcium affinity GC3 variants, the low calcium affinity double mutation variants, and the low calcium affinity triple and quadruple variants, respectively. The GCaMP3 control constructed was included in each of these statistical tests for combination mutants for comparison (Table 3).

2.4 ASSESSMENT OF GCAMP3 VARIANTS IN NEURONS

2.4.1 Primary Cell Culture of Hippocampal Neurons

Dissociated hippocampal cell cultures were used for the neuronal assessment of the sensitivity of GCaMP3 variants. Hippocampi were dissected from E18 Sprague-Dawley rat embryos (Charles River, Wilmington, MA, USA) and incubated for 15 min with 0.03% trypsin (Sigma, St. Louis, MO, USA). Trypsinized hippocampi were then dissociated using a fire-polished pasteur pipette. Cells were diluted in Neurobasal medium (Invitrogen) supplemented with 1% (v/v) B-27 (Invitrogen) 0.5 mM glutamine, 25 μM glutamate, and 5% Fetal Calf Serum (Invitrogen). The harvested dissociated hippocampi were then plated on 12-mm glass coverslips coated with 0.1% (w/v) poly-L-lysine (Peptides International, Louisville, KY, USA) at a density of $3–6\times10^3/cm^2$ and incubated at 5% CO_2 and 37°C. Four hours after plating, the medium was replaced with serum-free Neurobasal media supplemented with 1% B27 and placed back into the incubation chamber until transfection.

2.4.2 Subcloning GCaMP3 Calcium Affinity Variants into a Vector for Neuronal Protein Expression

GCaMP3 mutant constructs of interest from the *in vitro* portion of this project were prepared to determine if alterations in the affinity of calcium binding of GCaMP3 leads to changes in the sensitivity and saturation of the sensor in neurons. The mutation containing inserts of the GC3 variants to be tested were subcloned from the pRSET vector (used for the *in vitro* analysis) and inserted into pE vectors containing a cytomegalovirus (CMV) promoter to enable protein expression in neurons. Mutation containing inserts from the GCaMP3 variant constructs were excised and the vector construct pE(GC3) digested with the restriction enzyme BsrGI, which has two sites enclosing the CaM component of GCaMP3 (one site residing within the cpEGFP and the second site located 3' of CaM EF motif IV). After 1 h digestion times at 37°C, the pE(GCaMP3) was dephosphorylated with 2 µl Calf Intestinal Phosphatase (CIP, New England Biolabs) for 30 min to suppress re-ligation of vector not containing inserts. The digestion products were separated by agarose gel electrophoresis and the DNA fragments of interest were purified with the QIAEX II Gel Extraction Kit as described above. The insert and vector fragments were ligated with T4 DNA Ligase for either 1 h at 24°C or overnight at 16°C as described above. To verify the ligations, diagnostic digests similar to those described above were performed. The constructs that ligated successfully were further verified with nucleotide sequencing performed by Macrogen utilizing the reverse complement primer pE1600 (5'-TACATTGATGAGTTTGGACAAACCAC-3').

GCaMP3 variant constructs in the pE vector were verified by nucleotide sequencing and amplified for transfection of dissociated hippocampal cell cultures.

Briefly, 100 ng of each construct was transformed into electrocompetent *E. coli* bacteria and plated on antibiotic selective agar plates. Single colonies were selected for inoculation of 2 ml of LB media containing 0.1 µg/ml of Kanamycin (Gold BioTechnology Inc.) (the pE vector encodes a gene rendering bacteria Kanamycin resistant) and grown for 8 h at 37°C before being transferred to 500 ml of LB media also containing 0.1 µg/ml of Kanamycin for overnight incubation at 37°C. The bacterial pellets obtained from overnight cultures were subjected to a Plasmid Maxi Prep (Invitrogen) protocol, which includes the alkaline lysis of bacteria and subsequent purification of the plasmid DNA using anion exchange chromatography and precipitation with isopropanol.

2.4.3 Transfection of pE(GCaMP3) Constructs

Dissociated hippocampal cell cultures were transfected with the plasmid DNA of GCaMP3 mutation variants 10-17 days after plating utilizing a calcium phosphate precipitation transfection protocol as the neurons form synapses approximately two weeks after plating. For each culture dish (60 mm diameter), which contained five coverslips, separate precipitation mixes were prepared with 80 µg of a plasmid containing the cDNA of one of each GCaMP3 mutant variant per transfection and 0.25 M $CaCl_2$. In a subset of experiments, 80 µg of a plasmid encoding tdTomato-Bassoon was included in this mix to allow for the identification of presynaptic active zones, The precipitation mixes were slowly added to a second solution containing (in mM) 274 NaCl, 10 KCl, 1.4 Na_2HPO_4, 15 D-glucose, 42 -(2-hydroxyethyl)-1-piperazineethanesulfonic acid (Hepes), pH 7.10, vortexed and kept at room temperature for 20 min to allow for precipitate formation. The mix was then applied to culture dishes in which the conditioned medium

had been replaced by Minimal Essential Medium (MEM) (Invitrogen) containing 1% (v/v) B27 (Invitrogen). The cell cultures were incubated at 5% CO_2 and 37°C with the precipitate mix for 3–4 h and then washed three times with a buffer containing (in mM) 144 NaCl, 3 KCl, 2 $MgCl_2$, 10 Hepes, pH 6.70. The last wash was replaced with original conditioning medium in which the cultures were maintained (Neurobasal with 1% B27) and incubated at 5% CO_2 and 37°C until used for fluorescence imaging 2–3 days after transfection.

2.4.4 Stimulation and Cellular Imaging

Coverslips with transfected dissociated hippocampal cell cultures were mounted in a stimulation chamber with platinum electrodes placed 0.5 cm apart from one another. The coverslips were bathed in an Hepes buffered saline (HBS) solution containing (in mM) 124 NaCl, 3 KCl, 2 $CaCl_2$, 1 $MgCl_2$, 10 Hepes, and 5 D-glucose adjusted to pH 7.30, and supplemented with 10 μM 6,7-dinitroquinoxaline-2,3-dione (DNQX) and 50 μM 2-amino-5-phosphonovaleric acid (APV) to block NMDA-type and AMPA-type glutamate receptors for current elimination. The stimulation chamber was then mounted on a heated microscope stage platform (Warner Instruments, Hamden, CT, USA) of an Nikon TE2000 inverted epifluorescence microscope equipped with a 60X oil immersion objective (1.4 numerical aperture), a Smart shutter controlled by a Lambda 10-2 control unit (Sutter Instruments, Novato, CA, USA), and fluorescence filter sets (Semrock, Rochester, NY, USA). For imaging of GCaMP3 variants, we used a 470/22 nm excitation filter, a dichroic with 500-800 nm transmission band, and a 525/50 nm emission filter. For the visualization of tdTomato-Bassoon, a 556/20 nm excitation filter, a dichroic with 584-679 nm transmission band and a 590/20 nm barrier filter were employed. Images

were acquired with a Hamamatsu ORCA CCD camera. 2X2 binning was used to allow full-frame imaging at an acquisition rate of 10 Hz. The acquisition was controlled by IPlab software (Scanalytics, Fairfax, VA, USA). Experiments were performed at 35 ± 2°C. At the onset of an experiment, we searched for a field in which axons exhibited GCaMP fluorescence. We then used a Stimulus Isolation Unit (Warner Instruments) to apply 1 ms squared bipolar current pulses yielding fields of approximately 10 V/cm between the electrodes of the stimulation chamber. Image acquisition and stimulation was synchronized using a Master-8 stimulator (A.M.P.I., Jerusalem, Israel). In each experiment, we delivered, in that order, 4 stimuli and 2 at 40 Hz, repeated 5 and 10 times, respectively, 20 stimuli at 0.5 Hz, as well as stimulus trains of 2 s at 2.5, 5, 10, 20, 40, and 80 Hz and acquired 12 (isolated stimuli), 15 (stimulus bursts with 2 or 4 action potentials) or 60 frames starting 300 ms (3 frames) before stimulus onset. After each stimulus train, we waited 1 min before beginning the next stimulation episode. After the experiment, we verified that GCaMP baseline fluorescence remained stable for the entire duration of the experiments

2.4.5 Image Analysis

Acquired images were analyzed using IPLab and IgorPro programs. Image stacks were aligned to correct for small field shifts during acquisition and background-subtracted. For each field, maps of stimulus induced changes in fluorescence intensity were generated by subtracting an average of three frames taken before the stimulation from an average of three frames following stimulation. Regions of interest were selected for analysis that displayed ‘hotspots’ of calcium influx along axons, which were presumably presynaptic specializations. In a subset of experiments, tdTomato-Bassoon

was also expressed to detect active zone cytomatrices, which allowed us to confirm the location of presynaptic specializations. To quantify GCaMP3 fluorescence intensity, 36-pixel segments were placed over the 6 'hotspots' of calcium influx deemed the strongest responses.

The maximum change in fluorescence, ΔF, for isolated stimuli and stimulus bursts of 2 and 4 action potentials was calculated by subtracting the average baseline fluorescence F_0 (the average of first three frames) from the fluorescence obtained 200 ms following stimulus onset. These values were divided by the baseline fluorescence and the resulting relative change in fluorescence $\Delta F/F_0$, expressed as percentage in tables 4 - 6. Graphs of the change in fluorescence (calculated as $[(F - F_{min})/F_{min}]$) vs time were plotted for single experiments (Figures 18A-B and 24A-C) and experiment averages (Figures 18E-F, 21A-E, and 25A-C). Error bars for average experiments represent the standard error calculated for the change in fluorescence at each time point. The fluorescence change in response to the 2 second stimulus trains at varying frequencies was calculated in two ways. For an average of experiments, fluorescence changes were normalized to 1 to indicate sensor saturation and calculated as $[(F - F_{min})/(F_{max} - F_{min})]$. The maximum fluorescence increase reported for each experiment for each 2 sec train stimuli frequency is depicted in Tables 4 and 6. Graphs indicating the average degree of sensor saturation in response to 2 second stimulus trains at varying frequencies were plotted as $[(F - F_{min})/(F_{max} - F_{min})]$ vs time (Figures 19A-B and 23A-C). To depict single experiments, fluorescence changes were calculated slightly different. For single experiments, the change in fluorescence per time point was calculated as $[(F - F_{min})/F_{min})]$ and graphed (Figures 18C-D and 24D-F).

The basal fluorescence, dynamic range, and SNR were also calculated for each GCaMP variant assessed in neurons. The basal fluorescence was determined by averaging the pre-stimulus fluorescence in the six regions of interest selected in each experiment for all stimulus paradigms involving isolated stimuli as well as stimulus bursts of two and four APs. This minimum fluorescence per pixel, indicated in tables 4 – 6, was calculated by dividing the average with the total area of the ROIs selected (216 pixels). The dynamic range was calculated by subtracting the basal fluorescence measured from the largest response obtained to a stimulus train at 40 or 80 Hz, and dividing this value by the basal fluorescence. The average dynamic range found across all experiments of the same construct is indicated in Tables 4 – 6. The SNR was calculated by dividing the fluorescence increase obtained 100-200 ms following the stimulation by the standard deviation of the fluorescence signal before stimulation (the first three images acquired for each stimulus paradigm) $[(F_{max} - F_{min})/SD_{pre\text{-}stim}]$. Signal-to-noise ratios, averaged across experiments for each stimulus paradigm, are indicated in Figures 20, 22, and 26. The decay rate (tau) was also calculated to provide an indication as to how fast the sensor unbinds calcium. For the calculation of the decay time constant, we fitted the fluorescence decay of transients elicited by bursts of 4 stimuli at 40 Hz with an exponential starting with the frame obtained 200 ms after stimulus onset and ending with the last frame recorded. The resulting tau values of each experiment within the same construct were averaged and indicated in Tables 4 and 5.

2.4.6 Statistical Analysis of Neuronal Data

Statistical analysis was performed to determine if the results for each stimulus paradigm was significantly different for the GCaMP3 variants compared to GCaMP3.

Two-tailed unpaired T-tests were performed to compare the maximum fluorescence responses to small bursts of stimuli and trains of stimuli at varying frequencies, dynamic range, and decay rates of the high calcium affinity GCaMP3 variant GC3_K21A_K77G_N97D with GCaMP3 and the significance (P-value) is reported on Table 4. Additional two-tailed T tests were performed to compare the SNR and basal fluorescence of GC3_K21A_K77G_N97D and GCaMP3 in response to small bursts of stimuli (Figure 20 and Table 4, respectively). ANOVA/Tukey HSD tests were performed to compare the maximum fluorescence increases in response to small stimulus bursts, trains of stimuli, and dynamic ranges between the low calcium affinity GCaMP3 variants GC3_D24N_E104Q and GC3_D24N_D60N_E140Q and GCaMP3. The significance for these tests is reported on Table 6. Finally, another series of ANOVA/Tukey HSD tests were performed to compare the SNR and basal fluorescence of two more treatment groups to GCaMP3 (GC3_K21A, GC3_N97D, and GC3_K21A_N97D; and GC3_D24N_E104Q and GC3_D24N_D60N_E140Q) in response to small bursts of stimuli (Tables 5 and 6, and Figures 22 and 26, respectively).

CHAPTER 3 RESULTS

3.1 *IN VITRO* CHARACTERIZATION OF GCAMP MUTATIONS

3.1.1 Single Point Mutations in EF Motifs

We set out to identify single point mutations introduced within the EF motifs of CaM that either increase the calcium affinity of the GECI to generate a more sensitive sensor for low calcium concentrations in the range of 100 to 200 nM, or decrease CaMs calcium affinity for the engineering of GCaMP variants that allow the accurate measurement of large calcium concentrations in the range of 2 to 20 μM. In the following section, I will describe the effect of substituting various EF motif position residues on the calcium affinity, Hill coefficient, and dynamic range of GCaMP, measured in calcium titration assays with bacterially expressed and purified protein. I will begin with the most severe mutations (position 12), followed by the less severe (positions 3 and 5) to more ambiguous positional mutations (positions 9, 2, and 11). A schematic illustration overlaying the four EF motifs of CaM shown in Figure 6 indicates the position in which each single mutation has been performed.

3.1.1.1 Position 12 Mutations of GCaMP3

Glutamic acid is present at chelating position 12 of each of CaMs four calcium binding EF motifs of wild type GCaMP3. A protein study that individually mutated each of these residues to glutamine of *Drosophilia melanogaster* CaM independently, revealed that point mutations at this position abolished calcium binding of the EF motif (Maune et al, 1992). Therefore, we generated four separate point mutation constructs with the same

substitution to investigate their potential for reducing the calcium affinity of GCaMP3, named GC3_E31Q, GC3_E67Q, GC3_E104Q, and GC3_E140Q. Calcium titration analysis of each construct revealed that these single mutations have the greatest effect of any EF motif position tested as all four of these point mutants significantly reduced the calcium affinity of GCaMP3 ($p<0.01$, see Table 1 and Figure 7). Furthermore, these mutants provided information regarding the relative importance of each EF motif in terms of overall calcium affinity and binding cooperativity of the GECI. The reduction of calcium affinity was relatively moderate for position 12 mutations in the C-terminal domain of CaM, being the lowest for the mutation E104Q in EF motif III (K_d = 1.1 μM) and slightly stronger for the corresponding mutation E140Q in EF motif IV (K_d = 3.5 μM). The Hill coefficients and dynamic ranges of position 12 mutants in EF motifs III and IV (GC3_E104Q and GC3_E140Q) were similar to that of GCaMP3. In contrast, mutations of EF motif position 12 in the N-terminal domain of CaM had much more pronounced effects. The homologous mutation in EF motif I, E31Q, resulted in an approximately 32-fold reduced calcium affinity (K_d =13.5 μM) as well as a more than two-fold reduced cooperativity of calcium binding (Table 1 and Figure 7). The substitution of glutamate 12 in EF motif II, E67Q, led to changes in the binding cooperativity that were insufficiently described using the Hill equation. The major fluorescence change in this mutant occurred between 30 μM and 100 μM. Moreover, the cooperativity of calcium binding in the E67Q construct was even more strongly reduced than in GC3_E31Q (Table 1). Moreover, GC3_E31Q and GC3_E67Q showed a severely reduced dynamic range (2.6 and 4.0 compared to 9.1 for GCaMP3, $p<0.01$). In summary, these data demonstrate that the mutations E104Q and E140Q are ideal to lower the

affinity of GCaMP indicators while maintaining the dynamic range and cooperativity of GCaMP3. Our results also indicate that, in the context of GCaMP, position 12 mutations in the N-terminal domain of calmodulin are less desirable, lowering the dynamic range and cooperativity of calcium binding.

3.1.1.2 Position 3 Mutations of GCaMP3

Calcium interacts with the carboxylate group of aspartic acid located at position 3, a conserved residue across CaMs four EF motifs of wild type GCaMP3. A study investigating structure/function relationships of EF motif III using small peptides encompassing this motif revealed that the calcium affinity of this loop decreased when aspartic acid was replaced with asparagines (Procyshyn and Reid; 1994). Therefore, four separate constructs containing this point mutation substituting aspartic acid with asparagine in each of the four EF motifs were generated to determine if the same effect would be observed in GCaMP3. These constructs were named GC3_D22N, GC3_ D58N, GC3_D95N, and GC3_D131N. A calcium titration analysis revealed varying results amongst this set of mutations. The D22N mutation produced significant decreases in calcium affinity, resulting in an affinity constant of 1.25 μM ($p<0.01$, see Figure 8). In contrast, the D95N and D131N mutations exhibited only marginal decreases in calcium affinity, while the D58N exhibited only a marginal increase in calcium affinity (Table 1 and Figure 8). Hill coefficients, dynamic ranges, and basal fluorescence were similar to that of wild type GCaMP3 for each mutation with the exception of D22N, which exhibited a significantly reduced Hill coefficient and basal fluorescence ($p<0.05$) (Table 1). In summary, due to its significantly reduced K_d, the D22N mutation of EF motif I may

be a useful mutation to lower the calcium affinity in GCaMP constructs designed to prevent saturation at intermediate calcium concentrations.

3.1.1.3 Position 5 Mutations of GCaMP3

Position 5 of calmodulin's EF binding motifs is relatively conserved, being mostly occupied by an aspartic acid. Synthetic peptide studies performed on this calcium chelating site have revealed that the independent replacement of aspartic acid with glutamic acid within EF motif III and IV distorts the binding cavity due to its longer side chain, resulting in a significant reduction of calcium affinity (Reid and Procyshyn, 1995). We attempted to address whether the replacement of aspartic acid with asparagine (the third most frequently found residue at this site across calcium binding proteins; Marsden et al, 1990) at this position would lower the calcium affinity of CaM for the generation of a GCaMP variant that does not saturate at intermediate calcium concentrations. To accomplish this, we generated three separate GCaMP3 constructs with point mutations at position 5 of EF motifs I, II, and IV (the motifs containing aspartic acid at this coordination site), and named them GC3_D24N, GC3_D60N, and GC3_D133N. The D60N mutation reverses the point mutation performed by Tian et al (2009) in their generation of GCaMP3. We have tested GC3_D60N as the effect of this mutation has not been assessed in isolation. In addition, we mutated an asparagine at position 5 in the third EF motif to an aspartate with the intent to create a GCaMP3 variant with higher calcium affinity (GC3_N97D). However, upon calcium titration analysis, only the D24N and D133N mutations had significant shifts in calcium affinity with a K_d of 1.31 and 1.12 μM, respectively ($p<0.01$) (see Figure 9). For the D60N mutant only a marginal decrease in calcium affinity was noted (Table 1). In contrast, the N97D mutant slightly, but not

significantly, increased the calcium affinity of GCaMP3 (Table 1). All four mutant constructs exhibited similar Hill coefficients that were not different from GCaMP3. However, cooperative binding was marginally attenuated for the D24N mutant (Hill coefficient 1.62 ± 0.04 compared to 2.26 ± 0.07 for GCaMP3), reminiscent of the significant reduction observed for the D22N at position 3 in the same EF motif. Dynamic ranges of the position 5 mutations were not significantly different to that of wild type GCaMP3. However, the baseline fluorescence of the D24N, N97D, and D133N was significantly decreased (see Table 1). In summary, the D24N and D133N mutations of EF motif I and IV may be useful to lower the calcium affinity in GCaMP constructs designed to prevent saturation at intermediate calcium concentrations.

3.1.1.4 Position 9 Mutations of GCaMP3

The position 9 coordination site is less conserved across EF motifs of CaM than positions 3 and 5 due to the fact that the complexation of calcium at this position occurs via a bridged water molecule. A synthetic peptide model study indicated that when a native serine residue is replaced in this position, the calcium affinity of the loop is somewhat reduced (Procyshyn and Reid; 1994). Therefore, with the intention of increasing GCaMP3s calcium affinity, we generated a point mutant to replace the aspartic acid of EF motif II with serine, named GC3_D64S. Furthermore, we substituted the serine of EF motif III with aspartic acid, generating GC3_S101D, to achieve the opposite result. In addition to these two point mutations, we also inserted an aspartic acid into position 9 of EF loop I to generate GC3_T28D as another attempt to reduce the calcium affinity of the loop. Upon performing a calcium titration analysis, we found that changes in this position had more subtle effects on calcium binding of GCaMP3. When

differences in calcium affinity of all position 9 mutants and unmutated GCaMP3 were tested by ANOVA, we found no significance (Table 1). However, the T28D displayed a clear trend towards lower affinity (K_d 651 ± 40 nM) whereas the D64S and S101D mutants had a slightly increased affinity relative to GCaMP3 (320 ± 31 and 355 ± 13 nM, respectively) (see Figure 10). Furthermore, the Hill coefficients and dynamic ranges did not differ significantly from that of GCaMP3, although these values trended towards being lower for the D64S mutation. The only significant difference discovered amongst these three GCaMP3 variants were their lower basal fluorescence values. In summary, mutations performed on position 9 of the EF motifs, with the possible exception of the T28D mutant, do not appear to be useful for the engineering of GCaMP3 variants with higher or lower calcium binding affinity.

3.1.1.5 Position 2 Mutations of GCaMP3

Positively charged lysine residues at EF motif position 2 may electrostatically interact with calcium, lowering the calcium affinity or slowing calcium binding. Alternatively, these residues may interact with negatively charged residues at positions 1, 3 and 5 with unknown effects on the stability of the apo- and calcium-bound states of CaM and its calcium affinity. Initially, we mutated lysine at position 2 of the first EF motif to the nonpolar alanine residue (K21A) to determine if this mutation would increase the calcium affinity of GCaMP3. We also mutated a similar lysine at position 2 in the third EF motif (K94A). Upon performing a calcium titration analysis, both mutant constructs were found to marginally increase the calcium binding affinity of GCaMP3 (Figure 11). Although differences in the Hill coefficient between GCaMP3 and its K21A and K94A mutants were not significant (ANOVA p=0.16), there was a clear trend of

K21A towards a higher Hill coefficient. In fact, a t-test performed before examining the K94A mutant suggested a significantly increased calcium binding cooperativity of the K21A mutant. Such an increase in the Hill coefficient may be desirable for the detection of small calcium transients. While the K21A construct also exhibited a slightly, but not significantly, increased dynamic range, the K94A construct was very similar to GCaMP3 in this property (Table 1 and Figure 11). Moreover, opposite trends were observed for the baseline fluorescence of the K21A mutant (lower) and K94A mutant (higher) (see Table 1). In summary, mutations at position 2 showed interesting properties for the construction of a GCaMP with higher sensitivity, such as trends towards an increased K_d and higher Hill coefficients

3.1.1.6 Position 11 Mutations of GCaMP3

The increase in affinity observed from replacing lysines with alanine at position 2 of CaMs EF motifs I and III led us to investigate if the substitutions of other charged residues in EF motif positions that are not directly involved in the chelation of calcium also affect the calcium affinity of GCaMP3. We thus mutated two charged residues at position 11 in EF motif I and IV, K30 and E139, to alanine. A calcium titration analysis performed on these new constructs showed promising results as both mutations marginally increased GCaMP3s affinity for calcium (see Figure 12 for curve traces). GC3_K30A also had a marginally increased Hill coefficient, whereas that of GC3_E139A were similar to that of GCaMP3.The dynamic ranges and baseline fluorescence of these mutants were similar to GCaMP3 as well (see Table 1).

3.1.2 Linker Mutations of GCaMP3

Point mutations were also performed within the flexible interdomain linker region of CaM as basic amino acid residues of the linker have shown to be critical for stabilizing the apo- conformation of the N-terminal domain EF motifs and thus lowering their affinity for calcium (Faga et al, 2003; VanScyoc et al, 2002). Initially, we generated three constructs, named GC3_R74A, GC3_K75G, and GC3_K77G, and then a fourth construct, GC3_R90G, towards the end of our studies, in an attempt to increase GCaMP3s calcium binding capabilities. Conversely, we also inserted two basic residues at positions 80 and 84 of the linker, generating two more linker constructs GC3_D80R and GC3_E84R to determine if these mutations have the potential to decrease the overall calcium binding affinity of GCaMP3 (see Figure 13). A calcium titration analysis produced the results we predicted for all but one of these mutant constructs. The mutations of R74A, K75G, and K77G significantly increased GCaMP3s affinity for calcium (see Figure 14A, Table 2). The Hill coefficient also significantly increased for the K75G mutation, while trending towards higher cooperativity values for R74A and K77G. The dynamic ranges for K75G and K77G constructs were similar for that of GCaMP3 (Table 2). In contrast, the dynamic range for the R74A construct was significantly lower, decreasing by approximately 40% relative to GCaMP3. The R90G mutation resulted in only marginal increases in GCaMP3s affinity for calcium, Hill coefficient, and dynamic range.

Constructs in which an acidic residue in the linker region was substituted by a basic residue displayed variable effects. The mutation of D80R was found to significantly decrease calcium affinity while maintaining similar a similar Hill coefficient and

dynamic ranges compared to GCaMP3 (Figure 14B, Table 2). Moreover, both constructs significantly increased the basal fluorescence of GCaMP3 (Table 2). In contrast, the mutation E84R had no noticeable impact on the calcium affinity of GCaMP3, nor differed in dynamic range. However, the Hill coefficient of this mutant (h = 3.02) was significantly higher. In summary, the significant increase in K_d without a noticeable difference in dynamic range for the K75G and K77G mutations suggests these two GCaMP3 variants may be useful for measuring small calcium transients. Furthermore, a combinatorial approach for engineering a GCaMP3 calcium sensor that includes these two linker mutations alongside other EF motif mutations that trended towards higher calcium affinities, such as K21A and K94A (position 2), may have additive effects to create a higher affinity GCaMP3 variant more suitable for measuring smaller calcium transients. The D80R mutation may also be useful for measuring lower calcium concentrations due to its significantly lower K_d value.

3.1.3 Generation of GCaMP Variants with High Calcium Affinity Using a Combinatorial Approach

The first aim of this study was to generate a GCaMP variant with a substantially higher calcium affinity (100 to 200 nM) relative to GCaMP3. Single mutations in the EF motifs did not yield to significant increases in K_d although several did exhibit trends towards higher calcium affinity. Although single mutations in the linker region did significantly increase calcium affinity, they did not reach the desired K_d of our aim. Furthermore, although not significant, several single mutations in the EF motifs did exhibit trends towards increasing calcium affinity. This led us to pursue a combinatorial approach in which we combined multiple mutations, both within EF motifs and in the

interdomain linker region, to engineer GCaMP3 variants with larger increases in calcium affinity. Of the mutations tested in the initial phase of the project, three mutations appeared especially promising for such an approach. The asparagine to aspartate substitution at position 5 in EF motif III, N97D, was predicted to have increased calcium affinity and indeed resulted in a marginal increased K_d relative to GCaMP3. Similarly, the first linker mutation we characterized, 77G, displayed a significantly increased calcium affinity with an essentially unchanged dynamic range. Finally, a mutation at position 2 in the first EF motif, K21A, showed not only a marginal increase in K_d, but in addition a slight increase in its Hill coefficient, a property that may be desirable to increase the sensitivity of a high affinity GCaMP variant. For these reasons, we proceeded to generate a GCaMP3 variant with all of the above mutations, GC3_K21A_K77G_N97D. Toward the end of my studies, we generated two more combination constructs that included the K75G that also exhibited a significant increase in calcium affinity in addition to a significantly higher Hill coefficient, GC3_K21A_K75G_N97D and GC3_K21A_K75G_K77G_N97D. A calcium titration analysis of these constructs revealed that our prediction was in fact true. The calcium affinities were significantly increased relative to wild type GCaMP3 yielding a K_d values of 201.7 ± 9.6, 175.5 ± 12.4, and 176.6 ± 16.5 nM (K21A_K75G_N97D, K21A_K77G_N97D, and K21A_K75G_K77G_N97D, respectively) (Table 3, and see Figure 15 for relative shifts in affinity for each construct compared to one significant component, K77G). The Hill coefficients and dynamic ranges of each construct were similar to that of GCaMP3 with the exception of the quadruple mutant which trended towards a lower dynamic range (Table 3). However, the basal fluorescence of each

combination construct was significantly reduced. In summary, these three constructs proved to be our best sensors for increasing GCaMP3s calcium affinity as each of them may be useful for monitoring small calcium transients.

3.1.4 Generation of GCaMP Variants with Low Calcium Affinity Using a Combinatorial Approach

The second aim of this Masters project was to generate GCaMP variants with lower calcium affinity that allow the accurate measurement of larger calcium transients that saturate GCaMP3. None of the GCaMP variants generated by single amino acid substitutions had affinities in the of 10 μM range while maintaining a Hill coefficient or dynamic range to that was comparable to GCaMP3. We proceeded to combine amino acid substitutions with significantly lower calcium affinities and unaltered Hill coefficients and dynamic ranges. The glutamate to glutamine substitution at position 12 in EF motifs III and III, E104Q and E140Q, resulted in significant increases in K_d relative to GCaMP3 while maintaining similar Hill coefficients. Moreover, the position 5 mutations of aspartate to asparagine in EF motifs I and II, D24N and D60N, also significantly and marginally reduced the calcium affinity of GCaMP3, respectively. Therefore, we initially created two series of double mutation constructs (and E104Q series and E140Q series) combining both position 5 mutations of the N-terminal domain with position 12 mutations of the C-terminal domain (GC3_D24N_E104Q, GC3_D60N_E104Q and GC3_D24N_E140Q, GC3_D60N_E140Q).

The 104Q series of mutations (Figure 16A) significantly reduced the calcium affinity of GCaMP3 yielding K_d values of 2.7 ± 0.08 and 1.9 ± 0.15 μM (for D24N_E104Q and D60N_E104Q, respectively). Although the dynamic ranges for the

104Q series was significantly higher than GCaMP3, their basal fluorescence were significantly lower in addition to the Hill coefficient for the D60N_E104Q double mutant being significantly lower as well (Table 3). However, this E104Q series did not achieve calcium affinities low enough to measure larger calcium transients (10 – 20 μM) without concerns of saturating the sensor.

In comparison to the E104Q series constructs, the respective constructs in the E140Q series displayed an even lower calcium affinity (Figure 16B), exhibiting K_d values of 9.7 ± 0.3 and 3.5 ± 0.3 μM for the D24N_E140Q and D60N_E140Q mutations, respectively. This series of double mutations maintained similar Hill coefficients to GCaMP3 and significantly higher dynamic ranges, although also displayed significantly lower basal fluorescence properties, similar to those in the E104Q series (Table 3). These data of the two position 12 series indicate that the D24N of EF motif I and E140Q of EF motif IV have the largest impact on reducing the calcium affinity of GCaMP3.

More recently, we generated two more combinatorial GCaMP3 constructs that added additional mutations to the GC3_D24N_E140Q construct in an attempt to engineer a GECI to measure calcium concentrations without saturating in the range of 10 – 20 μM (GC3_D24N_D60N_E140Q and GC3_D24N_D60N_D95N_E140Q). The position 3 D95N mutation of EF motif III was included in this series as it marginally decreased the calcium affinity of GCaMP3 while maintaining the sensors Hill coefficient and dynamic range. Upon calcium titration analysis, these two constructs significantly reduced the calcium affinity of GCaMP3 (Figure 16B), resulting in K_d values lower than that the E140Q series (12.6 ± 0.3 and 11.6 ± 0.7 μM for D24N_D60N_E140Q and D24N_D60N_D95N_E140Q, respectively). Furthermore, they both maintained a similar

Hill coefficient to that of GCaMP3. Moreover, the GCaMP3_D24N_D60N_E140Q construct displayed a significantly higher dynamic range (Table 3). A notable difference between these two constructs was in their basal fluorescence. The basal fluorescence of the quadruple mutation construct was similar to that of GCaMP3 while the triple mutation construct exhibited a significantly lower value (Table 3).

In summary, the combinatorial approach was successful for engineering GCaMP3 variants with appropriate calcium affinities to measure large calcium transients or concentrations in the range of 10 – 20 μM without concerns of sensor saturation. The most viable constructs for this purpose were GC3_D24N_D60N_E140Q and GC3_D24N_D60N_D95N_E140Q.

3.2 Characterization of GCaMP Mutations in Cultured Hippocampal Neurons

GCaMP3 mutant constructs of interest from the *in vitro* portion of this project were further investigated to determine if alterations in the affinity of calcium binding of GCaMP3 lead to changes in the sensitivity and saturation characteristics in neurons. Therefore, due to our lab's interest in the mechanisms involved in neurotransmitter release regulation, selected constructs were transfected into dissociated rat hippocampal cell cultures and axonal calcium transients were measured, rather than somatic or dendritic calcium transients as performed by previous studies that attempted to improve the sensitivity of GECIs. The fluorescent responses of the GCaMP3 variants selected were observed at presynaptic localizations in response to isolated stimuli and stimulus trains and compared to fluorescent responses of GCaMP3.

3.2.1 Detection of Presynaptic Calcium Transients in Neurons

Dissociated hippocampal cell cultures were transfected with either GCaMP3 or variants thereof. In a subset of neurons, the active zone cytomatrix protein Bassoon, tagged with the red fluorescent protein tdTomato, was also transfected to identify the location of presynaptic specializations. Whereas tdTomato-Bassoon localization was restricted to presynaptic specializations (Figure 17A), GCaMP3 and its variants were distributed throughout the cytosol (Figures 17B). With the high affinity GCaMP variant GC3_21A|77G|97D, and to some extent with the unmodified GCaMP3, we observed spatially confined calcium transients in response to isolated stimuli. These "hotspots" of calcium influx overlapped with clusters of the presynaptic active zone cytomatrix protein Bassoon, which indicates that calcium influx in axons is largely restricted to presynaptic specializations (Figure 17C). Upon repetitive stimulation (20 stimuli at 20 Hz), an increase in calcium could also be observed in the axonal shaft (Figure 17D), indicating the diffusion of calcium out of presynaptic varicosities. These experiments suggest that presynaptic calcium transients can be measured with the high calcium affinity GCaMP3 mutant. Moreover, it is possible to measure calcium transients at individual synapses as long as they are sufficiently spaced apart, preventing diffusion of calcium from nearby synapses. Subsequently, we utilized this ability to measure presynaptic calcium transients for the comparison of the GC3 with our engineered high and low calcium affinity variants.

3.2.2 GCaMP Mutants with Higher Calcium Affinity

The triple mutations construct GC3_K21A_K77G_N97D, which exhibited a significant increase in calcium affinity while maintaining a similar Hill coefficient and dynamic range to that of the control GCaMP3 upon *in vitro* calcium titration analysis, was tested in neurons and compared to that of wild type GCaMP3. Of most importance, this triple mutant construct proved to be significantly more sensitive than GCaMP3 for detecting calcium in neurons. The fluorescence change (ΔF/F) for the triple mutant was 3.7 fold larger than GCaMP3 in response to isolated action potentials. Furthermore, it displayed roughly two-fold and 1.7 fold increase in fluorescence in response to bursts of 2 and 4 stimuli at 40 Hz, relative to GCaMP3 (unpaired two-tailed T-Test; see Figure 18A, B, E, and F, and Table 4). In addition, the SNR for this construct was 4.4-, 2.3-, and 1.5-fold higher than GCaMP3 in response to isolated and small bursts of 2 and 4 stimuli at 40 Hz ($p<0.01$ for isolated and 4 stimuli, $p<0.05$ for 2 stimuli, unpaired two-tailed T-Test, Figure 20) and displayed a 44% increase in basal fluorescence ($p=0.01$, unpaired, two-tailed T-Test; Table 4). The ΔF/F was also significantly higher for the triple mutant construct in response to 2 second trains of stimuli at 2.5, 5, 10, and 20 Hz (unpaired two-tailed T-Test) (Figure 18C and D, and Table 4). Furthermore, unlike the results from the *in vitro* analysis, the dynamic range of this triple mutant was significantly higher than that of GCaMP3 by approximately 20% when tested in neurons (unpaired two-tailed T-Test) (Table 4).

Due to GC3_K21A_K77G_N97D having an increased affinity for calcium, it is conceivable that this GCaMP3 variant is saturated at lower calcium concentrations than its parent GECI and thus unable to provide accurate, nearly linear measurements at

intermediate calcium concentrations. To investigate this possibility, we plotted relative fluorescence changes, normalized to the maximum fluorescence change ($[F-F_{min}]-[F_{max}-F_{min}]$) for 2 second stimulus trains at 2.5, 5, 10, 20, and 40 Hz. A statistical analysis indeed revealed a higher degree of receptor saturation at all frequencies examined. For example, the degree of saturation was approximately 15-17% higher for the triple mutant than GCaMP3 in response to 2 second trains at 5 and 10 Hz (Table 4). Furthermore, although the saturation of the triple mutant and GCaMP3 remained approximately linear to upwards of 2 second train stimuli of 20 Hz, the triple mutant achieve roughly 90% receptor saturation at 20 Hz, while GCaMP3 required 40 Hz to reach similar saturation levels (Figure 19A and B). While differences in sensor saturation between GCaMP3 and GC3_K21A_K77G_N97D are significant, they are relatively mild and should not interfere with the use of this sensor to assess calcium transients in response to action potential burst frequencies and durations normally encountered in cortical neurons. In summary, these results indicate that GC3_K21A_K77G_N97D, which has a significantly higher K_d for calcium, exhibits a significantly higher sensitivity for small calcium transients than GCaMP3 when used in neurons. Moreover, this triple mutant variant showed significantly higher saturation values in response to trains of stimuli at multiple frequencies and maximized at a lower frequency than GCaMP3.

As described in the *in vitro* analysis, the point mutation K77G significantly increased the calcium binding affinity of GCaMP3 while K21A and N97D showed only marginal increases in K_d. Following our finding that GC3_K21A_K77G_N97D exhibits a greater sensitivity for small calcium transients, we sought to determine the relative contribution of each of its mutations to the increased SNR of this triple mutant or if their

combination was required when applied to neurons. The three constructs of GC3_K21A, GC3_K77G, and GC3_N97D were thus transfected individually into neurons to investigate their relative fluorescence changes in response to stimuli compared to that of wild type GCaMP3. Surprisingly, we discovered that the K21A mutation provided a larger contribution towards improving the sensitivity of GCaMP for calcium detection rather than K77G. In response to small bursts (2 and 4) of stimuli, GC3_K21A significantly increased the ΔF/F signals (41 ± 8% and 105 ± 12%, respectively) for calcium detection compared to GCaMP3 (ΔF/F = 14 ± 2% and 40 ± 5%, respectively) (see Figure 21A, B, and C). For isolated stimuli, ΔF/F was increased three-fold over GCaMP3, although this increase was not significant (Table 5). SNRs for isolated stimuli, as well as bursts of 2 and 4 action potentials, was marginally increased as well (Figure 22). Moreover, only K21A resulted in a significant increase in dynamic range compared to that of wild type when stimulated by 2 second trains of varying frequencies ranging from 2.5 to 80 Hz (ANOVA analysis) (Table 5). In contrast, and N97D were not different from that of GCaMP3 in response to isolated stimulation as well as bursts of 2 and 4 stimuli upon an ANOVA analysis (Figure 21A and D, and Table 5). Furthermore, the SNR and basal fluorescence of mutations K77G and N97D were similar to GCaMP3 (Figure 22 and Table 5).

Interestingly, the significant increase in K_d was noted for K77G but not for K21A (258.8 and 356.9 nM, respectively) from the *in vitro* analysis. Therefore, the impact of the K21A in the triple mutant construct might be of more importance for other reasons than its affect on calcium affinity. To explore this possibility, we investigated how alterations in the kinetics of GCaMP3 due to its mutations may lead to an increase in

sensitivity to calcium transients elicited by isolated APs and small bursts of stimuli. Therefore, we determined the decay rates of K21A, K77G, and N97D and compared them to that of GCaMP3 (the Hamamatsu ORCA CCD camera used limited our ability to determine the binding kinetics of calcium transients as its acquisition rate was slower than the fast rise times of calcium transients). We discovered that from the maximal ΔF/F in response to a 4 stimuli burst, the fluorescence signal of K21A mutant decayed approximately twice as fast as GCaMP3. In contrast, no significant difference was observed for N97D, while K77G trended towards a slower decay upon an ANOVA analysis (Table 5). In comparison, the decay rate of the triple mutation was marginally smaller than that of GCaMP3 (Table 4). Furthermore, we also transfected neurons with another construct comprised of two of these mutations, K21A and N97G to determine if the presence of all three mutations was required to produce the significant sensitivity increase observed with the triple mutant construct. The GC3_K21A_N97D construct showed similar fluorescence increases to isolated action potentials as well as 40Hz bursts of 2 and four action potentials than the triple mutant also containing 77G (Figure 21E and Table 5). Moreover, for this mutant, we also observed only a marginally reduced decay rate and a dynamic range that was very similar to that of GCaMP3 (Table 5). In summary, this analysis suggests that the K21A is of most importance in increasing the sensitivity of the GC3_21A_77G_97D.

3.2.3 GCaMP Mutants with Lower Calcium Affinity

Two of the significantly decreasing calcium affinity mutant constructs, GC3_D24N_E104Q and GC3_D24N_D60N_E140Q, were selected to investigate if their decreased calcium affinity leads to more linear fluorescence increases in response to large

calcium transients in neurons. These two mutant constructs were selected over the other *in vitro* tested constructs as they exhibited the reduced calcium affinities of 3 and 12.5 μM, respectively, approximately 6- and 30-fold lower than GCaMP3, and similar to many low-affinity calcium indicators in use. The response of each mutant construct to 2 second stimulus trains at 2.5, 5, 10, 20, 40, and 80 Hz was assessed to determine if these GCaMP3 combination mutants would be good candidates to measure larger calcium transients or calcium concentrations more accurately than with GCaMP3. Upon plotting saturation curves for each reduced calcium affinity mutant sensor, we discovered that both sensors were not as easily saturated by larger calcium transients as they reported larger transients in a more linear manner than GCaMP3. Both mutant sensors revealed a decrease in sensitivity with significantly lower ΔF/F responses to 10 and 20 Hz stimuli (38 and 23% lower for GC3_D24N_E104Q, and 49 and 52% lower for GC3_D24N_D60N_E140Q, respectively), while D24N_D60N_E140Q was also significantly less sensitive in response to a 40 Hz stimulus (by 30%) upon an ANOVA analysis (Figure 24D, E, and F, and Table 6). It should also be noted that, although not significant, both sensors reported marginal sensitivity decreases relative to GCaMP3 in response to a 2 second train stimulus at 5 Hz (Table 6). In addition, while GCaMP3 became mostly saturated in response to a 20 Hz stimulus (86 ± 2%), the D24N_E104Q and D24N_D60N_E140Q constructs only saturated upon a 40 and 80 Hz stimulus, respectively (Figure 23A, B, and C and Table 6). Interestingly, D24N_E104Q had a significantly higher dynamic range (24% increase) when tested in neurons even though neither of the two sensors differed from the wild type control in this regard *in vitro* (Table 6). We also investigated the response of these two mutant sensors to a single stimulus and

bursts of 2 and 4 stimuli. While the 24N_104Q construct displayed fluorescence responses to isolated action potentials as well as bursts of two and four action potentials that were very similar to GCaMP3, the D24N_D60N_E140Q trended towards much reduced responses with ΔF/F values that were approximately 7-fold lower for bursts of two APs and about 3-fold lower for bursts of four APs (Figures 24A, B, and C; 25A, B, and C). In addition, although the basal fluorescence of both low calcium affinity mutants were similar to GCaMP3 in neurons, the SNR of the triple mutant was significantly reduced in response to bursts of 2 and 4 stimuli by approximately 10- and 6-fold, respectively (ANOVA/Tukey HSD) (Figure 26 and Table 6). However, due to the low number of experiments performed, with the exception of the SNR analysis, these data did not reach significance in an ANOVA analysis (Figure 19A, B, C, 20A, B, and C, and Table 6). In summary, both mutant sensors GC3_D24N_E104Q and GC3_D24N_D60N_E140Q are less easily saturated by larger calcium transients in neurons and can be utilized to accurately measure larger calcium transients than GCaMP3.

CHAPTER 4 DISCUSSION

4.1 GENERATION OF GCAMP VARIANTS WITH A LARGER RANGE OF CALCIUM AFFINITY

In this study, we succeeded to design GCaMP-based GECIs with a broad range of calcium affinities. The first aim was to generate a GCaMP variant with an increased sensitivity to detect lower calcium concentrations or transients in the range of 100 to 200 nM. The second aim of this study was to optimize GCaMP3 for the measurement of large calcium transients by reducing its affinity for calcium to 2 to 20 μM to avoid sensor saturation. A calcium titration analysis was used to investigate the altered calcium affinities, Hill coefficients, dynamic ranges, and basal fluorescence of all engineered GCaMP3 variants with the most promising constructs selected to assess their performance in cultured hippocampal neurons. The findings of the neuronal data indicate that both aims of the study were achieved. We successfully generated one construct, GC3_K21A_K77G_N97D, which is significantly more sensitive than GCaMP3 and is able to detect calcium transients at presynaptic specializations in response to single stimuli when tested in neurons. Moreover, we engineered two GCaMP variants, GC3_24N_104Q and GC3_D24N_D60N_E140Q, which exhibit a significantly lower sensitivity for calcium binding, allowing us to accurately measure larger calcium concentrations without concerns of sensor saturation.

4.1.1 High Calcium Affinity Sensor

Our extensive mutagenesis screen of calmodulin led us to identify several mutations in the interdomain linker that increased the calcium affinity significantly, as

well as mutations in the EF motifs that marginally elevated the K_d of GCaMP3 for calcium. While none of the EF motif mutations alone resulted in a large shift of the calcium association constant, the combination of several of these mutations led to the generation of a GCaMP variant with the desired high affinity for calcium. The effectiveness of this high affinity GCaMP3 variant, GC3_K21A_K77G_N97D, was substantiated by both an *in vitro* calcium titration analysis testing and its functional capabilities in neurons. The calcium titration analysis indicated that this high affinity construct exhibited a significantly increased calcium affinity of 179 ± 15.1 nM compared to GCaMP3 (419 ± 23.9 nM) which is within the desired range of between 100 and 200 nM. Most importantly, however, the K21A_K77G_N97D sensor, when expressed in neurons, significantly increased GCaMP3s response for single stimuli as well as small bursts of 2 and 4 stimuli. For isolated action potentials, the ΔF/F was increased three- to fourfold relative to GCaMP3, leading to a large increase in SNR of the sensor for small calcium transients. In summary, the creation of GC3_K21A_K77G_N97D achieved the first goal of creating a GCaMP variant with higher sensitivity that is suitable to report small calcium transients induced by single action potentials.

The *in vitro* and neuronal assessment of the individual components of GC3_K21A_K77G_N97D suggested that the most relevant parameter for constructing a variant with higher sensitivity may not be the calcium affinity conferred by each mutation. In isolation, the K77G was the only mutation of the three to provide a significant increase in calcium affinity upon *in vitro* calcium titration analysis. However, in contrast to K77G and N97D, K21A was the only mutation to exhibit a significant ΔF/F increase in response to small calcium transients elicited by burst stimulation in

presynaptic specializations of hippocampal neurons. A possible explanation for the significantly increased ΔF/F responses of the K21A mutant in neurons could be that its dynamic range was significantly higher than its parent GECI when tested in neurons which contrast the similar reported dynamic ranges of K77G and N97D compared to GCaMP3. However, the increase in the dynamic range is relatively small and unlikely to account for the much larger increase in ΔF/F in response to presynaptic calcium transients elicited by isolated action potentials or small action potential bursts. Alternatively, it is possible that the K21A mutation alters the calcium binding kinetics of GCaMP. Faster calcium binding would likely lead to an increase in sensitivity of the sensor to fast calcium transients. The 21A mutation removes a positively charged lysine from EF motif I that may cause some electrostatic repulsion of calcium ions which may slow down calcium binding to this site. While we were not able to measure the rise time of the calcium signal in neurons directly (the acquisition rate of our CCD camera was too low), we did measure the decay kinetics and found a significant increase in the decay time constant of the K21A mutant. This finding may indicate that the calcium binding kinetics may indeed be altered by this mutation. Therefore, the significant increase in sensitivity exhibited by GC3_K21A_K77G_N97D may result from not only the higher dynamic range or combination of the significantly increased calcium affinity properties of K77G and the marginal increase in K_d of the K21A and N97D mutants, but may also be due to altered binding kinetics of K21A.

4.1.2 Low Calcium Affinity Sensors

The effectiveness of the low calcium affinity sensors were also substantiated by both *in vitro* and neuronal data. In calcium titration experiments, GC3_D24N_E104Q and

GC3_D24N_D60N_E140Q displayed significantly reduced the calcium affinities compared to GCaMP3 with K_d values of 2.7 ± 0.07 and 12.6 ± 0.28 μM, respectively. Furthermore, the dynamic ranges of these sensors were also significantly higher than GCaMP3, which presumably could aid in the accurate detection of larger calcium transients. The results of the neuronal data for these constructs corresponded to the *in vitro* data as both of the low calcium affinity sensors saturated at much higher calcium concentrations. GCaMP3 approached saturation levels in response to a 2 second trains stimuli at 20 Hz (87 %) compared to only a 63% saturation observed by GC3_D24N_E104Q at 20 Hz. The GC3_D24N_D60N_E140Q variant showed an even lower tendency to saturate in response to large calcium transients, displaying, for example a 62% saturation observed by GC3_D24N_D60N_E140Q at 40 Hz compared to a 92% saturation of GCaMP3 in response to the same stimulus paradigm. These data allow us to conclude that the GC3_D24N_E104Q and GC3_D24N_D60N_E140Q sensors achieved the second aim of the study as they can be used to measure significantly larger concentrations of calcium accurately without concerns of saturation as observed with GCaMP3.

4.2 Further Improvements to the High and Low Calcium Affinity GCaMP3 Variants

4.2.1 Further Increases in Calcium Affinity

Currently, our high calcium affinity measures calcium concentrations around 175 nM. It may be desirable to engineer GCaMP variants with even higher calcium affinity, in the 50 – 100 nM range. A sensor in this affinity range could, for example, allow for an

accurate measurement of basal calcium concentrations in neurons at rest, which cannot be accomplished by current GECIs. In order to generate a GCaMP variant with very high affinity, other mutations that individually resulted in marginal increases in calcium affinity could be combined with the mutations in our current high affinity sensor. Specifically, the position 11 mutation of K30A in EF motif I and the R90G mutation in the interdomain linker exhibited marginal increases in calcium affinity and Hill coefficient compared to GCaMP3 during the *in vitro* analysis. Interestingly, the 90G mutation has also recently been assessed by another group (Akerboom et al, in press) and found it to increase calcium affinity. Furthermore, the same study indicated that two other mutations (D78Y located in the linker region of CaM and an A to V mutation at position 12 of the M13 peptide) also increase the calcium affinity of GCaMP (Akerboom et al, in press). These mutations are excellent candidates to use in combination with the mutations of our current high calcium affinity sensor to generate an additional GCaMP3 variant that would likely exhibit a further increase in its calcium affinity. This new GCaMP variant could then be applied to report changes in basal or resting calcium concentrations in neurons at rest. Fused to another fluorescent protein with clearly distinct excitation and emission spectra, such as mCherry, a high-affinity GCaMP variant could be engineered into a ratiometric sensor that would also allow an absolute measurement of basal calcium concentrations, enabling comparisons of resting calcium concentrations between populations of neurons or between subcellular compartments.

4.2.2 Improvement of the Signal-to-Noise Ratio with which GCaMPs Detect Small Calcium Transients

Although our GC3_K21A_K77G_N97D construct appears to be adequately altered to detect small calcium transients, it may be of interest to further improve the SNR of the sensor to ensure the detection of fast calcium transients. GCaMPs currently in use, including our high calcium affinity variant, still have a low SNR compared to that of synthetic calcium dyes. Previous approaches to increase SNR of GCaMPs for action potential-evoked calcium transients have mainly focused on increasing, the fraction of correctly folded and monomeric, functional sensor (Akerboom et al, 2009; Muto et al, 2011), its dynamic range (Tian et al, 2009; Zhao et al, 2011b; Akerboom et al, in press) and its calcium affinity as well as its Hill coefficient (our work; Akerboom et al, in press). However, of equal or possibly more importance for optimizing the SNR may be improving the calcium binding kinetics of GCaMP3. As previously discussed, the SNR increase for the K21A mutation may be due to altered calcium binding kinetics. This finding suggests that basic residues at position 2, and possibly at other positions within the EF motifs of calmodulin, affect the kinetics calcium binding, presumably due to electrostatic repulsion of calcium cations, Based on this hypothesis, two basic residues in EF motifs, lysine 94 at position 2 of EF motif III and lysine 30 at position 11 of EF motif I, may also affect calcium binding kinetics. Consequently, mutations in these positions, K30A and K94A, which have already been characterized *in vitro* in calcium titration experiments, should be analyzed for their effect on SNR for small action potential-evoked calcium transients in neurons.

In addition to basic residues in EF motifs, amino acid side chains in the interdomain linker of calmodulin may also affect the SNR of the sensor for small calcium transients. In the recent study by Akerboom and co-workers, the R90G mutation within the linker region of CaM was shown to not only increase the calcium affinity of GCaMP, as discussed above, but also increase the SNR of the optimized GCaMP in which it appeared by an unknown mechanism (Akerboom et al, in press). This mutation would also be interesting to test in neurons in combination of the mutations identified by us. Finally, a more thorough approach to further improve the SNR of GCaMP to action potential-evoked would be to perform a random mutagenesis screening on either CaM or on the entire GCaMP protein to identify mutations that improve the kinetics of GCaMP3, rather than calcium affinity or dynamic range. Mutant GCaMPs that demonstrate faster rise times of fluorescence responses to isolated action potentials or small bursts of action potentials could be identified in neurons in a medium throughput approach in multiple rounds of mutagenesis and selection. In order to accurately assess the possible altered kinetics conferred by mutations, a faster image acquisition rate would be required than what was performed in this study. In addition, targeting of the GECI to calcium microdomains where the diffusion of calcium does not contribute to the delayed rise time of the sensor would also be ideal to measure the altered kinetics of the GCaMP variants for attaining an improved SNR sensor that accurately detects fast calcium transients.

4.2.3 Further Improvements of Low Calcium Affinity Sensors

The affinities of our low calcium affinity sensors are, at 3 and 12 μM, ideal to investigate large calcium transients in the cytosol of excitable cells. Measurement of calcium in organelles, such as the ER and lysosomes, may require even further lower

affinity sensors, which could be accomplished by the combination of multiple position 12 mutations, but are not desired for our purposes. Further useful improvements, however, could be related to an increased dynamic range of the sensor. In this respect, mutations performed by Zhao and co-workers in their attempts to optimize the GECI identified additional mutations that led to an approximately a two-fold increase in dynamic range compared to GCaMP3 (Zhao et al, 2011b). These mutations resulted in a construct they termed G-GECO1 and included two residue substitutions in the cpEGFP (K119I and L173Q) and two in the CaM component of the sensor (S101G, position 9 of EF motif III; and E127V which is between EF motifs III and IV). Their inclusion in our low calcium affinity sensor could possibly improve its dynamic range when used in neurons. Furthermore, D 78Y, a mutation in the interdomain linker identified by Akerboom et al, (in press) increased the dynamic range of GCaMP3 and would also be a suitable candidate to increase the dynamic range of the low calcium affinity GCaMP variants.

Secondly, it may be advantageous for some applications, such as the use of low calcium affinity sensors in calcium micro- and nanodomains, to optimize the kinetics of these sensors in similar fashion to the optimization of the SNR of the high calcium affinity sensor. Thus, the K21A mutant may increase the on-rate of calcium binding and make the low-affinity sensors more suitable for the detection of large, but extremely fast calcium transients. A third possibility for improving the low affinity sensors would be to perform mutations that make the GCaMP variants less pH-sensitive. GCaMP3 and earlier GCaMP versions are extremely pH sensitive and almost entirely quenched in their fluorescence at pH 6. Large calcium transients often occur in conjugation with noticeable pH changes in the cytosol, such as during ischemia, and it may be desirable for some

applications to have GCaMPs that are much less sensitive to a drop in pH. Some GECO variants developed by Zhao and colleagues (2011b), such as B-GECO1, are much more pH-insensitive and only slightly quenched at a pH value of 6 (approximately 20%). Therefore, the mutations performed to create the low affinity calcium sensors could be introduced into B-GECO to obtain largely pH-insensitive calcium sensors.

4.3 APPLICATIONS FOR GCAMP3 AFFINITY VARIANTS

4.3.1 Measurement of Action Potential-Evoked Presynaptic Calcium Transients

We are interested in examining the long-term regulation of presynaptic calcium transients and molecular mechanisms that lead to sustained changes in presynaptic calcium influx. GECIs have several advantages over synthetic calcium indicator dyes for the observation of axonal calcium transients. The use of GECIs, for example, is less invasive than techniques involving loading of indicator dyes through a patch pipette, and does not suffer from dye leakage during prolonged experiments. Furthermore, whereas indicator dyes are difficult to target to presynaptic localizations and are limited to recording calcium within a single or only a few cells, GECIs circumvent these issues. In fact, several recent studies have used previous versions of GCaMP targeted to presynaptic specializations to report action potential-evoked presynaptic calcium conductances (Dreosti et al, 2009, Zhao et al, 2011a). However, the previous versions of GCaMP used in these studies had a relatively low SNR. As a consequence, calcium transients elicited by isolated action potentials could be detected only at a small subset of large and efficacious synapses. Our new calcium affinity sensors could be applied in two

ways to detect small calcium transients at these sites. The high calcium affinity sensor, GC3_K21A_K77G_N97D, is more sensitive than previous versions of GCaMP, making it suitable to accurately measure small calcium transients in the cytosol. A second fluorescent marker, such as the active zone cytomatrix protein bassoon labelled with tdTomato, could be used in conjunction to identify synapses. In an alternative approach, the low calcium affinity sensors generated by this study can be targeted to calcium micro- and nanodomains by fusing them with active zone cytomatrix proteins such as bassoon or VGCCs. For this second approach, it would be ideal to use a low calcium affinity sensor with fast kinetics as such sensors would be insensitive to calcium diffusing into presynaptic specializations from adjacent synapses while responding maximally to the fast and large calcium transients likely encountered at presynaptic locations. Our preliminary results and work from other groups (Dreosti et al, 2009, Zhao et al, 2011a, Tay et al, 2012) suggests that both strategies are feasible and can be used to investigate the mechanisms of long-term changes of calcium transients at synapses.

4.3.2 "Mapping" of Calcium Micro- and Nanodomains

A second application for our newly generated GCaMP3 variants would be to utilize the lower calcium affinity sensors to "map" the spatial extent of calcium micro- and nanodomains. Calcium signals at presynaptic specializations are extremely inhomogeneous and it is known that calcium transients in micro- or nanodomains provide the signal required for synaptic vesicle fusion to release neurotransmitters (Südhof, 1995). However, the exact spatial extent of these domains remains elusive. Low calcium affinity sensors could be applied in a systematic fashion to report or "map" the spatially defined calcium micro- and nanodomain regions. For this purpose N- and P/Q-type

VGCCs, cytomatrix proteins that anchor these channels, such as RIM and RIM-BP (Kaeser et al, 2011, Hibino et al, 2002), and active zone cytomatrix proteins located at likely increasing distances from the calcium influx source, such as Munc13, Bassoon, or Piccolo, could be tagged with GCaMPs of varying affinities. Theoretically, the calcium signals would depend on their distance from the calcium channels, with low-affinity sensors only providing signals in response to isolated stimuli if they are present in nanodomains. As a possible technical challenge, current low affinity calcium sensors may exhibit kinetic properties that are insufficient to detect large, but potentially short-lived calcium transients. Therefore, it may be necessary to improve the kinetic properties of our low affinity sensors. The information gathered from this systematic application of the low affinity calcium sensors as well as our knowledge about protein-protein interactions between VGCCs and active zone cytomatrix proteins and interactions among cytomatrix scaffolding proteins, could be used to gather important information about the spatiotemporal extent of calcium nanodomain and spatial restrictions of calcium signalling at presynaptic specializations.

4.3.3 Compartmentalization of Calcium Homeostasis in Neurons at Rest and Under Conditions of Sustained Calcium Influx

Another interesting application of these calcium sensors would be to determine the compartmentalization of calcium across a neuron as a whole. As outlined in the previous section, calcium signalling elicited by isolated action potentials or synaptic activation is known to be highly compartmentalized and limited to a small cytosolic volume around open voltage-gated calcium channels or calcium-conducting ligand-gated channels. It is unclear, however, whether the compartmentalization of calcium signals

persists under conditions of sustained calcium influx due to persistent depolarization or ongoing exposure to ligands activating calcium conductances, Moreover, it is unknown whether basal cytosolic calcium concentrations in the absence of depolarizing stimuli or ligands that activate calcium conductances are regulated globally or locally, allowing for independent regulation of basal calcium concentrations, for example, in somatodendritic and axonal compartments. The low- and high-affinity sensors we have developed could be used to quantify calcium elevations in neurons in response to sustained activation high frequency trains of stimuli. This approach would allow us to address whether sustained calcium influx through plasma membrane calcium conductances whose distribution is often highly polarized (e.g. NMDA-type glutamate receptors and L-type calcium channels in the somatodendritic domain) affect calcium concentrations only in the respective compartment or whether saturation of extrusion mechanisms leads to significant "spillover" of calcium in the adjacent compartment. A sensor with extremely high calcium affinity (50 to 100 nM range), coupled to a second fluorescent protein for ratiometric imaging could be used to determine if the basal calcium concentrations in somatodendritic and axonal compartments of visually identified neurons are equal and, if so, if they are differentially susceptible to pharmacological manipulation of individual calcium conductances and transporters with polarized distribution in neurons, such a T-type calcium channels and calcium pumps in the smooth endoplasmic reticulum (SERCA). This application would especially be interesting for the investigation of neurodegenerative diseases in which chronic elevations in calcium could play a major role.

REFERENCES

Akerboom J, Rivera JDV, Guilbe MMR, Malave ECA, Hernandez HH, Tian L, Hires SA, Marvin JS, Looger LL, and Schreiter ER (2009) Crystal structures of the GCaMP calcium sensor reveal the mechanism of fluorescent signal change and aid rational design. *J Biol Chem*. 284: 6455-64.

Akerboom J, Chen TW, Wardill TJ, Tian L, Marvin JS, Mutlu S, Calderón NC, Esposti F, Borghuis BG, Sun XR, Gordus A, Orger MB, Portugues R, Engert F, Macklin JJ, Filosa A, Aggarwal A, Kerr R, Takagi R, Kracun S, Shigetomi E, Khakh BS, Baier H, Lagnado L, Wang SS, Bargmann CI, Kimmel BE, Jayaraman V, Svoboda K, Kim DS, Schreiter ER, and Looger LL (in press) Optimization of a GCaMP calcium indicator for neural activity imaging. *J Neurosci.*

Baimbridge KG, Celio MR, and Rogers JH (1992) Calcium-binding proteins in the nervous system. *Trends Neurosci.* 15: 303-8.

Baird GS, Zacharias DA, and Tsien RY (1999) Circular permutation and receptor insertion within green fluorescent proteins. *Proc. Natl. Acad. Sci. USA*. 96: 11241-46.

Becker PL and Fay FS (1987) Photobleaching of fura-2 and its effect on determination of calcium concentrations. *Am. J. Physiol.* 253: C613-8.

Berridge MJ (1993) Inositol trisphosphate and calcium signaling. *Nature* 361: 315-25.

Berridge MJ (1998) Neuronal calcium signaling. *Neuron.* 21: 13-26.

Bers DM, Patton CW, and Nuccitelli R (2010) A practical guide to the preparation of Ca^{2+} buffers. *Methods Cell Biol.* 99: 1-26.

Bianchi K, Rimessi A, Prandini A, Szabadkai G, and Rizzuto R (2004) Calcium and mitochondria: mechanisms and functions of a troubled relationship. *Biochim. Biophys. Acta.* 1742: 119-31.

Birnboim HC and Doly J (1979) A rapid alkaline extraction procedure for screening recombinant plasmid DNA. *Nucleic Acids Res.* 7: 1513-23.

Borghuis BG, Tian L, Xu Y, Nikonov SS, Vardi N, Zemelman BV, and Looger LL (2011) Imaging Light Responses of Targeted Neuron Populations in the Rodent Retina. *J. Neurosci.* 31:2855-67.

Brownlee C (2000) Cellular calcium imaging: so, what's new? *Trends Cell Biol*. 10: 451-57.

Catteral WA (2000) Structure and regulation of voltage-gated Ca^{2+} channels. *Annu. Rev. Cell Dev. Biol.* 16: 521-55.

Celio MR (1990) Calbindin D-28k and parvalbumin in the rat nervous system. *Neurosci.* 35: 375-475.

Chad JE and Eckert R (1984) Calcium domains associated with individual channels can account for anomalous voltage relations of Ca-dependent responses. *Biophys J.* 45: 993-99.

Chalasani SH, Chronis N, Tsunozaki M, Gray JM, Ramot D, Goodman MB and Bargmann CI (2007) Dissecting a circuit for olfactory behaviour in *Caenorhabditis elegans*. *Nature* 450: 63-70.

Cheung WY (1970) Cyclic 3`, 5`-nucleotide phosphodiesterase: demonstration of an activator. *Biochem. Biophys. Res. Commun.* 38: 533-38.

Clapham DE (1995) Calcium Signalling. *Cell* 80: 259-68.

Di Virgilio F, Fasolato C, and Steinberg TH (1988) Inhibitors of membrane transport system for organic anions block fura-2 excretion from PC12 and N2A cells. *Biochem. J.* 256: 959-63.

Di Virgilio F, Steinberg TH, and Silverstein SC (1990) Inhibition of fura-2 sequestration and secretion with organic anion transport blockers. *Cell Calcium* 11: 57-62.

Dombeck DA, Harvey CD, Tian L, Looger LL, and Tank DW (2010) Functional imaging of hippocampal place cells at cellular resolution during virtual navigation. *Nat. Neurosci.* 13: 1433-40.

Dreosti E, Odermatt B, Dorostkar MM, and Lagnado L (2009) A genetically encoded reporter of synaptic activity *in vivo*. *Nat. Methods* 6: 883-89.

Edmonds B, Reyes R, Schwaller B, and Roberts WM (2000) Calretinin modifies presynaptic calcium signaling in frog saccular hair cells. *Nat. Neurosci.* 3: 786-90.

Faga LA, Sorensen BR, VanScyoc WS, and Shea MA (2003) Basic interdomain boundary residues in calmodulin decrease calcium affinity of sites I and II by stabilizing helix-helix interactions. *Proteins* 50: 381-91.

Filippin L, Abad MC, Gastaldello S, Magalhães PJ, Sandonà D, and Pozzan T (2005) Improved strategies for the delivery of GFP-based Ca^{2+} sensors into the mitochondrial matrix. *Cell Calcium*. 37: 129-36.

Gao ZH, Krebs J, VanBerkum MF, Tang WJ, Maune JF, Means AR, Stull JT, and Beckingham K (1993) Activation of four enzymes by two series of calmodulin mutants with point mutations in individual Ca^{2+} binding sites. *J. Biol. Chem.* 268: 20096-104.

Garaschuk O, Griesbeck O, and Konnerth A (2007) Troponin C-based biosensors: A new family of genetically encoded indicators for *in vivo* calcium imaging in the nervous system. *Cell Calcium.* 42: 351-61.

Garaschuk O, Yaari Y, and Konnerth A (1997). Release and sequestration of calcium by ryanodine-sensitive stores in rat hippocampal neurons. *J. Physiol.* 502: 13-30.

Griesbeck O, Baird GS, Campbell RE, Zacharias DA, and Tsien RY (2001) Reducing the environmental sensitivity of yellow fluorescent protein. *J. Biol. Chem.* 276: 29188-94.

Hasan MT, Friedrich RW, Euler T, Larkum ME, Giese G, Both M, Duebel J, Waters J, Bujard H, Griesbeck O, Tsien RY, Nagai T, Miyawaki A, and Denk W (2004) Functional fluorescent Ca^{2+} indicator proteins in transgenic mice under TET control. *PLoS Biol.*2: e163.

Heidelberger R, Heinemann C, Neher E, and Matthews G (1994) Calcium dependence of the rate of exocytosis in a synaptic terminal. *Nature* 371: 513-15.

Heim N and Griesbeck O (2004) Genetically encoded indicators of cellular calcium dynamics based on troponin C and green fluorescent protein. *J. Biol. Chem.* 279: 14280-86.

Heim N, Garaschuk O, Friedrich MW, Mank M, Milos R I, Kovalchuk Y, Konnerth A, and Griesbeck O (2007) Improved calcium imaging in transgenic mice expressing a troponin C-based biosensor. *Nat. Method* 4, 127–129.

Hibino H, Pironkova R, Onwumere O, Vologodskaia M, Hudspeth AJ, and Lesage F (2002) RIM binding proteins (RBPs) couple Rab3-interacting molecules (RIMs) to voltage-gated Ca^{2+} channels. *Neuron* 34: 411-23.

Higashijima S, Masino MA, Mandel G, and Fetcho JR (2003) Imaging neuronal activity during zebrafish behavior with a genetically encoded calcium indicator. *J. Neurophysiol.* 90: 3986-97.

Higley MJ and Sabatini BL (2008) Calcium signaling in dendrites and spines: practical and functional considerations. *Neuron* 59: 902-13.

Jaffe DB, Johnston D, Lasser-Ross N, Lisman JE, Miyakawa H, and Ross WN (1992) The spread of Na^{+} spikes determines the pattern of dendritic Ca^{2+} entry into hippocampal neurons. *Nature*. 357: 244-46

Ji G, Feldman M, Deng KY, Greene KS,Wilson J, Lee J, Johnston R, Rishniw M, Tallini Y, Zhang J,WierWG, Blaustein MP, Xin HB, Nakai J & Kotlikoff MI (2004). Ca2+-sensing transgenic mice: postsynaptic signaling in smooth muscle. *J Biol Chem* 279, 21461–68.

Kaeser PS, Deng L, Wang Y, Dulubova I, Liu X, Rizo J, and Südhof TC (2011) RIM proteins tether Ca^{2+} channels to presynaptic active zones via a direct PDZ-domain interaction. *Cell* 144: 282-95.

Kasai H (1993) Cytosolic Ca2+ gradients, Ca2+ binding proteins and synaptic plasticity. *Neurosci Res.* 16:1-7.

Kerr R, Lev-Ram V, Baird G, Vincent P, and Tsien RY (2000) Optical imaging of calcium transients in neurons and pharyngeal muscle of *C. elegans*. *Neuron.* 26: 583-94.

Klee CB and Vanaman TC (1982) Calmodulin. *Advances in Prot. Chem.* 35: 213-321.

Knopfel T, Lin MZ, Levskaya A, Tian L, Lin JY, and Boyden ES (2010) Toward the second generation of optogenetic tools. *J. Neurosci.* 30: 14998-15004.

Kostyuk P and Verkhratsky A (1994). Calcium stores in neurons and glia. *Neurosci.* 63: 381-404.

Kotlikoff MI (2007) Genetically encoded Ca^{2+} indicators: using genetics and molecular design to understand complex physiology. *J. Physiol.* 578: 55-67.

Kuboniwa H, Tjandra N, Grzesiek S, Ren H, Klee CB, and Bax A (1995) Solution structure of calcium-free calmodulin. *Nat. Struct. Biol.* 2: 768-76.

Kuhn B, Ozden I, Lampi Y, Hasan MT, and Wang SS (2012) An amplified promoter system for targeted expression of calcium indicator proteins in the cerebellar cortex. *Front. Neural Circuits.* 6 – Epub.

Llinás R, Sugimori M, and Silver RB (1992) Microdomains of high calcium concentration in a presynaptic terminal. *Science* 256: 677-79.

Looger LL and Griesbeck O (2011) Genetically encoded neural activity indicators. *Curr. Opin. Neurobiol.* 22:1-6.

Malgaroli AD, Milani JM, and Pozzan T (1987) Fura-2 measurement of cytosolic free Ca^{2+} in monolayers and suspensions of various types of animal cells. *J. Cell Biol.* 105: 2145-55.

Mank M and Griesbeck O (2008) Genetically encoded calcium indicators. *Chem. Rev.* 108: 1550-64.

Mank M, Reiff DF, Heim N, Friedrich MW, Borst A, and Griesbeck O (2006) FRET-Based calcium biosensor with fast signal kinetics and high fluorescence change. *Biophys. J.* 90: 1790-96.

Mao T, O`Connor DH, Scheuss V, Nakai J, and Svoboda K (2008) Characterization and subcellular targeting of GCaMP-type genetically-encoded calcium indicators. *PLoS One.* 3: e1796.

Maravall M, Mainen ZF, Sabatini BL, and Svoboda K (2000) Estimating intracellular calcium concentrations and buffering without wavelength ratioing. *Biophys J.* 78: 2655-67.

Marsden BJ, Shaw GS, and Sykes BD (1990) Calcium binding proteins. Elucidating the contributions to calcium affinity from an analysis of species variants and peptide fragments. *Biochem. Cell Biol.* 68: 587-601.

Maune JF, Klee CB, and Beckingham K (1992) Ca^{2+} binding and conformational change in two series of point mutations to the individual Ca^{2+}-binding sites of calmodulin. *J. Biol. Chem.* 267: 5286-95.

McDonough PM and Button DC (1989) Measurement of cytoplasmic calcium concentration in cell suspensions: correction for extracellular Fura-2 through use of Mn^{2+} and probenecid. *Cell Calcium* 10: 171-80.

Mittmann W, Wallace DJ, Czubayko U, Herb JT, Schaefer AT, Looger LL, Denk W, and Kerr JN (2011) Two-photon calcium imaging of evoked activity from L5 somatosensory neurons in vivo. *Nat. Neurosci.* 14: 1089-93.

Miyawaki A, Griesbeck O, Heim R & Tsien RY (1999). Dynamic and quantitative Ca2+ measurements using improved cameleons. *Proc. Natl. Acad. Sci. USA* 96, 2135–40.

Miyawaki A, Llopis J, Heim R, McCaffery JM, Adams JA, Ikura M, and Tsien RY (1997) Fluorescent indicators for Ca^{2+} based on green fluorescent proteins and calmodulin. *Nature* 388: 882-27.

Müller W and Connor JA (1991) Dendritic spines as individual neuronal compartments for synaptic Ca^{2+} responses. *Nature*. 354: 73-76.

Munsch T and Deitmer JW (1995) maintenance of fura-2 fluorescence in glial cells and neurones of the leech central nervous system. *J. Neurosci. Methods* 57: 195-204.

Muto A, Ohkura M, Kotani T, Higashijima S, Nakai J, and Kawakami K (2011) Genetic visualization with an improved GCaMP calcium indicator reveals spatiotemporal activation of the spinal motor neurons in zebrafish. *Proc Natl Acad Sci USA*. 108: 5425-30.

Nagai T, Sawano A, Park ES, and Miyawaki A (2001) Circularly permuted green fluorescent proteins engineered to sense Ca^{2+}. *Proc Natl Acad Sci USA*. 98: 3197-3202.

Nagai T, Yamada S, Tominaga T, Ichikawa M, and Miyawaki A (2004) Expanded dynamic range of fluorescent indicators for Ca^{2+} by circularly permuted yellow fluorescent proteins. *Proc. Natl. Acad. Sci. USA*. 101: 10554-59.

Nakai J, Ohkura M, and Imoto K (2001) A high signal-to-noise Ca^{2+} probe composed of a single green fluorescent protein. *Nat. Biotechnol.* 19: 137-41.

Nakajima K, Harada K, Ebina Y, Yoshimura T, Ito H, Ban T, and Shingai R (1993) Relationship between resting cytosolic Ca21 and responses induced by *N*-methyl D-aspartate in hippocampal neurons. *Brain Res.* 603:321–23.

Neher E (1998) Vesicle pools and Ca^{2+} microdomains: New tools for understanding their roles in neurotransmitter release. *Neuron* 20: 389-99.

Ohkura M, Matsuzaki M, Kasai H, Imoto K, and Nakai J (2005) Genetically encoded bright Ca^{2+} probe applicable for dynamic Ca^{2+} imaging of dendritic spines. *Anal. Chem.* 77: 5861-69.

Palmer AE, Giacomello M, Kortemme T, Hires SA, Lev-Ram V, Baker D, and Tsien RY (2006) Ca^{2+} indicators based on computationally redesigned calmodulin-peptide pairs. *Chem. Biol.* 13: 521-30.

Palmer AE, Jin C, Reed JC, and Tsien RY (2004) Bcl-2-mediated alterations in endoplasmic reticulum Ca^{2+} analyzed with an improved genetically encoded fluorescent sensor. *Proc. Natl. Acad. Sci. USA.* 101: 17404-49.

Paredes RM, Etzler JC, Watts LT, Zheng W, and Lechleiter JD (2008) Chemical calcium indicators. *Methods* 46: 143-51.

Pologruto TA, Yasuda R, and Svoboda K (2004) Monitoring neural activity and [Ca^{2+}] with genetically encoded Ca^{2+} indicators. *J. Neurosci.* 24: 9572-9.

Procyshyn RM and Reid RE (1994a) A structure/activity study of calcium affinity and selectivity using a synthetic peptide model of the helix-loop-helix calcium-binding motif. *J. Biol. Chem.* 269: 1641-47.

Procyshyn RM and Reid RE (1994b) An examination of glutamic acid in the –X chelating position of the helix-loop-helix calcium binding motif. *Arch. Biochem. Biophys.* 311: 425-29.

Reid and Procyshyn (1995) Engineering magnesium selectivity in the helix-loop-helix calcium-binding motif. *Arch. Biochem. Biophys.* 323: 115-19.

Reiff DF, Ihring A, Guerrero G, Isacoff EY, Joesch M, Nakai J, and Borst A (2005) *In vivo* performance of genetically encoded indicators of neural activity in flies. *J. Neurosci.* 25: 4766-78.

Reuter H and Porzig H (1995) Localization and functional significance of the Na^{+}/Ca^{2+} exchanger in presynaptic boutons of hippocampal cells in culture. *Neuron* 15: 1077-84.

Rhoads AR and Friedberg F (1997) Sequence motifs for calmodulin recognition. *FASEB J.* 11: 331-40.

Roberts WM, Jacobs RA, and Hudspeth AJ (1990) Colocalization of ion channels involved in frequency selectivity and synaptic transmission at presynaptic active zones of hair cells. *J. Neurosci.* 10: 3664-84.

Rocheforte NL, Jia H, and Konnerth A (2008) Calcium imaging in the living braing: prospects for molecular medicine. *Trends Mol. Med.* 14: 389-99.

Romoser VA, Hinkle PM, and Persechini A (1997) Detection in living cells of Ca^{2+}-dependent changes in the fluorescence emission of an indicator composed of two green fluorescent protein variants linked by a calmodulin-binding sequence. *J. Biol. Chem.* 272: 13270-74.

Schlatterer C, Knoll G, and Malchow D (1992) Intracellular calcium during chemotaxis of *Dictyostelium descoideum*: a new fura-2 derivative avoids sequestration of the indicator and allows long-term calcium measurements. *Eur. J. Cell Biol.* 58: 172-81.

Schneggenburger R, Meyer AC, and Neher E (1999) Released fraction and total size of a pool of immediately available transmitter quanta at a calyx synapse. *Neuron* 23: 399-409.

Seelig JD, Chiappe ME, Lott GK, Dutta A, Osborne JE, Reiser MB and Jayaraman V (2010) Two-photon calcium imaging from head-fixed *Drosophila* during optomotor walking behavior. *Nat. Methods.* 7: 535-40.

Shigetomi E, Kracun S, and Khakh BS (2010) Monitoring astrocyte calcium microdomains with improved membrane targeted GCaMP reporters. *Neuron Glia Biol.* 6: 183-91.

Simpson PB, Challis RAJ, and Nahorski SR (1995). Neuronal Ca^{2+} stores: activation and function. *Trends Neurosci.* 18: 299-306.

Sorensen BR, Faga LA, Hultman R, and Shea MA (2002) An interdomain linker increases the thermostability and decreases the calcium affinity of the calmodulin N-domain. *Biochem.* 41: 15-20.

Spafford JD and Zamponi GW (2003) Functional interactions between presynaptic calcium channels and the neurotransmitter release machinery. *Curr. Opin. Neurobiol.* 13: 308-14.

Stanley EF and Atrakchi AH (1990) Calcium currents recorded from a vertebrate presynaptic nerve terminal are resistant to the dihydropyridine nifedipine. *Proc Natl Acad Sci USA.* 87**:** 9683-7.

Starovasnik MA, Su D, Beckingham K, and Klevit R (1992) A series of point mutations reveal interactions between the calcium-binding sites of calmodulin. *Protein Sci.* 1: 245-53.

Steinberg SF, Bilezikian JP, and Al-Aqwati AL (1987) Fura-2 fluorescence is localized to mitochondria in endothelial cells. *Am. J. Physiol.* 253: C744-7.

Südhof TC (1995) The synaptic vesicle cycle: a cascade of protein-protein interactions. *Nature*. 375: 645-53.

Takahashi A, Camacho P, Lechleiter JD, and Herman B (1999) Measurement of intracellular calcium. *Physiol Rev*. 79: 1089-1125.

Tay LH, Dick IE, Yang W, Mank M, Griesbeck O, and Yue DT (2012) Nanodomain Ca^{2+} of Ca^{2+} channels detected by a tethered genetically encoded Ca^{2+} sensor. *Nat. Commun.* 3: Article 778.

Tallini YN, Ohkura M, Choi BR, Ji G, Imoto K, Doran R, Lee J, Plan P, Wilson J, Xin HB, Sanbe A, Gulick J, Mathai J, Robbins J, Salama G, Nakai J, and Kotlikoff MI (2006) Imaging cellular signals in the heart *in vivo*: Cardiac expression of the high-signal Ca^{2+} indicator GCaMP2. *Proc Natl Acad Sci USA.*103: 4753-58.

Tian L, Hires SA, Mao T, Huber D, Chiappe ME, Chalasani SH, Petreanu L, Akerboom J, McKinney SA, Schreiter ER, Bargmann CI, Jayaraman V, Svoboda K, and Looger L (2009) Imaging neural activity in worms, flies and mice with improved GCaMP calcium indicators. *Nat. Methods*. 6: 875-81.

Truong K, Sawano A, Mizuno H, Hama H, Tong KI, Mal TK, Miyawaki A & Ikura M (2001). FRET-based in vivo Ca2+ imaging by a new calmodulin-GFP fusion molecule. *Nat Struct Biol* 8, 1069–73.

Tsalkova TN and Privalov PL (1985) Thermodynamic study of domain organization in troponin C and calmodulin. *J. Mol. Biol.* 181: 533-44.

Tsien RW and Tsien RY (1990) Calcium channels, stores, and oscillations. *Annu Rev Cell Biol*. 6: 715-60.

VanScyoc WS, Sorensen BR, Rusinova E, Laws WR, Ross JB, and Shea MA (2002) Calcium binding to calmodulin mutants monitored by domain-specific intrinsic phenylalanine and tyrosine fluorescence. *Biophys. J.* 83: 2767-80.

Wallace DJ, zum Alten Borgloh SM, Astori S, Yang Y, Bausen M, Kügler S, Palmer AE, Tsien RY, Sprengel R, Kerr JND, Denk W and Hasan MT (2008) Single-spike detection *in vitro* and *in vivo* with a genetic Ca^{2+} sensor. *Nat. Methods* 5: 797-804.

Wang Q, Shui B, Kotlikoff MI, and Sondermann H (2008) Structural basis for calcium sensing by GCaMP2. *Structure* 16: 1817-27.

Wu X and Reid RE (1997a) Conservative D133E mutation of calmodulin site IV drastically alters calcium binding and phosphodiesterase regulation. *Biochem.* 36: 3608-16.

Wu X and Reid RE (1997b) Structure/Calcium affinity relationships of site III of calmodulin: Testing acid pair hypothesis using calmodulin mutants. *Biochem.* 36: 8649-56.

Ye Y, Lee HW, Yang W, Shealy S, and Yang JJ (2005) Probing site-specific calmodulin calcium and lanthanide affinity by grafting. *J. Am. Chem. Soc.* 127: 3743-50.

Zacharias DA, Violin JD, Newton AC, and Tsien RY (2002). Partitioning of lipid-modified monomeric GFPs into membrane microdomains of live cells. *Science.* 296: 913-16.

Zhao CJ, Dreosti E, and Lagnado L (2011a) Homeostatic synaptic plasticity through changes in presynaptic calcium influx. *J. Neurosci.* 31: 7492-96.

Zhao Y, Araki S, Wu J, Teramoto T, Chang YF, Nakano M, Abdelfattah AS, Fujiwara M, Ishihara T, Nagai T, and Campbell RE (2011b) An expanded palette of genetically encoded Ca^{2+} indicators. *Science* 333: 1888-91.

APPENDIX A: PRIMER SEQUENCES

EF Motif I Mutations	Primer Name	Sequence	SDM TYPE
K21A	GC3_22_F	GACGGGGATGGGACAATAACAACC	E
	GC3_K21A_R	GGCGTCAAATAGGGAGAAAGCCTCTTTAAATTCTG	
D22N	GC3_22N24DN_F	AACGGGRATGGGACAATAACAACC	E
	GC3_21_R	CTTGTCAAATAGGGAGAAAGCCTCTTTAAATTC	
D24N	GC3_D24N_F	AATGGGACAATAACAACCAAGGAGC	E
	GC3_23_R	CCCGTCCTTGTCAAATAGGGAGAAAG	
T28DE	GC3_T28DE_F	GAWACCAAGGAGCTGGGGACG	E
	GC3_27_R	TATTGTCCCATCCCCGTCCTTG	
K30AE	GC3_K30AE_F	GMGGAGCTGGGGACGGTGATG	E
	GC3_29_R	GGTTGTTATTGTCCCATCCCCGTC	
E31Q	GC3_E31Q_F	CAGCTGGGGACGGTGATGCGGTC	E
	GC3_30_R	CTTGGTTGTTATTGTCCCATCCCCGTC	
EF Motif II Mutations	**Primer Name**	**Sequence**	**SDM TYPE**
D58N	GC3_59_F	ACGGTGACGGCACAATCGAC	E
	GC3_D58N_R	TGGCATCTACTTCATTGATCATGTCCTG	
N60D	GC3_D60N_F	AACGGCACAATCGACTTCCCTG	E
	GC3_59_R	ACCGTCGGCATCTACTTCATTGATC	
D64NST	GC3_D64NST_F	AVCTTCCCTGAGTTCCTGACAATGATGG	E
	GC3_63_R	GATTGTGCCGTCACCGTCG	
E67Q	GC3_E67Q_F	CAGTTCCTGACAATGATGGCAAGAAAAATG	E
	GC3_66_R	AGGGAAGTCGATTGTGCCGTC	
EF Motif III Mutations	**Primer Name**	**Sequence**	**SDM TYPE**
K94AEV	GC3_95_F	GATGGCAATGGCTACATCAGTGCAG	E
	GC3_K94AEV_R	CDCATCAAACACACGGAACGCTTCTC	
D95N	CaM_D95N_F	AATGGCAATGGCTACATCAGTGC	E
	CaM_94_R	CTTATCAAACACACGGAACGCTTCTC	
N97D	CaM_N97D_F	GTGTTTGATAAGGATGGCGATGGCTACATCAGTGCAG	C
	CaM_N97D_R	CTGCACTGATGTAGCCATCGCCATCCTTATCAAACAC	
S101D	CaM_S101D_F	GGATGGCAATGGCTACATCGATGCAGCAGAGCTTCGCCAC	C
	CaM_S101D_R	GTGGCGAAGCTCTGCTGCATCGATGTAGCCATTGCCATCC	
E104Q	GC3_E104Q_F	CAGCTTCGCCACGTGATGACAAACC	E
	GC3_103_R	TGCTGCACTGATGTAGCCATTG	

EF Motif IV Mutations	Primer Name	Sequence	SDM TYPE
D131N	CaM_D131N_F	CAGGGAAGCAGACATCAATGGGGATGGTCAGG	C
	CaM_D131N_R	CCTGACCATCCCCATTGATGTCTGCTTCCCTG	
D133N	CaM_D133N_F	GAAGCAGACATCGATGGGAATGGTCAGGTAAACTACG	C
	CaM_D133N_R	CGTAGTTTACCTGACCATTCCCATCGATGTCTGCTTC	
E139A	GC3_E139A_F	GCAGAGTTTGTACAAATGATGACAGCGAAG	E
	GC3_138_R	GTAGTTTACCTGACCATCCCCATCG	
E140Q	GC3_E140Q_F	CAGTTTGTACAAATGATGACAGCGAAGTAAAAGC	E
	GC3_139_R	TTCGTAGTTTACCTGACCATCCCCATC	
Linker Mutations	**Primer Name**	**Sequence**	**SDM TYPE**
R74AG	GC3_R74AG_F	GSCAAAATGAAAGACACAGACAGTGAAGAAG	E
	GC3_73_R	TGCCATCATTGTCAGGAACTCAG	
K75AG	GC3_K75AG_F	GSAATGAAAGACACAGACAGTGAAGAAGAAATTAG	E
	GC3_74_R	TCTTGCCATCATTGTCAGGAACTC	
K77AG	GC3_K77AG_F	GSAGACACAGACAGTGAAGAAGAAATTAGAGAAG	E
	GC3_76_R	CATTTTTCTTGCCATCATTGTCAGGAACTC	
K75AG, K77G	GC3_75AG77G_F	GSAATGGGAGACACAGACAGTGAAG	E
	GC3_74_R	TCTTGCCATCATTGTCAGGAACTC	
D80GR	GC3_81_F	AGTGAAGAAGAAATTAGAGAAGCGTTCC	E
	GC3_D80GR_R	CCYTGTGTCTTTCATTTTTCTTGCCATCATTG	
D84GR	GC3_85_F	ATTAGAGAAGCGTTCCGTGTGTTTG	E
	GC3_D84GR_R	CCYTTCTTCACTGTCTGTGTCTTTCATTTTTCTTG	
R90AG	GC3_R90AG_F	GSTGTGTTTGATAAGGATGGCAATGGCTAC	E
	GC3_89_R	GAACGCTTCTCTAATTTCTTCTTCACTGTC	

Primer sequences used for Site Directed Mutagenesis in GCaMP3. Positions of mutations are indicated relative to calmodulin. Letter in front of position indicates amino acid residue present in GCaMP3, letter after position designates mutaion introduced. In some instances we used degenerate primers to be able to introduce any one of several amino acid residues designated after the position number. Oligonucleotides with which a mutation is introduced contain respective mutation in their name. F indicates sense (forward), R antisense (reverse complement) primer. Primer sequences are given in 5' to 3' direction. Abbreviations for nucleotide mixes at degenerate positions are R = A,G; Y =

C,T; M = A,C; K = G,T; S = C,G; W = A,T; H = A,C,T; B = C,G,T; V = A,C,G; D = A,G,T; N = A,C,G,T. In the “Site directed mutagenesis (SDM) type”column, E indicates mutation at the end of one primer (primers were phosphorylated and purified PCR fragments subjected to blunt-end ligation), C denotes SDMs in which largely complementary primers with mutations in the center were used (primers not phosphorylated and directly transformed after DpnI digest without ligation).

APPENDIX B: TABLES

Mutations	K_D (nM)	Hill Coef.	Dynamic Range (F_{max}-F_{min})/F_{min}	F_0(Mut)/ F_0(WT)	n
Control					
GC3 Wild Type	**419** ± 23.9	**2.26** ± 0.07	**9.07** ± 0.35	**1**	31
Pos 2					
GC3 K21A	**356.9** ± 35.7	**2.58** ± 0.15	**11.31** ± 0.47	**0.77** ± 0.05	8
GC3 K94A	**320.6** ± 15.1	**2.34** ± 0.1	**9.13** ± 0.48	**1.68** ± 0.65	4
Pos 3					
GC3 D22N	**1249.2** ± 46.2**	**1.53** ± 0.16*	**11.85** ± 1.09	**0.28** ± 0.01*	4
GC3 D58N	**349.1** ± 28	**2.29** ± 0.07	**10.43** ± 1.1	**0.743** ± 0.06	4
GC3 D95N	**602.1** ± 52.3	**2.3** ± 0.2	**7.83** ± 0.47	**0.92** ± 0.05	3
GC3 D131N	**676.1.8** ± 134.7	**2.49** ± 0.24	**7.86** ± 0.99	**1.00** ± 0.30	5
Pos 5					
GC3 D24N	**1310** ± 89.2**	**1.62** ± 0.04	**11.1** ± 0.89	**0.55** ± 0.06**	6
GC3 D60N	**568.3** ± 59.1	**2.26** ± 0.27	**9.62** ± 0.86	**0.8** ± 0.06	4
GC3 N97D	**339.3** ± 42.2	**2.04** ± 0.06	**11.53** ± 0.64	**0.7** ± 0.05**	4
GC3 D133N	**1118.7** ± 63**	**2.21** ± 0.21	**11.48** ± 0.29	**0.76** ± 0.08*	4
Pos 9					
GC3 T28D	**650.5** ± 40.3	**2.01** ± 0.07	**9.33** ± 0.53	**0.46** ± 0.01**	3
GC3 D64S	**319.6** ± 30.6	**1.66** ± 0.07	**6.56** ± 0.6	**0.69** ± 0.09**	3
GC3 S101D	**354.6** ± 13.3	**1.86** ± 0.03	**9** ± 0.95	**0.16** ± 0.03**	3
Pos 11					
GC3 K30A	**275.5** ± 10.2	**2.7** ± 0.06	**9.15** ± 0.35	**1.33** ± 0.28	4
GC3 E139A	**330.6** ± 9.9	**2.2** ± 0.1	**9.77** ± 0.28	**0.89** ± 0.03	3
Pos 12					
GC3 E31Q	**13.5 µM** ± 1.1**	**0.93** ± 0.03**	**2.61** ± 0.05**	**2.74** ± 0.08**	5
GC3 E67Q	**≥30 µM†**	**≤0.6†**	**4.02** ± 0.38**	**0.24** ± 0.03**	6
GC3 E104Q	**1122.9** ± 64**	**2** ± 0.16	**11.65** ± 0.28	**0.53** ± 0.06**	4
GC3 E140Q	**3476.5** ± 192.7**	**2.02** ± 0.05	**13.77** ± 0.57**	**0.62** ± 0.11*	6

Table 1. Dissociation constants (K_d), Hill coefficients, dynamic ranges, basal fluorescence, and sample sizes from the *in vitro* characterization of single point mutant GCaMP3 constructs performed within the four CaM calcium binding EF motifs. Red text indicates point mutants that significantly decrease the calcium affinity relative to GCaMP3. Statistical analysis was performed on groups separated by horizontal lines, including GCaMP3 control. Values indicate means ± standard error (* = $p<0.05$; ANOVA/Tukey HSD Test) (** = $p<0.01$; ANOVA/Tukeys HSD Test) († = cannot be fitted with a Hill model of cooperative binding.)

Mutations	K_D (nM)	Hill Coef.	Dynamic Range (F_{max}-F_{min})/F_{min}	F_0(Mut)/ F_0(WT)	n
Control					
GC3 Wild Type	**419** ± 23.9	**2.26** ± 0.07	**9.07** ± 0.35	**1**	31
Linker					
GC3 R74A	**227.9** ± 7.2**	**2.48** ± 0.07	**5.8** ± 0.21**	**0.94** ± 0.15	5
GC3 K75G	**254.2** ± 8.7*	**2.88** ± 0.21**	**9.6** ± 0.56	**1.07** ± 0.19	5
GC3 K77G	**258.8** ± 22.8*	**2.48** ± 0.89	**8.43** ± 0.38	**0.59** ± 0.03	8
GC3 D80R	**745.9** ± 55.7**	**2.28** ± 0.04	**8.1** ± 0.17	**1.37** ± 0.27*	3
GC3 E84R	**372.9** ± 16.7	**3.02** ± 0.20**	**8.53** ± 0.3	**1.47** ± 0.28**	3
GC3 R90G	**292.9** ± 28.2	**2.66** ± 0.26	**11.23** ± 0.18	**0.73** ± 0.15	3

Table 2. Dissociation constants (K_d), Hill coefficients, dynamic ranges, basal fluorescence, and sample sizes from the *in vitro* characterization of single point mutant GCaMP3 constructs performed within the flexible linker region between the N-terminal and C-terminal CaM domains. Green text indicates point mutants that significantly increase the calcium affinity of GCaMP3. Red text indicates point mutants that significantly decrease the calcium affinity of GCaMP3. Statistical analysis was performed on groups separated by horizontal lines and GCaMP3 control. Values indicate means ± standard error. * denotes significance of $p<0.05$; ** at $p<0.01$ level (ANOVA/Tukey HSD Test).

Mutations	K_D (nM)	Hill Coef.	Dynamic Range (F_{max}-F_{min})/F_{min}	F_0(Mut)/ F_0(WT)	n
Control					
GC3 Wild Type	**419** ± 23.9	**2.26** ± 0.07	**9.07** ± 0.35	**1**	31
INCREASING AFFINITY C0MBINATIONS:					
GC3 K21A|K75G|N97D	**201.7** ± 9.6**	**2.13** ± 0.03	**9.06** ± 0.19	**0.75** ± 0.02**	5
GC3 K21A|K77G|N97D	**175.5** ± 12.4**	**2.01** ± 0.06	**8.92** ± 0.40	**0.50** ± 0.05**	10
GC3 K21A|K75G|K77G|N97D	**176.6** ± 16.5**	**2.00** ± 0.08	**7.32** ± 0.14	**0.79** ± 0.02**	5
DECREASING AFFINITY C0MBINATIONS:					
Double					
GC3 D24N|E104Q	**2711.2** ± 74.9**	**1.95** ± 0.06	**11.7** ± 0.35*	**0.41** ± 0.03**	12
GC3 D60N|E104Q	**1862.5** ± 147.8**	**1.66** ± 0.1**	**11.98** ± 0.46**	**0.12** ± 0.01**	8
GC3 D24N|E140Q	**9661** ± 252.1**	**1.94** ± 0.02	**11.67** ± 0.58*	**0.34** ± 0.01**	6
GC3 D60N|E140Q	**3474.7** ± 319.3**	**1.97** ± 0.06	**12.9** ± 0.52**	**0.01** ± 0.03**	10
Triple					
GC3 D24N|D60N|E140Q	**12586.8** ± 282.1**	**2** ± 0.02	**12.03** ± 0.45**	**0.28** ± 0.03**	6
Quadruple					
GC3 D24N|D60N|D95N|E140Q	**11614.4** ± 670.8**	**2.26** ± 0.08	**10.27** ± 0.26	**0.83** ± 0.21	6

Table 3. Dissociation constants (K_d), Hill coefficients, dynamic ranges, basal fluorescence, and sample sizes from the *in vitro* characterization of combination point mutant GCaMP3 constructs performed within the flexible linker region between the N-terminal and C-terminal CaM domains and within the four CaM calcium binding EF motifs. Green text indicates point mutants that significantly increase the calcium affinity of GCaMP3. Red text indicates point mutants that significantly decrease the calcium affinity of GCaMP3. Statistical analyses were separately performed on (a) the high-affinity mutants and GCaMP3 as control, (b) low affinity constructs with two mutations

and GCaMP3 control, and (c) triple and quadruple mutant low affinity GCaMP constructs and GCaMP3 Values indicate means ± standard error. * denotes significance at $p<0.05$, ** at $p<0.01$ level.

Treatment	Constructs Tested	
ΔF/F	**GC3 Wild Type**	**GC3 K21A|K77G| N97D**
1 Stimulus	3.9 ± 1%	14 ± 3%
P Value	0.012	
2 Stimuli	14 ± 2%	32 ± 5%
P Value	0.005	
4 Stimuli	40 ± 5%	68 ± 9%
P Value	0.014	
Basal Fluorescence		
F_0	36.3 ± 4.4	64.5 ± 9.2
P Value	0.010	
Kinetics		
Decay Rate (tau)	1.49 ± 0.08	0.76 ± 0.07
P Value	0.404	
2 second Train Stimuli $(F - F_{min})/(F_{max} - F_{min})$		
2.5 Hz	0.10 ± 0.02	0.24 ± 0.05
P value	0.014	
5 Hz	0.29 ± 0.03	0.45 ± 0.05
P Value	0.016	
10 Hz	0.61 ± 0.03	0.78 ± 0.03
P Value	0.001	
20 Hz	0.86 ± 0.02	0.93 ± 0.02
P Value	0.006	
40 Hz	0.92 ± 0.01	0.90 ± 0.02
P Value	0.542	
Dynamic Range		
$(F_{max} - F_{min})$	2.38 ± 0.08	2.85 ± 0.16
P Value	0.018	

Table 4. Fluorescence changes in neurons expressing the high calcium affinity GCaMP3 variant, GC3_K21A_K77G_N97D (n=15 experiments, total of 90 synapses) compared to GCaMP3 control (n=23 experiments, total of 138 synapses). Fluorescence values in response to single and small bursts of 2 and 4 stimuli calculated as ΔF/F values are represented as percentage increases above baseline fluorescence, while fluorescence

change in response to 2 second train of stimuli at 2.5, 5, 10, 20, and 40 Hz are normalized as ($[F - F_{min}]/[F_{max} - F_{min}]$) to indicate degree of sensor saturation. Dynamic range values are calculated as the maximum fluorescence response subtracted by the minimum fluorescence response ($F_{max} - F_{min}$). Basal Fluorescence values indicate the minimum fluorescence observed prior to stimulation. Decay rates (tau) provide an indication as to how fast calcium dissociates from the sensor in response to bursts of 4 stimuli. Values indicate means ± standard error. Significance values for each treatment were calculated with two-tailed unpaired T-tests.

Treatment	Constructs Tested				
ΔF/F	**GC3 Wild Type**	**GC3 K21A**	**GC3 K77G**	**GC3 N97D**	**GC3 K21A|N97D**
1 Stimulus	3.9 ± 1%	12 ± 3%	3.0 ± 2%	3.0 ± 1%	14 ± 6%
Significance		NS	NS	NS	P < 0.05
2 Stimuli	14 ± 2%	41 ± 8%	11 ± 4%	12 ± 3%	27 ± 6%
Significance		P < 0.01	NS	NS	NS
4 Stimuli	40 ± 5%	105 ± 12%	26 ± 7%	30 ± 3%	54 ± 4%
Significance		P < 0.01	NS	NS	NS
Basal Fluorescence					
F_0	36.3 ± 4.4	24.0 ± 5.6	ND	63.8 ± 11.6	56.4 ± 8.6
Significance		NS		NS	NS
Kinetics					
Decay Rate (tau)	1.49 ± 0.08	0.70 ± 0.18	1.64 ± 0.05	2.00 ± 0.58	1.09 ± 0.17
Significance		P < 0.05	NS	NS	NS
Dynamic Range					
(F_{max} - F_{min})	2.38 ± 0.08	3.51 ± 0.22	2.08 ± 0.14	2.47 ± 0.29	2.16 ± 0.11
Significance		P < 0.01	NS	NS	NS

Table 5. Fluorescence changes in neurons expressing GC3_K21A (n=7 experiments, 42 synapses), GC3_K77G (n=5 experiments), GC3_N97D (n=5), and GC3_K21A_N97D (n=5), compared to GCaMP3 control (n=23). Fluorescence values in response to single and small bursts of 2 and 4 stimuli calculated as ΔF/F values are represented as percentage increases above baseline fluorescence. Dynamic range values are calculated as the maximum fluorescence response subtracted by the minimum fluorescence response ($F_{max} - F_{min}$). Basal Fluorescence values indicate the pre-stimulus fluorescence. Decay rates (tau) were calculated for responses to bursts of 4 stimuli. Values indicate means ± standard error. Significance values for each treatment were calculated with ANOVA/Tukey HSD analysis.

Treatment	Constructs Tested		
ΔF/F	**GC3 Wild Type**	**GC3 D24N|E104Q**	**GC3 D24N|D60N|E140Q**
1 Stimulus	3.9 ± 1%	3.0 ± 1%	1.0 ± 1%
Significance		NS	NS
2 Stimuli	14 ± 2%	10 ± 1%	3.0 ± 1%
Significance		NS	NS
4 Stimuli	40 ± 5%	36 ± 12%	12 ± 6%
Significance		NS	NS
Basal Fluorescence			
F_0	36.3 ± 4.4	49.0 ± 22.7	35.2 ± 8.6
Significance		NS	NS
2 second Train Stimuli $(F - F_{min})/(F_{max} - F_{min})$			
2.5 Hz	0.10 ± 0.02	0.01 ± 0.01	0.01 ± 0.02
Significance		NS	NS
5 Hz	0.29 ± 0.03	0.04 ± 0.01	0.04 ± 0.02
Significance		NS	NS
10 Hz	0.61 ± 0.03	0.23 ± 0.01	0.12 ± 0.07
Significance		P < 0.01	P < 0.01
20 Hz	0.86 ± 0.02	0.63 ± 0.04	0.34 ± 0.14
Significance		P < 0.05	P < 0.01
40 Hz	0.92 ± 0.01	0.87 ± 0.09	0.62 ± 0.12
Significance		NS	P < 0.01
Dynamic Range			
$(F_{max} - F_{min})$	2.38 ± 0.08	3.11 ± 0.07	2.37 ± 0.03
Significance		P < 0.05	NS

Table 6. Fluorescence changes in neurons expressing GC3_D24N_E104Q (n=3) and GC3_D24N_D60N_E140Q (n=3) compared to GCaMP3 control (n=23). Fluorescence change in response to single and small bursts of 2 and 4 stimuli calculated as ΔF/F values represented as percentage increases above baseline fluorescence, while fluorescence change in response to 2 second train of stimuli at 2.5, 5, 10, 20, and 40 Hz are normalized as $([F - F_{min}]/[F_{max} - F_{min}])$ to indicate degree of sensor saturation. Basal Fluorescence values indicate the pre-stimulus fluorescence observed. Dynamic range

values are calculated as the maximum fluorescence response subtracted by the minimum fluorescence response ($F_{max} - F_{min}$) for 2 second train stimuli treatments. Values indicate means ± standard error. Significance values for each treatment were calculated with ANOVA/Tukey HSD analysis.

APPENDIX C: FIGURES

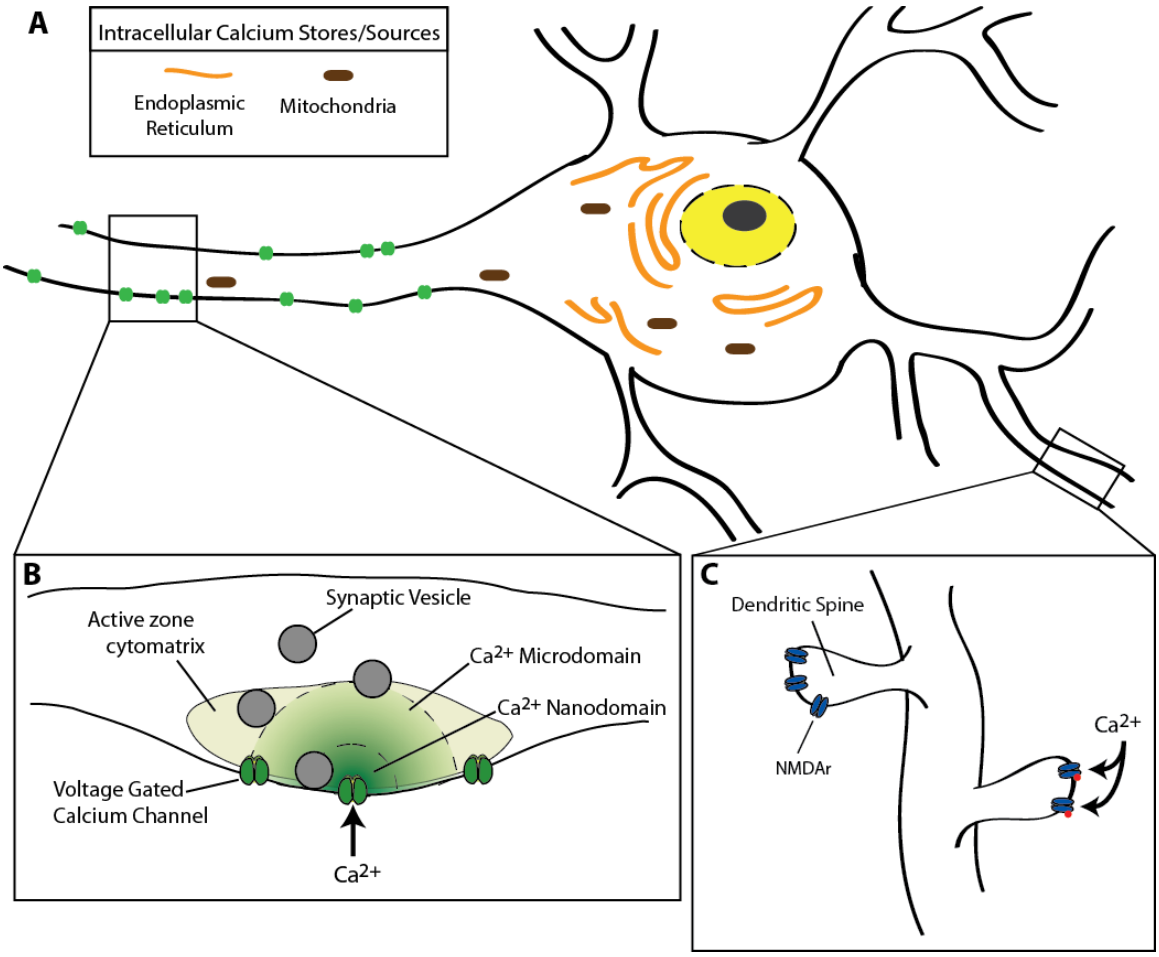

Figure 1. Schematic representation of compartmentalized calcium signalling in neurons. (**A**) Axonal (left) and somatodendritic (center/right) regions of a neuron. Calcium is stored in intracellular organelles such as mitochondria and the endoplasmic reticulum. (B) Magnified region of the axon depicting a presynaptic varicosity. Calcium influx occurs through VGCCs on the plasma membrane. Calcium micro- and nanodomains form around individual VGCCs or clusters of calcium channels. With increasing diffusional distance, the amplitude of calcium transients decreases. (**C**)

Magnified region of a dendrite with dendritic spines. Calcium influx occurs within this domain through ligand bound NMDA receptors.

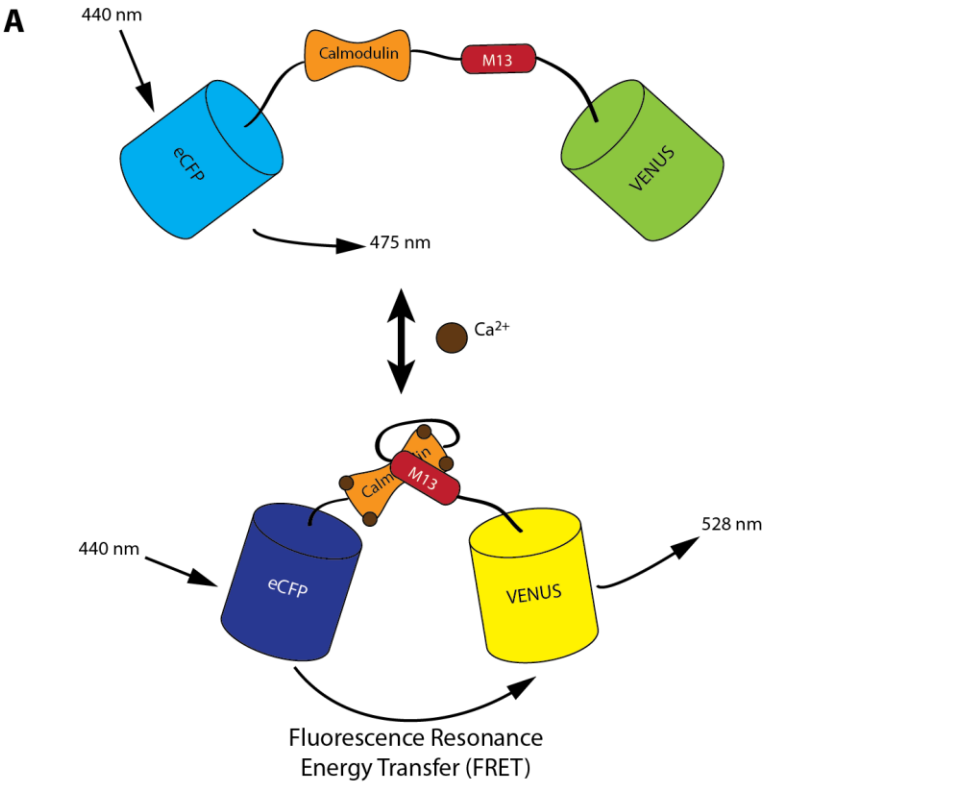
A
440 nm
Calmodulin
M13
eCFP
VENUS
475 nm
Ca2+
Calm
M13
440 nm
eCFP
VENUS
528 nm
Fluorescence Resonance
Energy Transfer (FRET)

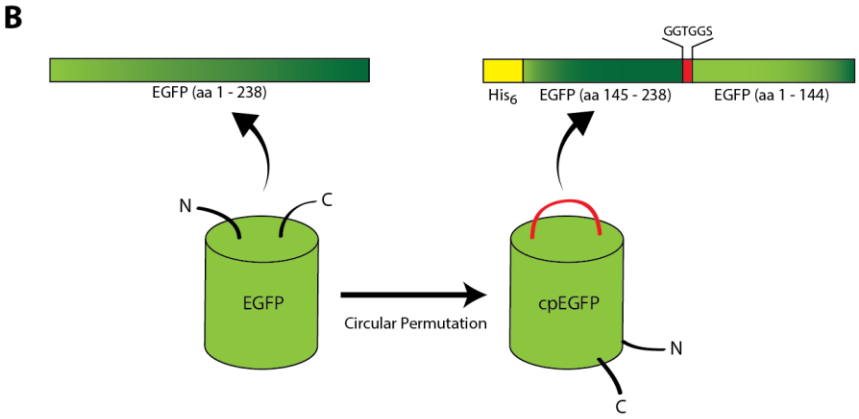
B
GGTGGS
EGFP (aa 1 - 238)
His6
EGFP (aa 145 - 238)
EGFP (aa 1 - 144)
N
C
EGFP
Circular Permutation
cpEGFP
N
C

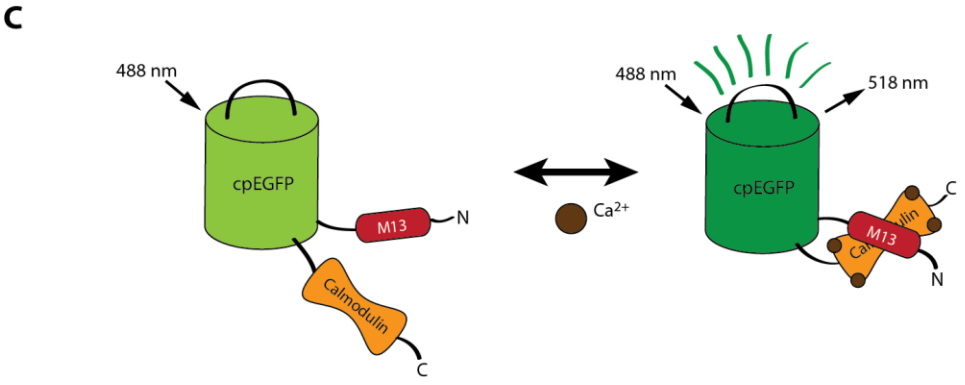
C
488 nm
cpEGFP
M13
N
Calmodulin
C
Ca2+
488 nm
518 nm
cpEGFP
C
M13
N

Figure 2. Schematic representation illustrating FRET-based calcium indicators and GCaMP-based calcium indicators. (**A**) FRET-based calcium indicator with two fluorophores. In the absence of calcium, the cyan fluorescent protein is excited by 440 nm wavelength. eCFP and Venus are spatially separated, preventing fluorescence energy transfer from eCFP to Venus. Energy from ecFP is emitted as light with 475 nm avelength. Upon calcium binding to CaM, conformational changes occur between the CaM/M13 peptide complex to bring the fluorophores close in proximity to each other and align their dipoles, thus allowing for fluorescence energy transfer. Fluorescence intensity at 475 nm (eCFP emission) diminishes, emission at 528 nm increases. (**B**) Schematic of the circular permutation of GFP. (**C**) Schematic of the calcium sensing mechanism for the single fluorescent protein GECI, GCaMP. Calcium induced conformational changes in the CaM/M13 peptide complex induce fluorescence changes in the circularly permutated EGFP (cpEGFP)

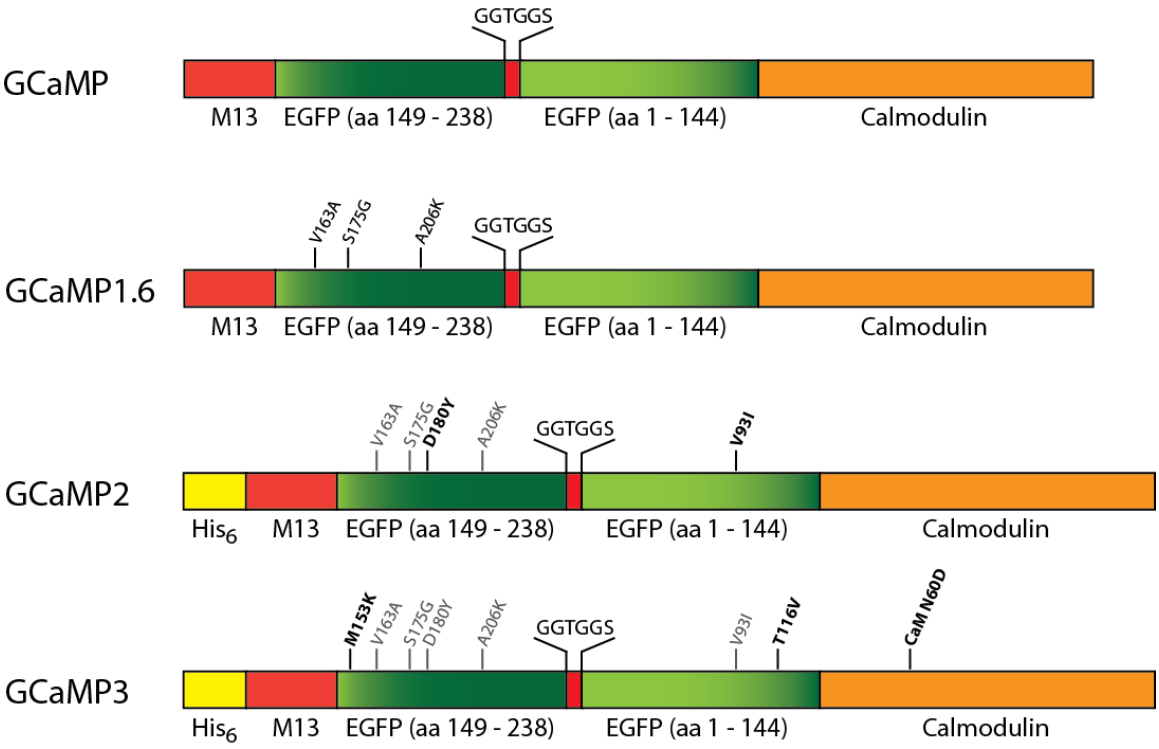

Figure 3. Overview of the optimization of the GECI, GCaMP, to generate GCaMP3. Three mutations were performed on GCaMP (V163A, S175G, and A206K) to obtain GCaMP1.6. Two more mutations were performed on GCaMP1.6 (D180Y and V93I) and a polyHis peptide region was inserted at the N-terminal of the sensor to generate GCaMP2. A total of three more mutations were introduced to GCaMP2 (M153K, T116V of the cpEGFP, and N60D of CaM) to engineer GCaMP3.

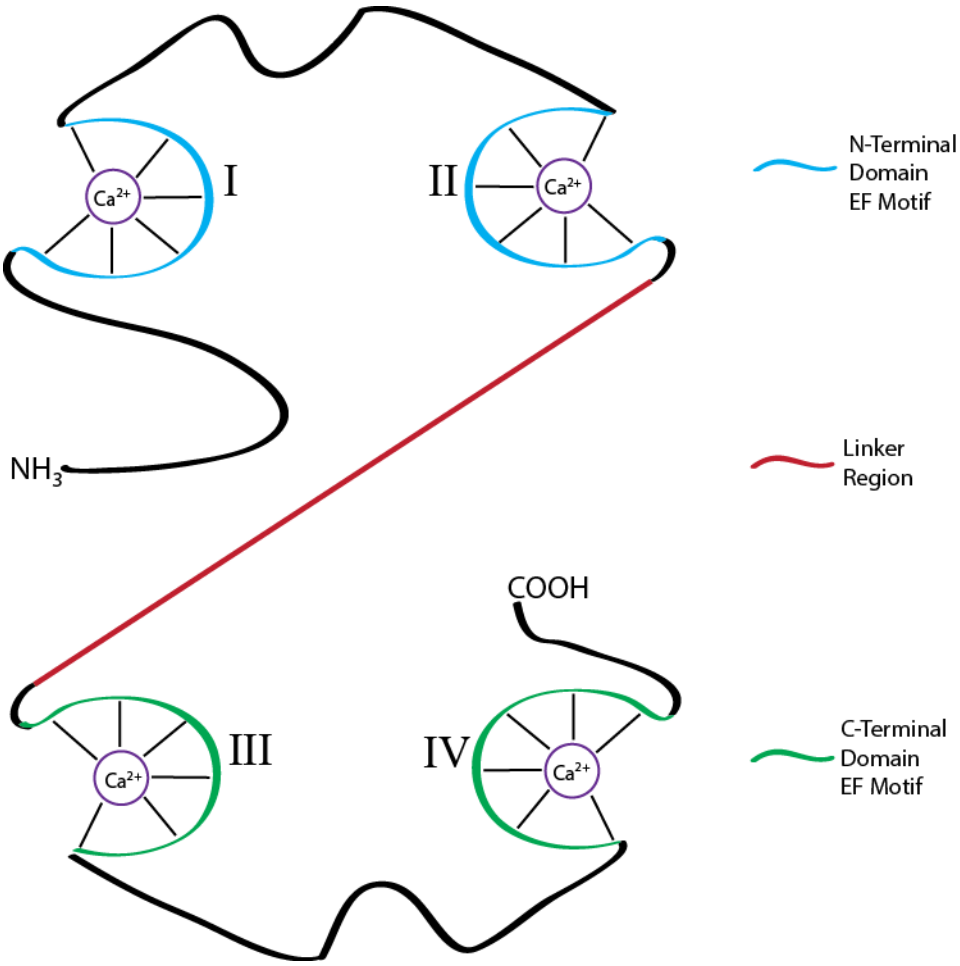

Figure 4. Schematic representation of the calcium chelating protein, calmodulin. The four EF motifs of CaM, which bind calcium ions via their six chelating residues, are shown in blue and green to indicate the N-terminal (I and II) and C-terminal (III and IV) sites, respectively. The flexible linker region connecting the N- and C- domains of CaM is illustrated in red.

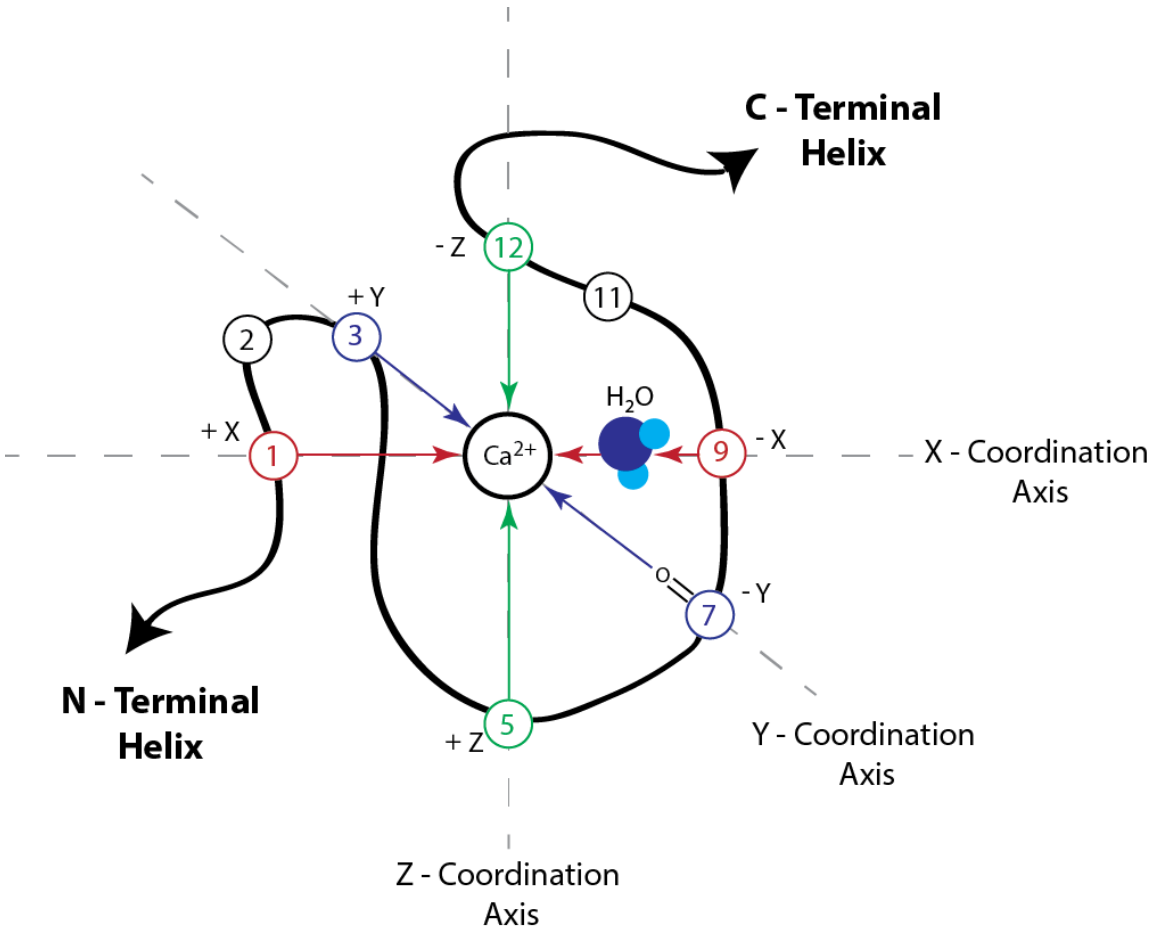

Figure 5. Schematic diagram illustrating the loop of an EF motif. The six chelating residues, numbered 1, 3, 5, 7, 9, and 12, are positioned on the X, Y, and Z coordination axes. Positions 2 and 11 are also indicated on the near octahedral coordination sphere as residues at these locations within select EF motifs were also mutated in our studies.

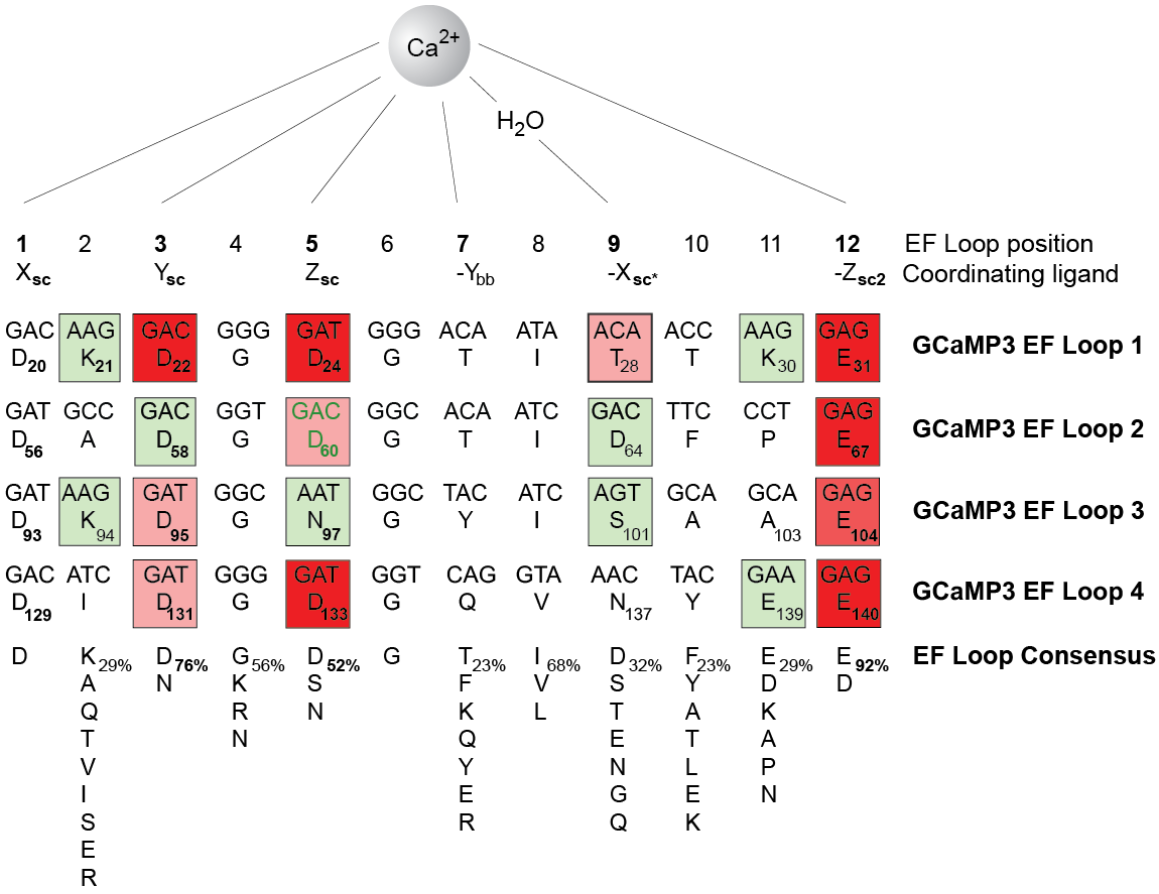

Legend

* Coordination directly via amino acid side chain (sc) or backbone (bb) or indirectly via water molecule (sc*)
* D60 (green) is point mutant in GCaMP3 relative to Calmodulin (N60)
* Boxed amino acids are EF loop positions containing point mutants
* Box fill colour indicates decrease (red/pink) or increase (green/light green) in affinity of single point mutant relative to WT, with darker shades indicating significant ($p<0.01$; ANOVA and Tukey HSD post hoc tests) affinity changes

Figure 6. Overlay of the four calcium binding EF motifs to illustrate the degree of amino acid residue conservation. Boxed amino acids indicate locations of point mutations with the darker shades of green and red demonstrating mutations resulting in significant increases and decreases in the calcium affinity of GCaMP3, respectively. Lighter shades of green and red indicate only marginal alterations in calcium affinity of GCaMP3.

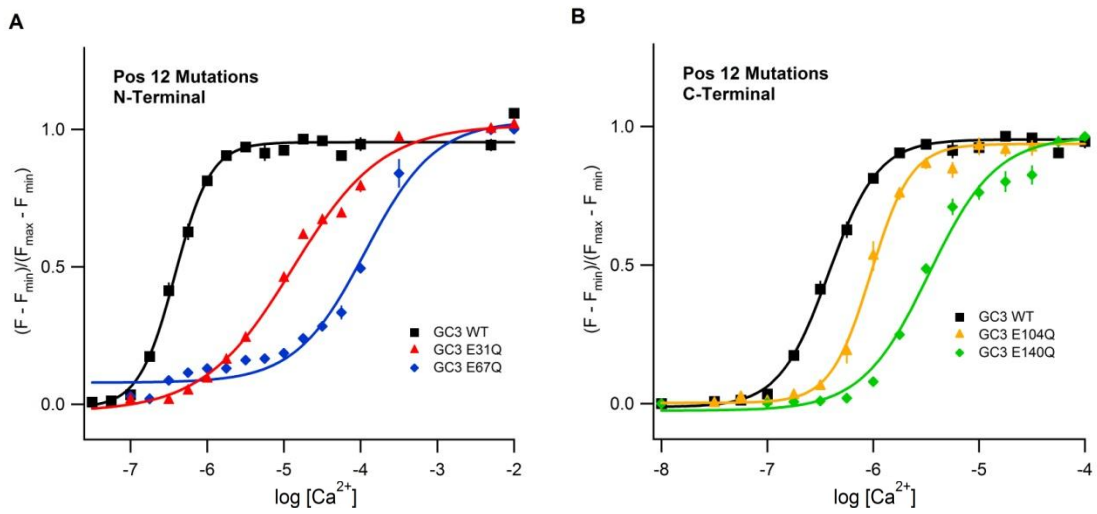

Figure 7. *In vitro* characterization of GCaMP3 constructs containing mutations at position 12 of the calcium binding EF motifs within the N-terminal (**A**) and C-terminal (**B**) domains of CaM (left). Ca^{2+} titration curve traces indicate the relative shifts in calcium affinity observed for constructs GC3 E31Q (red; n = 5) located in EF motif I, GC3 E67Q (blue; n = 6) located in EF motif II, GC3 E104Q (orange; n = 4) located in EF motif III, and GC3 E140Q (green; n = 6) located in EF motif IV, compared to that of the control construct, GC3 (black; n = 31). All samples (1 μM protein) in this and subsequent graphs were excited at 488 nm. Emitted light was sampled at 518 nm.

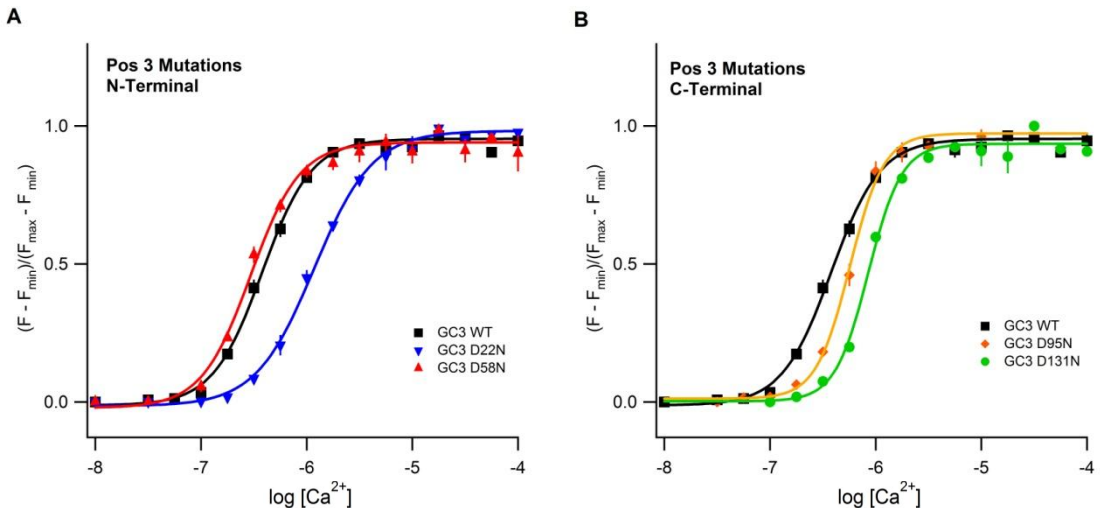

Figure 8. *In vitro* characterization of GCaMP3 constructs containing mutations at position 3 of the calcium binding EF motifs within the N-terminal (**A**) and C-terminal (**B**) domains of CaM. Ca^{2+} titration curve traces indicate the relative shifts in calcium affinity observed for constructs GC3 D22N (blue; n = 4) located in EF motif I, GC3 D58N (red; n = 4) located in EF motif II, GC3 D95N (orange; n = 3) located in EF motif III, and GC3 D131N (green; n = 5) located in EF motif IV, compared to that of the control construct, GC3 (black; n = 31).

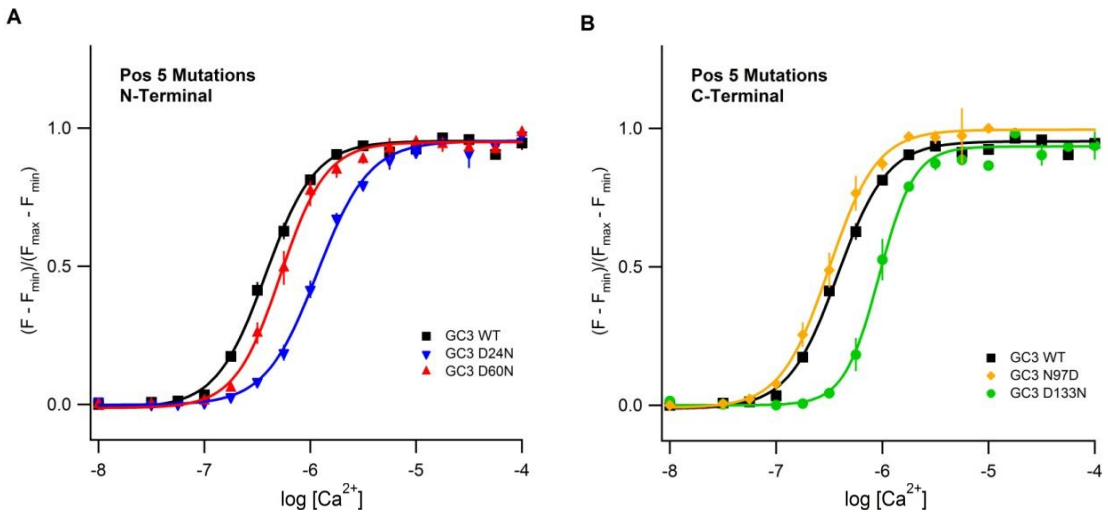

Figure 9. *In vitro* characterization of GCaMP3 constructs containing mutations at position 5 of the calcium binding EF motifs within the N-terminal (**A**) and C-terminal (**B**) domains of CaM. Ca^{2+} titration curve traces indicate the relative shifts in calcium affinity observed for constructs GC3 D24N (blue; n = 6) located in EF motif I, GC3 D60N (red; n = 4) located in EF motif II, GC3 N97D (orange; n = 4) located in EF motif III, and GC3 D133N (green; n = 4) located in EF motif IV, compared to that of the control construct, GC3 (black; n = 31).

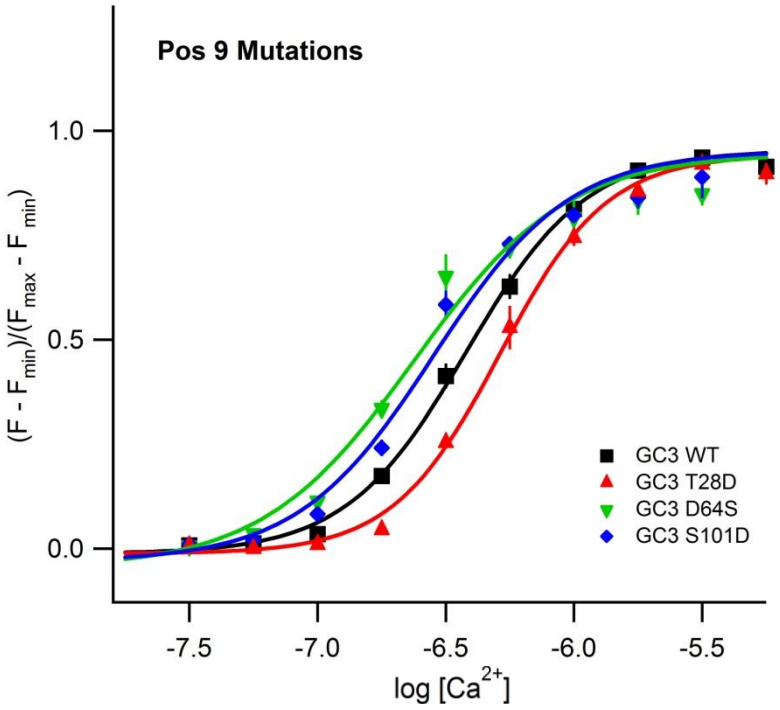

Figure 10. *In vitro* characterization of GCaMP3 constructs containing mutations at position 9 of the calcium binding EF motifs within CaM. Ca^{2+} titration curve traces indicate the relative shifts in calcium affinity observed for constructs GC3 T28D (red; n = 3) located in EF motif I, GC3 D64S (green; n = 3) located in EF motif II, and GC3 S101D (blue; n = 3) located in EF motif III, compared to that of the control construct, GC3 (black; n = 31).

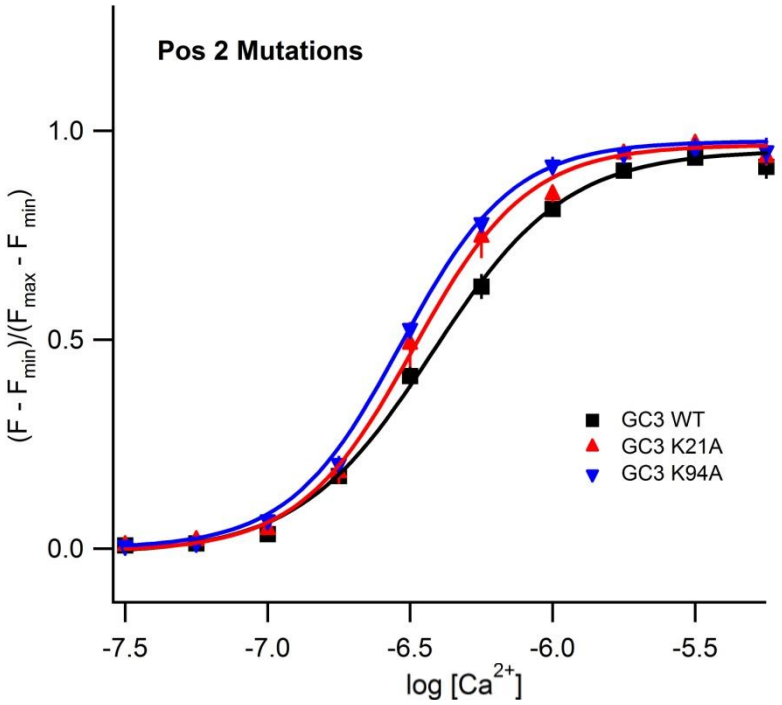

Figure 11. *In vitro* characterization of GCaMP3 constructs containing mutations at position 2 of the calcium binding EF motifs within CaM. Ca^{2+} titration curve traces indicate the relative shifts (increases) in calcium affinity observed for constructs GC3 K21A (red; n = 8) located in EF motif I and GC3 K94A (blue; n = 4) located in EF motif III compared to that of the control construct, GC3 (black; n = 31).

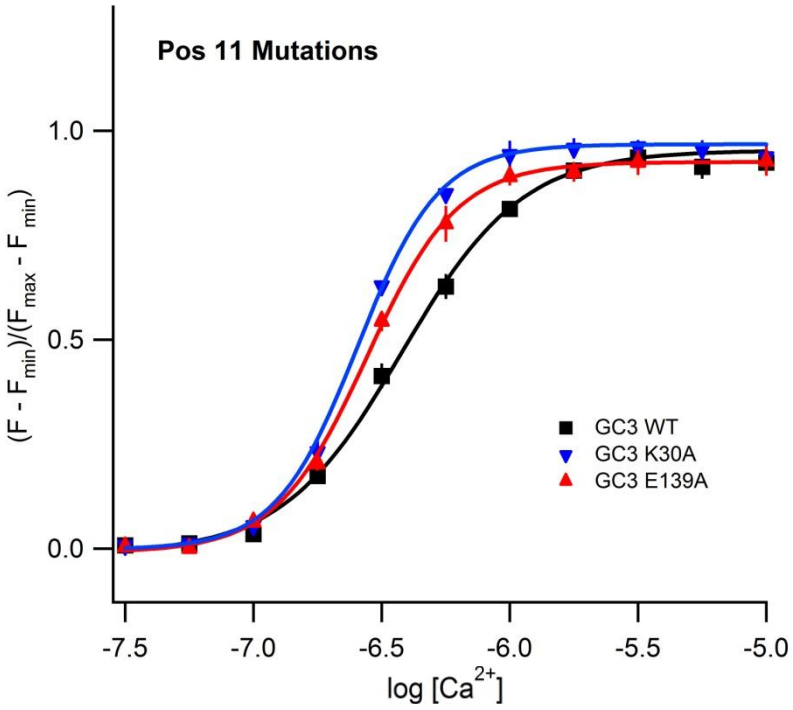

Figure 12. *In vitro* characterization of GCaMP3 constructs containing mutations at position 11 of the calcium binding EF motifs within CaM. Ca^{2+} titration curve traces indicate the relative shifts in calcium affinity observed for constructs GC3 K30A (blue; n = 4) located in EF motif I and GC3 E139A (red; n = 3) located in EF motif IV, compared to that of the control construct, GCaMP3 (black; n = 31).

Linker Region Connecting the N- and C-terminal Domains of CaM

Legend

* Boxed amino acids are EF loop positions containing point mutants
* Box fill colour indicates decrease (red/pink) or increase (green/light green) in affinity of single point mutant relative to WT, with darker shades indicating significant ($p<0.01$; ANOVA and Tukey HSD post hoc tests) affinity changes

Figure 13. Overview of the 25 amino acid residue flexible linker region of CaM that connects EF motif II located in the N-terminal domain with EF motif III of the C-terminal domain. Boxed amino acids indicate locations of point mutations with the darker shades of green and red demonstrating mutations resulting in a significant increase or decrease in the calcium affinity of GCaMP3, respectively. Lighter shades of green indicate marginal alterations in calcium affinity of GCaMP3.

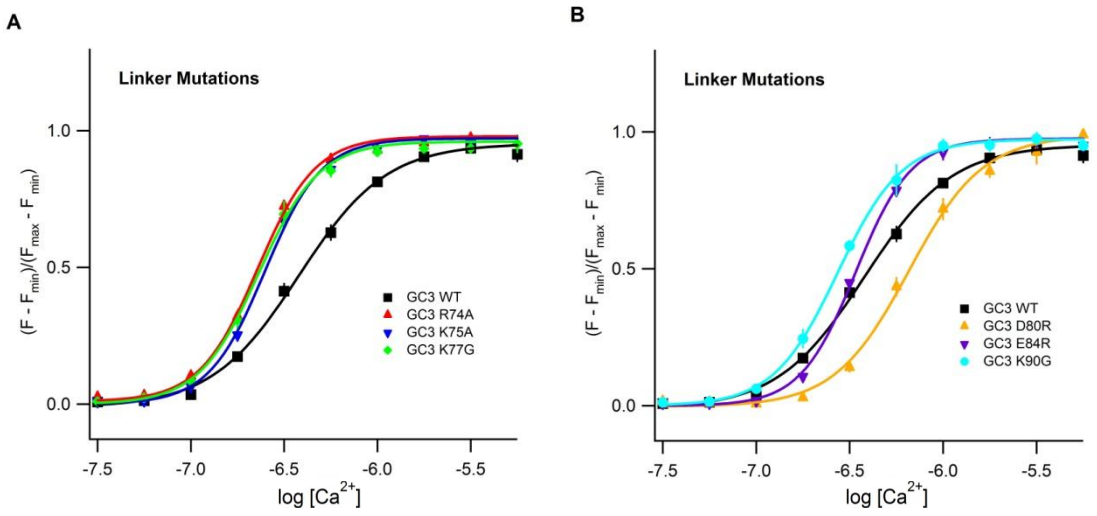

Figure 14. *In vitro* characterization of GCaMP3 constructs containing mutations within the linker region connecting the N- and C-terminal domains of CaM. Ca^{2+} titration curve traces indicate the relative shifts in calcium affinity observed for constructs: (**A**) GC3 R74A (red; n = 5), GC3 K75A (blue; n = 5), and GC3 K77G (green; n = 8); and (**B**) GC3 D80R (orange; n = 3), and GC3 E84R (purple; n = 3) compared to that of the control construct, GC3 (black; n = 31).

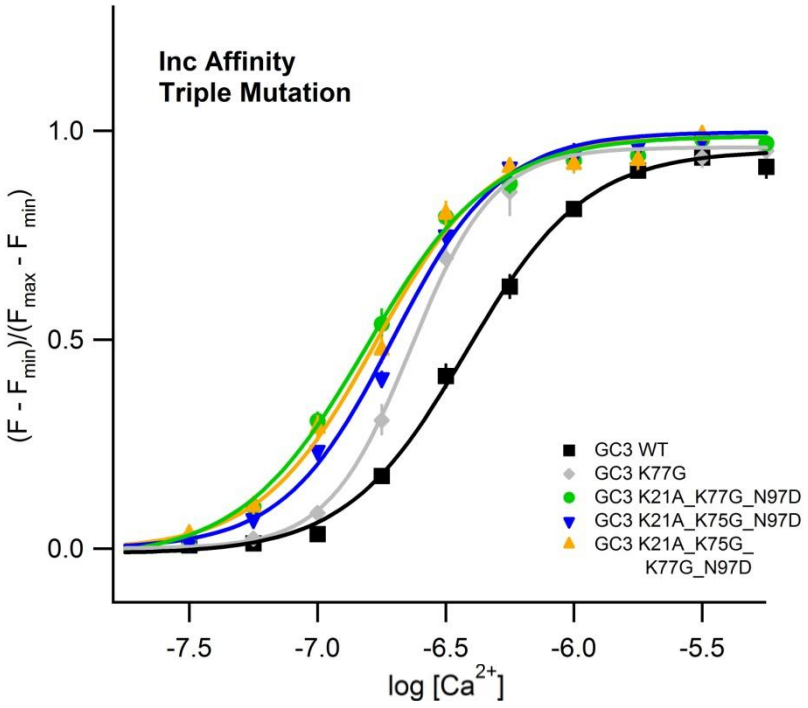

Figure 15. *In vitro* characterization of GCaMP3 constructs containing multiple mutations within the calcium binding EF motifs and linker region connecting the N- and C-terminal domains of CaM. Ca^{2+} titration curve traces indicate the relative shifts in calcium affinity observed for constructs GC3 K21A_K77G_N97D (green; n = 10), GC3 K21A_K75G_N97D (blue; n = 5), and GC3 K21A_K75G_K77G_N97D (orange; n = 5) compared to that of the control construct, GCaMP3 (black; n = 31). The grey trace shows the calcium titration curve of the single mutant K77G (as shown previously in Figure 14A) for comparison purposes.

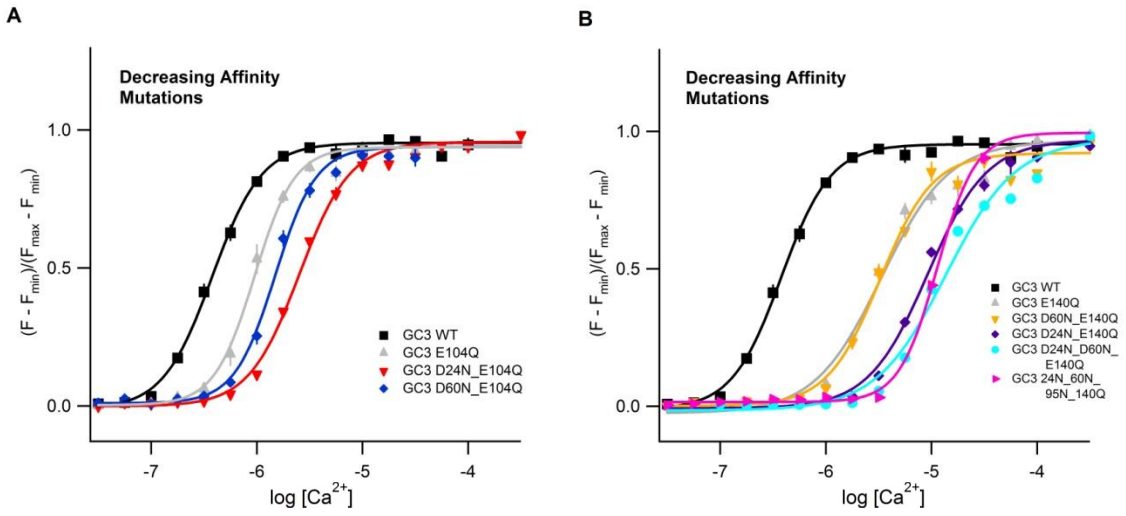

Figure 16. *In vitro* characterization of GCaMP3 constructs containing multiple mutations based on position 12 of the calcium binding EF motifs within CaM. Ca^{2+} titration curve traces indicate the relative shifts in calcium affinity observed for the constructs: **A**) GC3 D24N_E104Q (red; n = 12) and GC3 D60N_E104Q (blue; n = 8), and **B**) GC3 D24N_E140Q (purple; n = 6), GC3 D60N_E140Q (orange; n = 10), GC3 D24N_D60N_E140Q (cyan; n = 6), GC3 D24N_D60N_D95N_E140Q (pink; n = 6); compared to that of the control construct, GC3 (black; n = 31). Grey traces show the relative affinity shifts of the single mutants (E104Q in **A** and E140Q in **B** as shown previously in Fig. 7B) for comparison purposes.

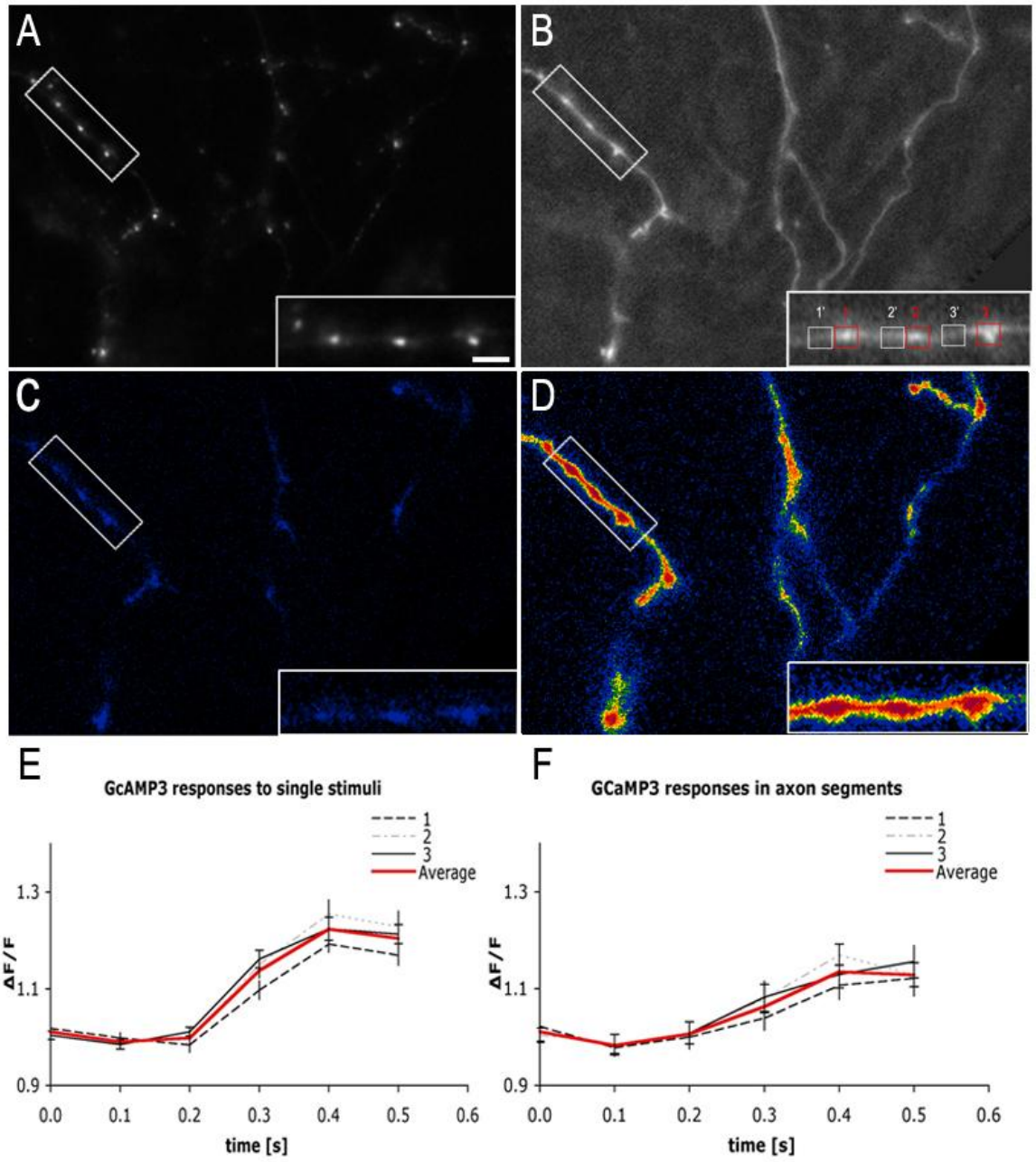

Figure 17. Images showing dissociated hippocampal neurons transfected with TdTomato-Bassoon and GC3_21A_77G_97D. **A)** TdTomato-Bassoon fluorescence. Region indicated by the white box in the upper left quadrant is shown at twice the magnification in the lower right. Scale bar, 5 µm (2.5 µm for magnified region). **B)** Basal

GCaMP_21A_77G_97D fluorescence. **C)** GCaMP3_21A_77G_97D fluorescence increase in response to isolated stimuli. Fluorescence increases are localized to regions that overlap with the synaptic active zone marker tdTomato-Bassoon indicating that presynaptic calcium influx is largely restricted to presynaptic specializations. **D)** GCaMP3_21A_77G_97D fluorescence increases in response to repetitive stimulation (20 stimuli at 20 Hz) showing the diffusion of calcium into the axonal shaft between synapses. Small increases in fluorescence in C and D are shown in blue, larger increases in green, yellow and red hues. **E)** Graph showing the time course of fluorescence changes at presynaptic specializations (E, regions of interest used for signal integration indicated with red boxes in B). **F)** Plot of fluorescence changes observed at adjacent extrasynaptic regions of the axonal shaft (white boxes in B).

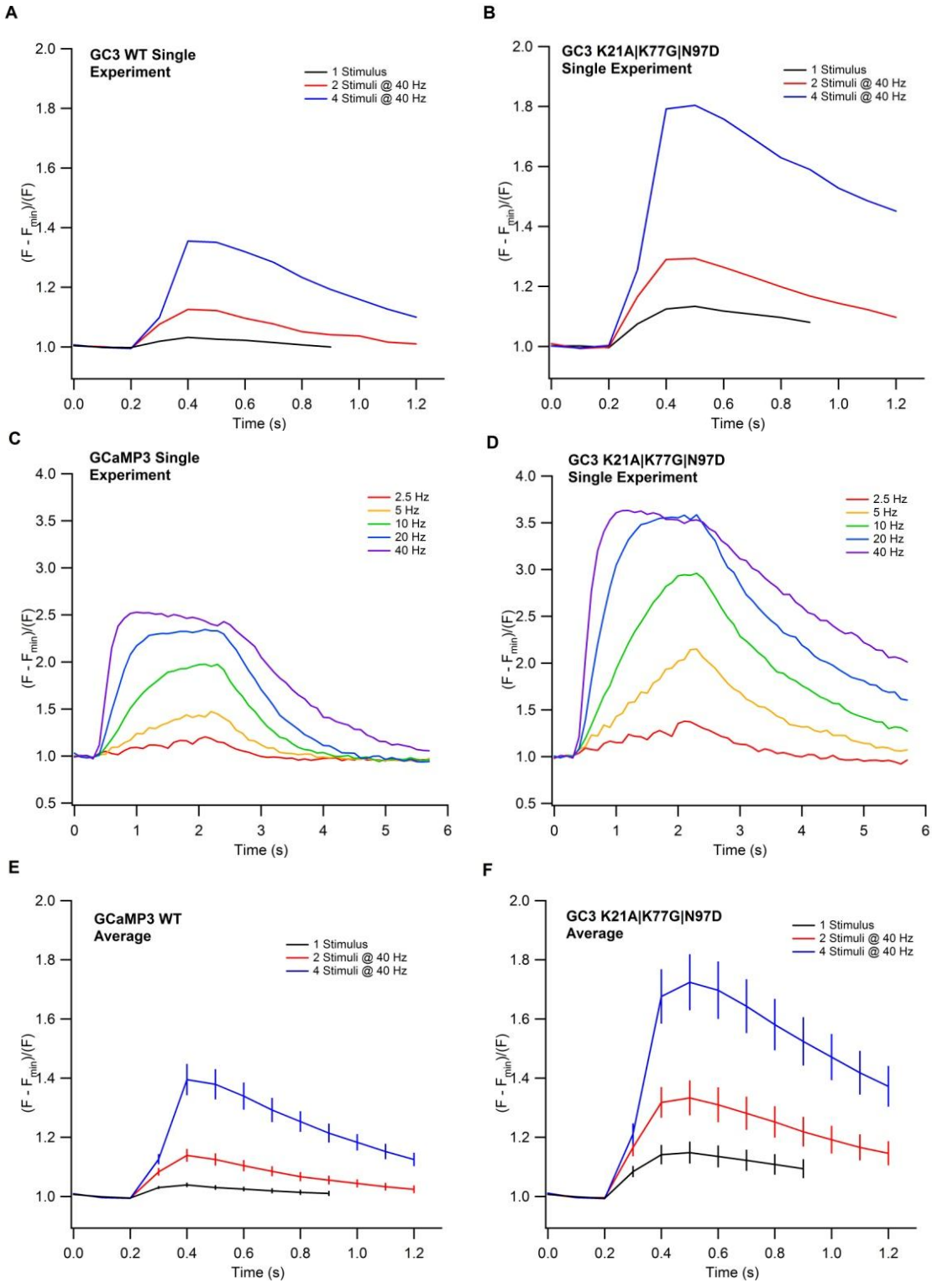
A
GC3 WT Single Experiment
1 Stimulus
2 Stimuli @ 40 Hz
4 Stimuli @ 40 Hz
(F - F_min)/(F)
Time (s)
B
GC3 K21A|K77G|N97D Single Experiment
1 Stimulus
2 Stimuli @ 40 Hz
4 Stimuli @ 40 Hz
(F - F_min)/(F)
Time (s)
C
GCaMP3 Single Experiment
2.5 Hz
5 Hz
10 Hz
20 Hz
40 Hz
(F - F_min)/(F)
Time (s)
D
GC3 K21A|K77G|N97D Single Experiment
2.5 Hz
5 Hz
10 Hz
20 Hz
40 Hz
(F - F_min)/(F)
Time (s)
E
GCaMP3 WT Average
1 Stimulus
2 Stimuli @ 40 Hz
4 Stimuli @ 40 Hz
(F - F_min)/(F)
Time (s)
F
GC3 K21A|K77G|N97D Average
1 Stimulus
2 Stimuli @ 40 Hz
4 Stimuli @ 40 Hz
(F - F_min)/(F)
Time (s)

Figure 18. Fluorescence changes of GCaMP3 and GC3_K21A_K77G_N97D in response to electrical stimulation. (**A** and **B**) Fluorescence increases (ΔF/F) in response to a single stimulus and bursts of 2 and 4 stimuli at 40 Hz for single experiments. (**C** and **D**) Fluorescence increase (ΔF/F) in response to 2 second trains at 2.5, 5, 10, 20, and 40 Hz for single experiments. (**E** and **F**) Average change in fluorescence (ΔF/F) in response to a single stimulus and bursts of 2 and 4 stimuli at 40 Hz (GCaMP3, n=23 experiments, total of 138 synapses; GC3_K21A_K77G_N97D, n=15 experiments, total of 90 synapses).

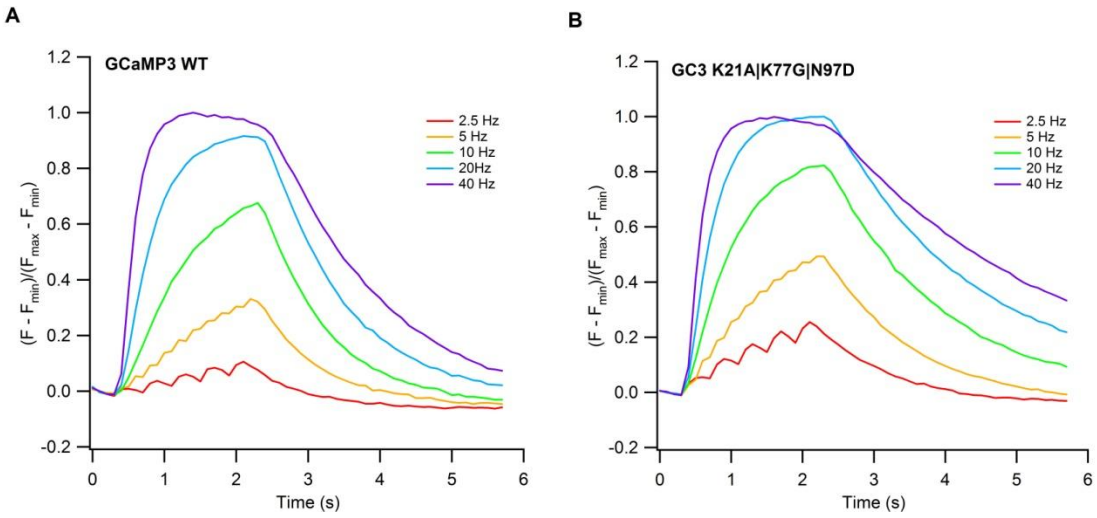

Figure 19. Normalized fluorescence changes ($[F - F_{min}]/ [F_{max}-F_{min}]$) of GCaMP3 (A) and GC3_K21A_K77G_N97D (B) in response to 2 second trains at 2.5, 5, 10, 20, and 40 Hz. Note that the high affinity construct saturates at slightly lower calcium concentrations than GCaMP3.

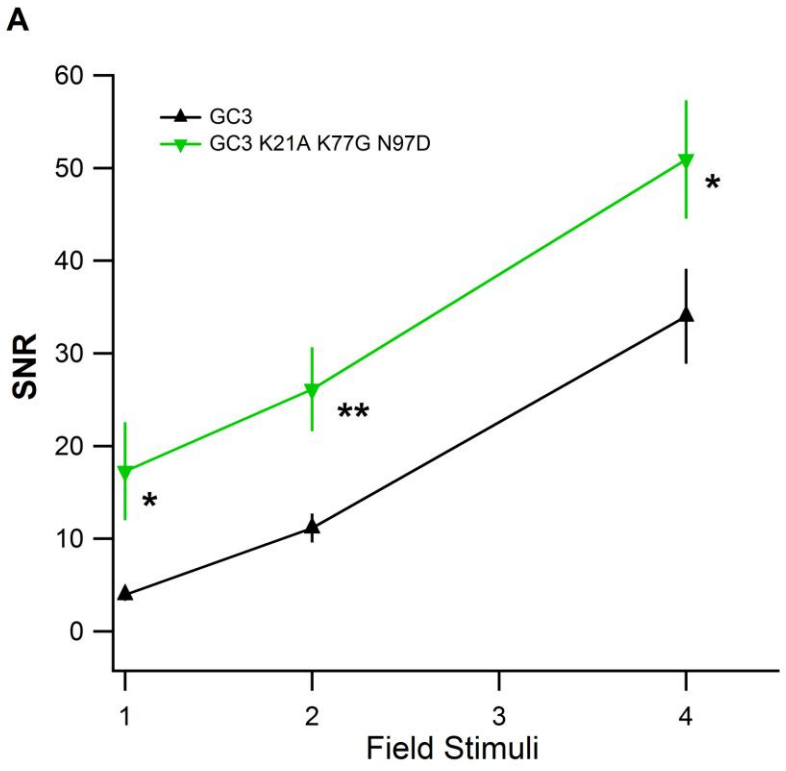

Figure 20. SNR for GC3 and the high calcium affinity sensor, GC3_K21A_K77G_N97D, in response to a single stimulus and bursts of 2 and 4 stimuli. SNR was calculated as the ratio between the peak fluorescence response amplitude (ΔF) and the standard deviation of fluorescence variations before stimulus onset (200 ms). (* = $p<0.05$; Two-tailed T-Test) (** = $p<0.01$; Two-tailed T-Test).

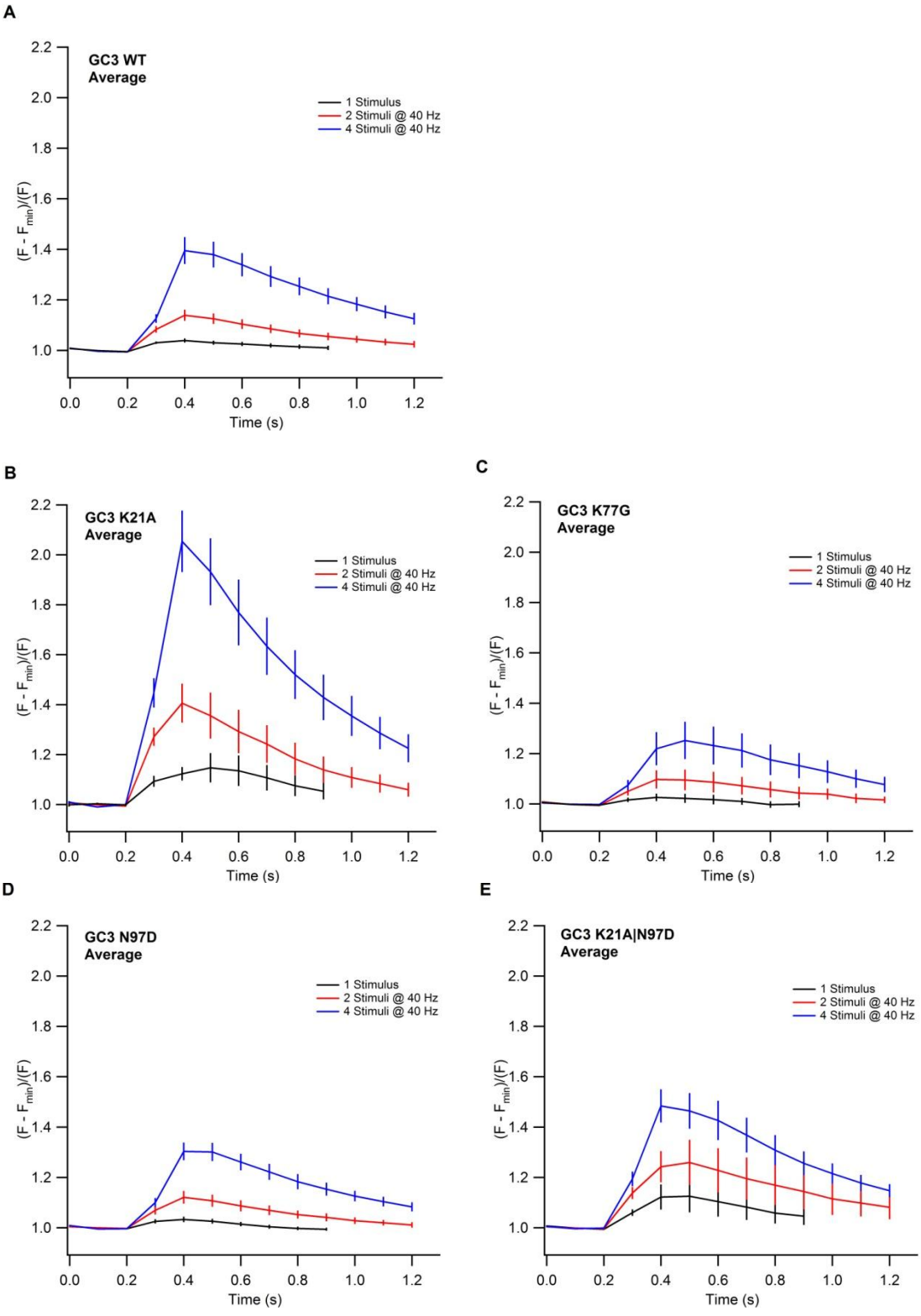
A
GC3 WT
Average
1 Stimulus
2 Stimuli @ 40 Hz
4 Stimuli @ 40 Hz
(F - F_min)/(F)
Time (s)
B
GC3 K21A
Average
C
GC3 K77G
Average
D
GC3 N97D
Average
E
GC3 K21A|N97D
Average

Figure 21. Average change in fluorescence (ΔF/F) observed in response to a single stimulus and bursts of 2 and 4 stimuli at 40 Hz for mutations comprising the high calcium affinity sensor, GC3_K21A_K77G_N97D. **A**) GCaMP3 (n=23). This graph is taken from Figure 17E and only included for comparison purposes. **B**) GC3_K21A (n=7). **C**) GC3_K77G (n=5). **D**) GC3_N97D (n=5). **E**) GC3_K21A_N97D (n=5).

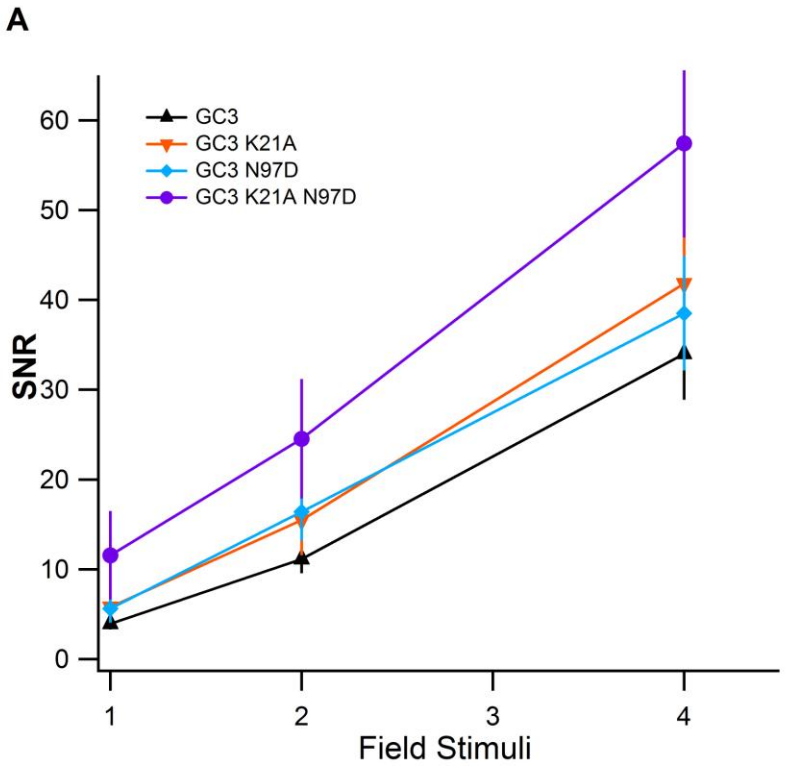

Figure 22. SNR for GC3, GC3_K21A, GC3_N97D, and GC3_K21A_N97D (select mutations comprising the high calcium affinity sensor, GC3_K21A_K77G_N97D) in response to a single stimulus and bursts of 2 and 4 stimuli. SNRs of these GCaMP variants were not significantly different (ANOVA, $p>0.05$).

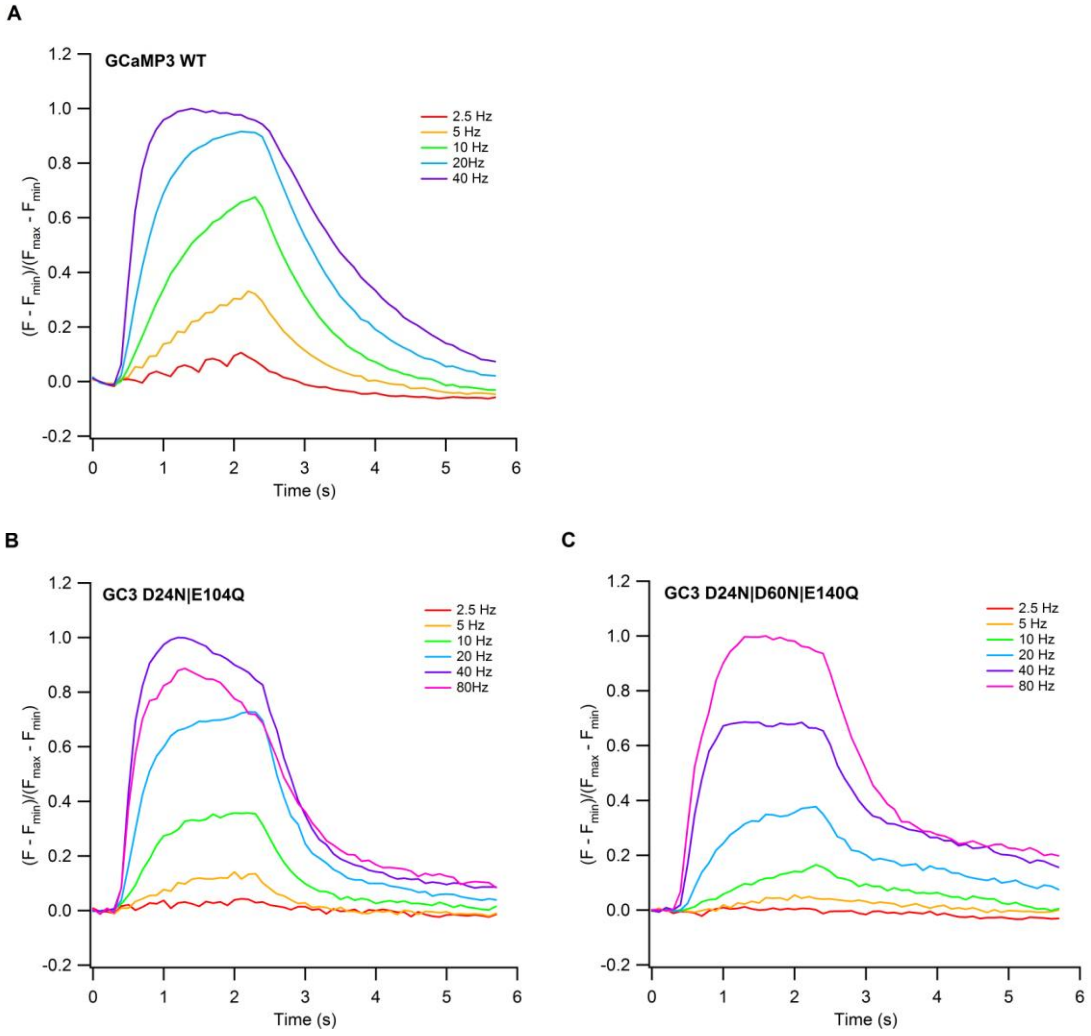

Figure 23. Normalized fluorescence changes ($[F - F_{min}]/ [F_{max}-F_{min}]$) of GCaMP3 (A, n=23; graph is taken from Figure 19A and included for comparison purposes) GC3_D24N_E104Q (B, n=3) and GC3_D24N_D60N_E140Q (C, n=3). Responses to 2s stimulus trains at 80 Hz was included for the low affinity constructs. Note that both of the low calcium affinity constructs become saturated at much higher calcium concentrations compared to GCaMP3.

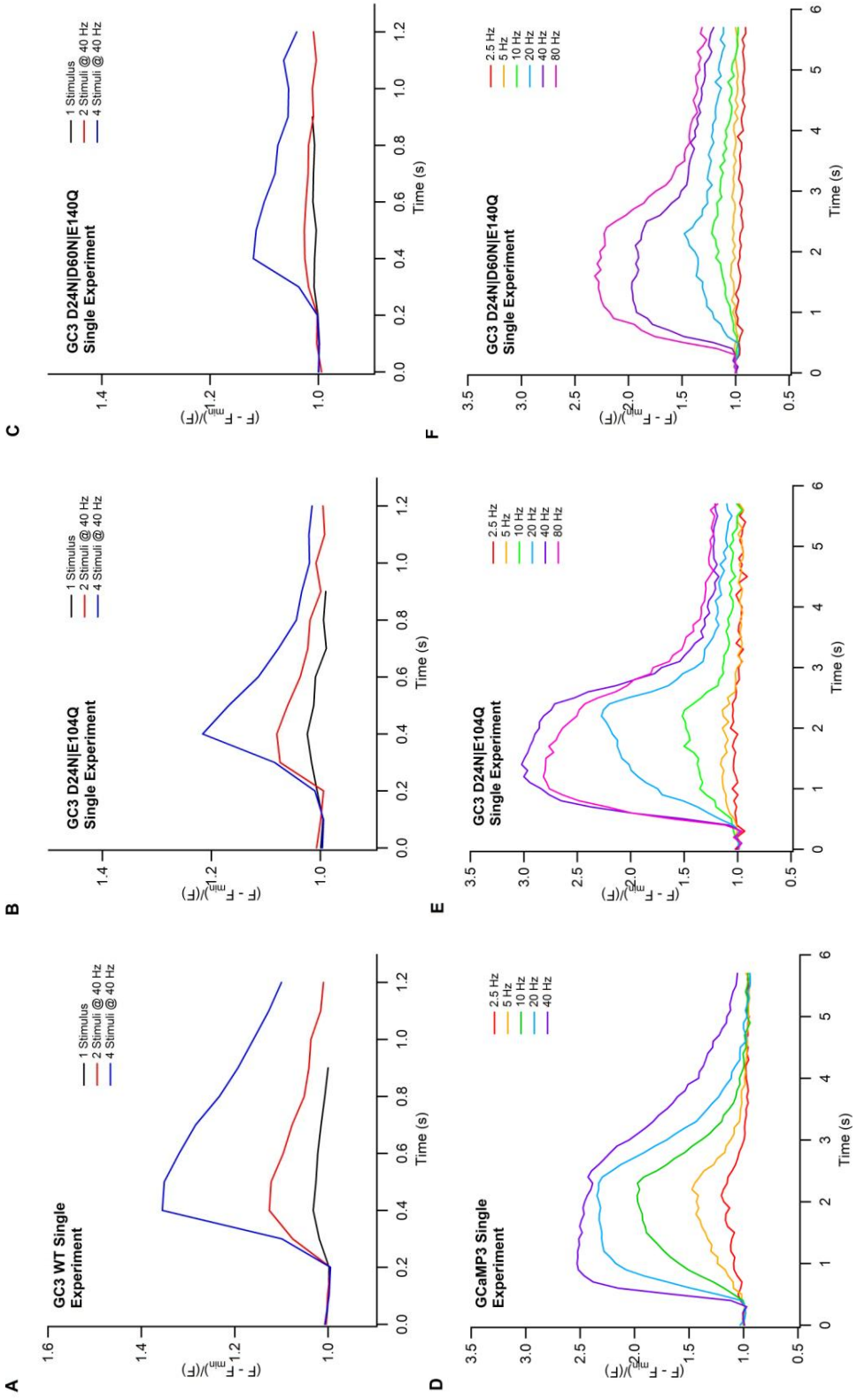
A
GC3 WT Single Experiment
1 Stimulus
2 Stimuli @ 40 Hz
4 Stimuli @ 40 Hz
B
GC3 D24N|E104Q Single Experiment
C
GC3 D24N|D60N|E140Q Single Experiment
D
GCaMP3 Single Experiment
2.5 Hz
5 Hz
10 Hz
20 Hz
40 Hz
E
GC3 D24N|E104Q Single Experiment
80 Hz
F
GC3 D24N|D60N|E140Q Single Experiment
Time (s)
(F - F_min)/(F)

Figure 24. Fluorescence changes for GCaMP3 and the low calcium affinity sensors. Fluorescence increases (ΔF/F) in response to a single stimulus and bursts of 2 and 4 stimuli at 40 Hz for single experiments with GCaMP3 (A), GC3_D24N_E104Q (B), and GC3_D24N_D60N_E140Q (C), respectively. The graph for GCaMP3 is taken from Figure 18A and included for comparison purposes. (**D, E** and **F**) Fluorescence increases (ΔF/F) in response to 2 second trains at 2.5, 5, 10, 20, and 40 Hz for single experiments with GCaMP3, GC3_D24N_E104Q, and GC3_D24N_D60N_E140Q, respectively.

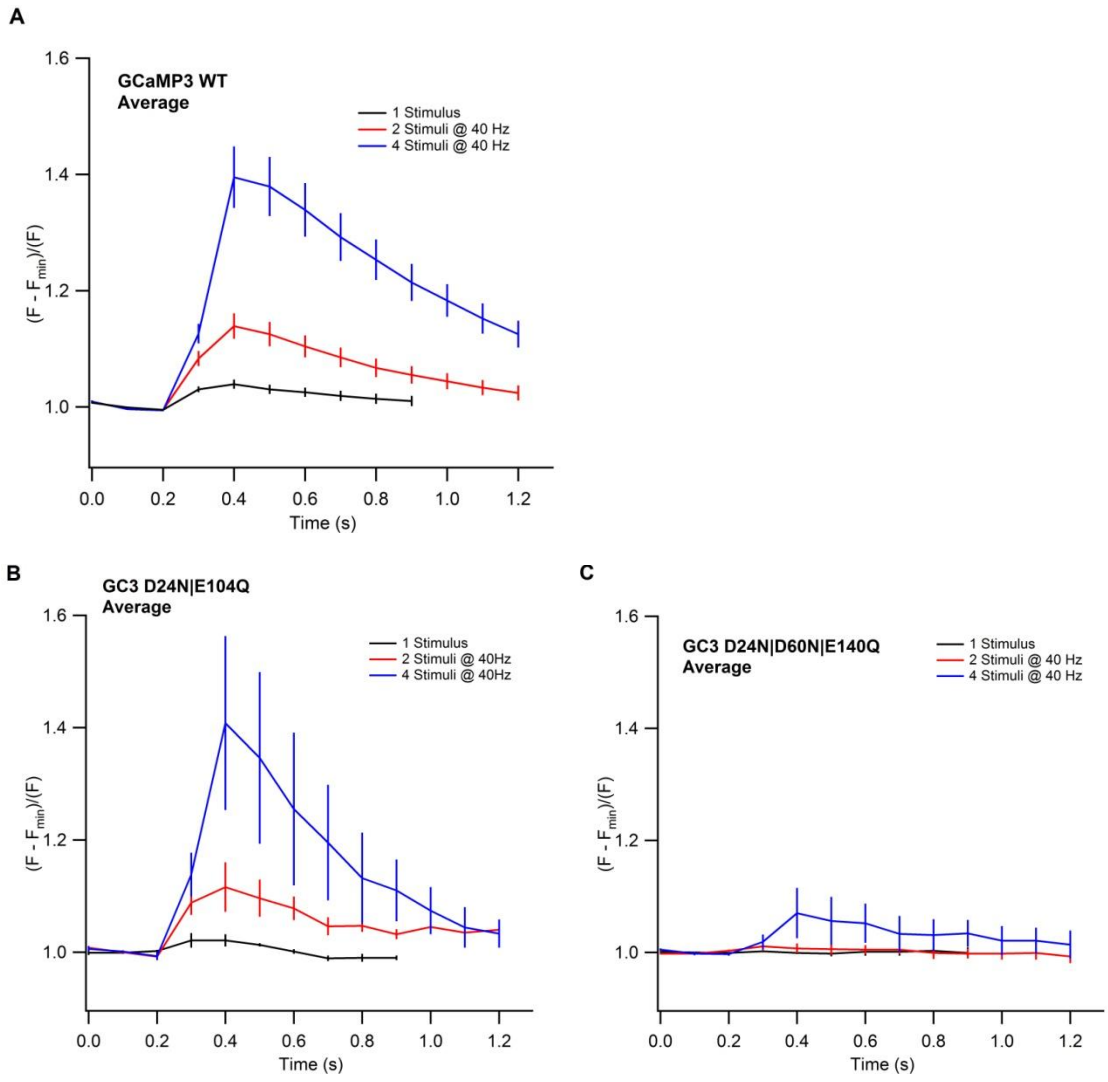

Figure 25. Average change in fluorescence (ΔF/F) observed in response to a single stimulus and bursts of 2 and 4 stimuli at 40 Hz for GCaMP3 (n=23, also shown in Fig 18E), GC3_D24N_E104Q (B, n=3), and GC3_D24N_D60N_E140Q (C, n=3).

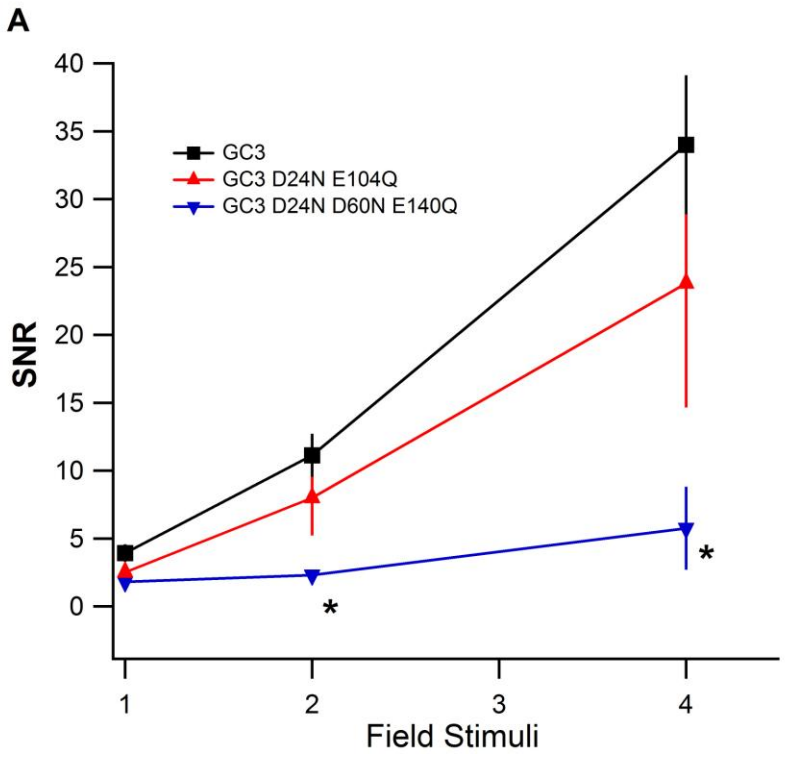

Figure 26. Average SNR for GC3 (black trace) and the low calcium affinity sensors, GC3_D24N_E104Q (red) and GC3_D24N_D60N_E140Q, (blue) in response to a single stimulus and bursts of 2 and 4 stimuli. SNR was calculated as the ratio between the peak fluorescence response amplitude (ΔF) and the standard deviation of the fluorescence trace before stimulus onset (200 ms). (* = $p<0.05$; ANOVA/Tukey HSD Test)